AD-A066 103 PACIFICA TECHNOLOGY DEL MAR CA F/G 18/3
GROUND SHOCK INTERACTIONS WITH NUCLEAR-EXPLOSION PRODUCED CHIMN--ETC(U)
MAY 78 D F PATCH, G I KENT, J E WELCH DNA001-78-C-0066
UNCLASSIFIED PT-U78-0197 DNA-4653T NL

| OF |
AD
A066103

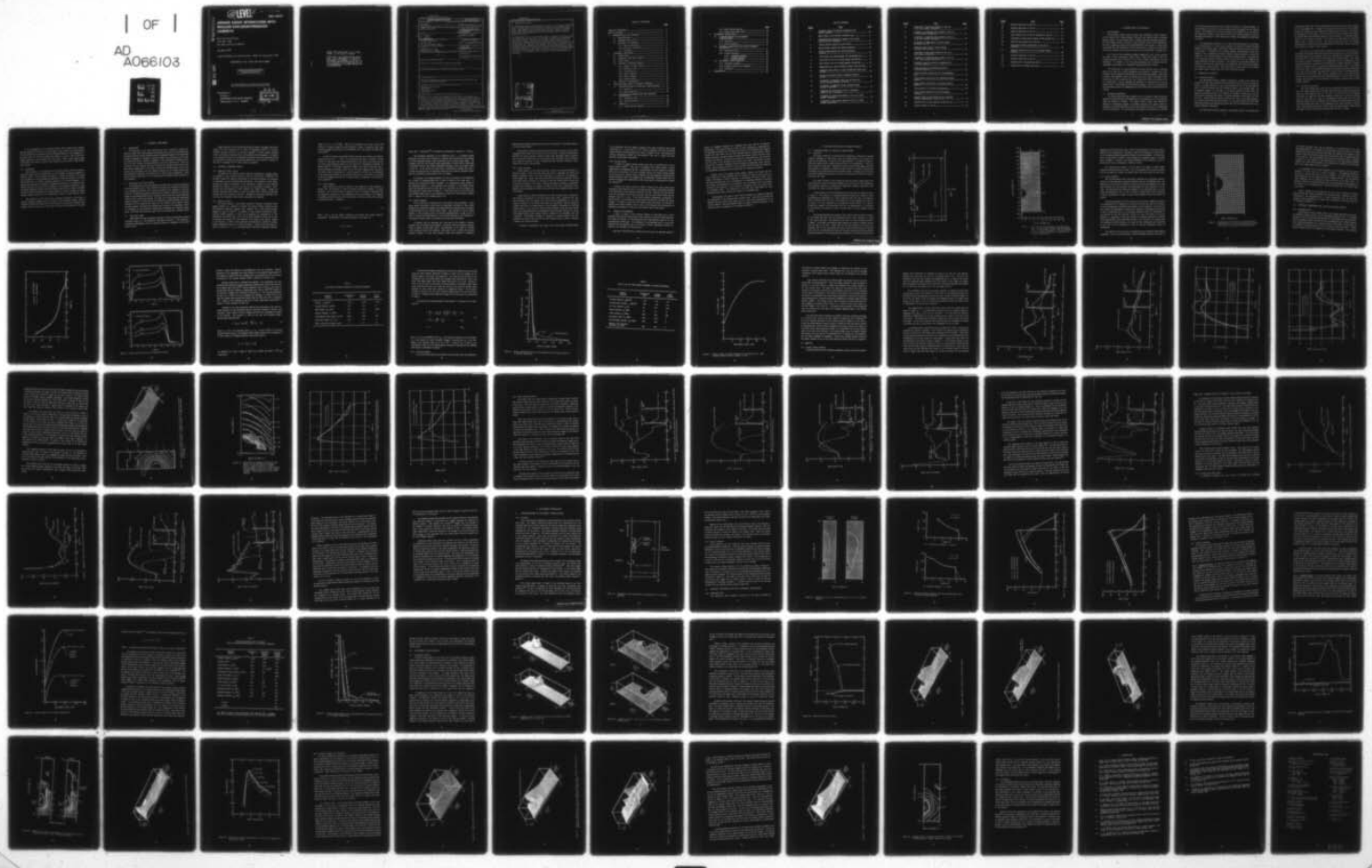

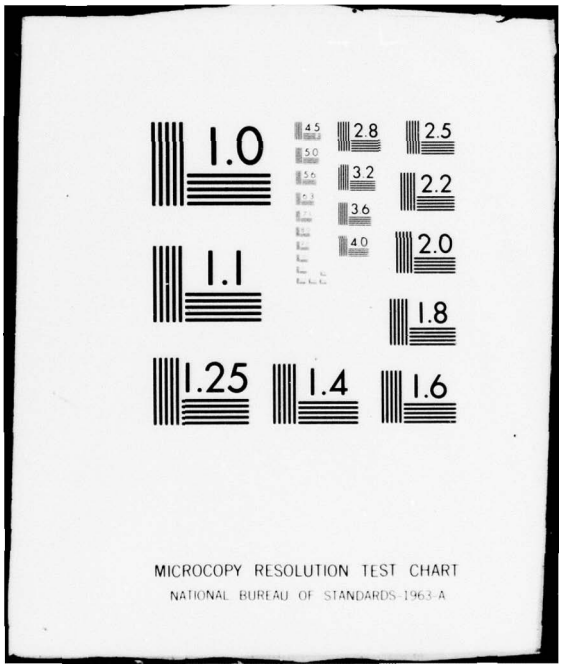
1.0
1.1
1.25
1.4
1.6
2.8
3.2
3.6
4.0
2.5
2.2
2.0
1.8
MICROCOPY RESOLUTION TEST CHART
NATIONAL BUREAU OF STANDARDS-1963-A

(12) LEVEL III

DNA 4653T

GROUND SHOCK INTERACTIONS WITH NUCLEAR EXPLOSION-PRODUCED CHIMNEYS

Pacifica Technology
P.O. Box 148
Del Mar, California 92014

20 May 1978

Topical Report for 15 November 1976—14 November 1977

CONTRACT No. DNA 001-78-C-0066

APPROVED FOR PUBLIC RELEASE;
DISTRIBUTION UNLIMITED.

THIS WORK SPONSORED BY THE DEFENSE NUCLEAR AGENCY
UNDER RDT&E RMSS CODE B345078462 J24AAXYX98354 H2590D.

Prepared for
Director
DEFENSE NUCLEAR AGENCY
Washington, D. C. 20305

Destroy this report when it is no longer needed. Do not return to sender.

PLEASE NOTIFY THE DEFENSE NUCLEAR AGENCY, ATTN: TISI, WASHINGTON, D.C. 20305, IF YOUR ADDRESS IS INCORRECT, IF YOU WISH TO BE DELETED FROM THE DISTRIBUTION LIST, OR IF THE ADDRESSEE IS NO LONGER EMPLOYED BY YOUR ORGANIZATION.

UNCLASSIFIED

SECURITY CLASSIFICATION OF THIS PAGE *(When Data Entered)*

REPORT DOCUMENTATION PAGE

READ INSTRUCTIONS BEFORE COMPLETING FORM

1. REPORT NUMBER: DNA 4653T
2. GOVT ACCESSION NO.:
3. RECIPIENT'S CATALOG NUMBER:

4. TITLE *(and Subtitle)*: GROUND SHOCK INTERACTIONS WITH NUCLEAR-EXPLOSION PRODUCED CHIMNEYS.

5. TYPE OF REPORT & PERIOD COVERED: Topical Report for Period 15 Nov 76—14 Nov 77

6. PERFORMING ORG. REPORT NUMBER: PT-U78-0197

7. AUTHOR(s): D. F. Patch, G. I. Kent, J. Eddie Welch

8. CONTRACT OR GRANT NUMBER(s): DNA 001-78-C-0066

9. PERFORMING ORGANIZATION NAME AND ADDRESS: Pacifica Technology, P.O. Box 148, Del Mar, California 92014

10. PROGRAM ELEMENT, PROJECT, TASK AREA & WORK UNIT NUMBERS: NWET Subtask J24AAXYX983-54

11. CONTROLLING OFFICE NAME AND ADDRESS: Director, Defense Nuclear Agency, Washington, D.C. 20305

12. REPORT DATE: 20 May 1978

13. NUMBER OF PAGES: 98

14. MONITORING AGENCY NAME & ADDRESS *(if different from Controlling Office)*:

15. SECURITY CLASS *(of this report)*: UNCLASSIFIED

15a. DECLASSIFICATION DOWNGRADING SCHEDULE:

16. DISTRIBUTION STATEMENT *(of this Report)*

Approved for public release; distribution unlimited.

(18) DNA, SBIE (19) 4653T, AD-E300 466

17. DISTRIBUTION STATEMENT *(of the abstract entered in Block 20, if different from Report)*

18. SUPPLEMENTARY NOTES

This work sponsored by the Defense Nuclear Agency under RDT&E RMSS Code B345078462 J24AAXYX98354 H2590D.

19. KEY WORDS *(Continue on reverse side if necessary and identify by block number)*

Underground Nuclear Test
Containment
Chimney Interaction
Ground Shock

20. ABSTRACT *(Continue on reverse side if necessary and identify by block number)*

Results from a series of two-dimensional ground motion calculations are reported. The calculations represent a first cut at understanding both the dynamic and late-time interactions between an underground nuclear test and an existing nuclear explosion-produced chimney. Two general configurations were examined: detonations adjacent to a nearby chimney and detonations at the working point of a prior explosion which has produced a chimney. In the adjacent chimney study, two chimney separation distances were investigated

(over)

DD FORM 1 JAN 73 1473 EDITION OF 1 NOV 65 IS OBSOLETE

UNCLASSIFIED

SECURITY CLASSIFICATION OF THIS PAGE *(When Data Entered)*

20. ABSTRACT (Continued)

for two bounding cases of chimney material strength. The effects of different material strength and chimney shape were studied in the in-chimney computations. Taken together, the computations show the importance of accurately knowing the material response of the chimney material. Material response models used in the computations and the data on which they are based are discussed in detail.

All computations for the nearby chimney predict a competent late-time residual hoop stress about the new cavity for the range of properties and separation distances considered. Decreasing the chimney material strength, and to a lesser extent, reducing the separation distance enhanced the influence of the chimney on the magnitude of the dynamic stress field in the region around the new shot point. Reducing the competence of the chimney material in the in-chimney computations dramatically altered both the ground motion and the residual stress field. This sensitivity of the results to the chimney properties suggests that extensive material properties data will be required if a new test is to be conducted, either very near or inside the chimney of an old event.

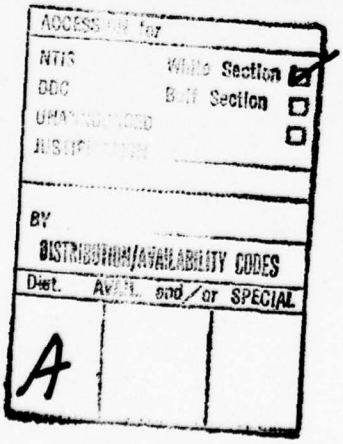

TABLE OF CONTENTS

LIST OF FIGURES

1. INTRODUCTION AND SUMMARY

1.1 BACKGROUND

DNA (formerly DASA) became involved with underground nuclear testing in the late 1960's when it became apparent that such tests could be useful in studying weapons effects. As the program grew, it became clear that planning personnel in the field needed criteria on which to select sites for future tunnel development. Earlier site separation criteria which were established[1] were chosen in a conservative way because the data available at the time were limited. However, the referenced criteria were adopted as the standard for lack of any rational basis to change them.

As a result of the containment program supported by DNA to help evaluate the safety of their underground nuclear tests, a large base of data in both the material properties area, as well as in the area of reentry observations, has been established. In addition to the data bases, analytical and numerical tools for considering various aspects of containment phenomenology have evolved.

The importance of siting horizontal line-of-site nuclear tests in materials which are at once low in shock attenuation, and moderate in strength, has led to extensive material properties determinations for site selection purposes. Some areas of Rainier and Aqueduct mesas are clearly better than others according to these criteria, and in order to maximize the use of these areas (which are considered best for containment) a conflict regarding the proximity of a proposed test to an old chimney arises. The computations reported here represent a first cut at understanding the interactions between an underground test and existing nuclear explosion-produced chimney.

1.2 STUDIES CONDUCTED

The studies which have been conducted are of two general types: detonations adjacent to nearby chimneys and detonations at the working point of a prior explosion which has produced a chimney. The nearby chimney studies have modeled the chimneys as disk-shaped regions of modified materials with centers located at distances of 122 meters (400 feet) and 152 meters (500 feet) from the working point of the new detonation. For each location, two companion computations at a nominal

10 kT yield were performed in order to bound the effects of material strength. In all calculations the volume from the chimnied cavity was spread over the chimney volume. The strength of the chimney material was considered to be the same as the undisturbed material in one case and zero (as an extreme bound) in the other. Preliminary discussions of these studies have already been published as References (2) and (3).

The compuations performed for the cases where detonation is to take place at the working point of a prior event consider the effects of different material properties and chimney shape. These latter studies are presented for the first time in this report. A cylindrical and a conoidal chimney, each presumed to have been caused by 10 kT explosions and having different material properties, provide the media for 5 kT explosions placed at the original detonation point. The properties of the cylindrical chimney material include a void volume from the original burst cavity distributed through the chimney. The material in the conoidal chimney was assumed to have the same properties as the undisturbed tuffs which would collapse into chimneys in Rainier Mesa. This material has a much lower air void content and exhibits higher strength than that in the cylindrical chimney.

1.3 SUMMARY OF RESULTS

1.3.1 Pancake Simulation

The disk-shaped chimney, "pancake", centered at a range of 152 meters was found to have very little influence on the stress fields around the cavity at anytime, however, a modest decrease in axial stress compared to that of the free-field did occur at about 120 meters near the immediate vicinity of the pancake edge. For the pancake centered at 122 meters, a 50 percent decrease in axial stress was observed immediately in front of the edge of the pancake at about 60 ms, but the cavity region experienced only about a 15 percent decrease in axial stress at a time of 80 ms. Neither chimney location produced more than a very slight change in the residual stress fields around the cavity. As one would expect, the stress field inside both chimneys was significantly altered from that of the free-field due to the material properties differences.

The "fluid filled" chimneys produced a much larger effect on the dynamic and

residual stress fields than did the chimneys which were given the same shear strength as the surrounding tuff. Although the compressive hoop stress was only slightly reduced, the thickness of the residual stress region around the cavity was modified by the presence of the pancakes. In the case in the chimney centered at 122 meters, the residual hoop stress decreased rapidly at about 65 meters to a "fractured" region whereas for the pancake centered at 152 meters, the rapid drop to a fractured region occurs at about 85 meters. The peak residual axial stress was reduced approximately 15 percent from the free-field value in the direction of the far chimney and 30 percent towards the near chimney.

The series of four calculations discussed here demonstrate the sensitivity of the dynamic and residual stress fields to the material properties of a nearby chimney. The pancake geometry is inherently conservative regarding the propagation of reflected waves from a nearby chimney back towards the detonation point. Data which has become available subsequent to the performance of these calculations on the material properties of fractured and reconstituted tuff samples indicates a strength reduction of approximately 25 percent at confining pressures above 1 kbar and 30 percent at 0.5 kbar. The unconfined strength for the disturbed material was measured to be zero, but the strength rose rapidly with small increases in confining pressure. On the basis of these test results and the recognition that at burst elevation the chimney tuff is recompacted to near its original properties, it is felt that the "strong" chimney material gives a better estimate of the chimney response than the zero strength material.

1.3.2 In-Chimney Detonation

The most striking result from all of the calculations reported here was the late time velocity retained by the chimney material for the cylindrical chimney case which was still moving at 350 ms. For the 5 kT yield used for the in-chimney calculations one expects the free-field stresses to settle down to their final configuration at about 200 ms. While the hemispherical region below the cavity was relatively unperturbed by the presence of the chimney, the material above the cavity had hoop stresses below that of the magnitude of the cavity pressure at 350 ms. Also, a tensile region was found to exist at that time which formed a valley around the region of high residual stress and intersected the tunnel horizon.

In the computation of the conoidal chimney which utilized more realistic material properties at least for the lower region of the chimney, the results showed that the presence of the chimney created small perturbations in the propagation of the shock wave, but that the residual stress fields at a time of 250 ms were only slightly perturbed in the direction above the cavity. While a small tensile region at the edge of the chimney existed, it was isolated from the cavity by high residual hoop stresses.

1.3.3 Conclusions

Taken together, the computations for both the pancake and the in-chimney detonation studies show the importance of the knowledge of material properties in chimney regions. For the pancake simulations, a chimney centered at 152 meters does not appear to create significant perturbations to either the dynamic or late-time stress fields from an adjacent explosion regardless of its material response. Considering the conservative assumptions regarding the geometry, it is expected that a chimney centered 122 meters from an explosion of the magnitude studied here would not produce significant effects unless the chimney material were of very low strength. In order to study the influence of a nearby chimney of very low strength, the simple pancake geometry would have to be abandoned in order to obtain realistic results.

The sensitivity of the results of the in-chimney detonation to the choice of material properties suggests that an extensive data acquisition program would be required to justify the utilization of an old chimney for execution of another event having a yield of factor of 2 lower than the event which produced the chimney.

2. TECHNICAL DISCUSSION

2.1 OBJECTIVES

The objectives of the work reported here were to determine whether any dramatic effects which could influence containment would occur due to ground shock interaction with prior event-produced chimneys at different locations. The information available regarding the strength of chimney material was nonexistent at the time the studies commenced. However, recognition of the importance of strength effects led to the zero strength bounding calculations which are reported here. What was anticipated was the possible occurrence of early-time dynamic effects which could cause large displacements in the region between the detonation point and the old chimney; also anticipated were the possible reduction of the residual stress fields which ordinarily accompany the detonation of a nuclear device underground. These stress fields are considered to aid in containing the radioactive gases produced by the detonation.

2.2 MODELING THE REAL WORLD

The configurations which best represent situations close to reality are generally three-dimensional in nature. This is especially true when one considers the interaction of an underground explosion with a chimney produced by an explosion at the same elevation. Furthermore, geologic layering and the effects of gravity are additional aspects of the phenomenology which if included would dictate that three-dimensional models would be required for analysis. The large cost of exercising three-dimensional computer programs is well-known and the hardware available generally puts severe limitations on the resolution with which one can compute a given region of space. For these reasons, and because the present work was only of an exploratory nature, the utilization of two-dimensional axisymmetric techniques was considered appropriate. The STAR code which was used for all the computations is discussed below.

2.3 THE STAR CODE

STAR solves the finite difference equations of motion of compressible, inviscid, continuous media in a two-dimensional Lagrangian framework. This approach is particularly advantageous when the constitutive relation is dependent on the deformation history.

Special features of STAR include generalized boundary conditions, much faster energy and stress iterations than in early 2D Lagrangian codes,[4] an improved artificial viscosity treatment, an improved capability to detect regions requiring rezone, an automatic rezoning routine, and subcycling of grid subregions. In addition to the person-time saved by not requiring intervention and manual operations during runs, automatic rezoning and subcycling techniques can save factors of between 10 and 100 in computing time for many classes of problems.

2.4 MATERIAL RESPONSE MODEL

2.4.1 Equation of State Library

All aspects of the material response model are computed in a separate library of equation of state routines which are called by either STAR or SIMONE. This procedure insures that identical descriptions of the material behavior are employed in comparable one and two-dimensional calculations. This equation of state library permits very general formulations of the constitutive response of real materials including the response of porous, visco-elastic and visco-plastic materials. Multi-material and multi-equation of state problems are readily treated. Energy and pressure dependent yield surfaces, as well as variable elastic moduli, are generally employed for most materials of interest. Although not used here, associative flow rule and strain dependent yield surface formulations are available.

2.4.2 Equation of State

The current equation of state library contains six different formulations which specify pressure as a function of density and internal energy: gamma-law gas, Mie-Gruneisen, polytropic, Tillotson, JWL explosive, and a very detailed tabular equation of state for water.[5] In addition to these response formulations, multi-material, tabular equations of state can be generated by combining up to four materials in any desired ratio. Any of the six basic equations of state can be used to represent the response of each component of the mixture. The tabular response of the mixture as a whole is then generated automatically by iteration to achieve pressure equilibrium between the various components. Common table dimensions are 128 by 32 entries in $\mu = (\rho/\rho_o - 1)$ and log(e) space, respectively, spanning a pressure

range of 0.1 to 1 x 10^5 MPa. There is no restriction in the code to limit the number of materials using the multi-component mixture formulation (other than increased storage requirements) and calculations with multi-tabular materials have been made.[6]

In both the chimney and pancake studies cavity gas was modeled as a uniform, gamma-law gas with $\gamma = 1.333$. For the regions and times of interest in these studies it is well known that detailed calculations of the device interaction with the zero room and surrounding medium are not required to satisfactorily reproduce the ground shock.[7] Additionally, parametric studies which model cavity gas with a chemical equilibrium equation of state for the rock vapor suggested that the gamma law source model is equivalent to a modest increase in device yield in comparison to the chemical equilibrium source, and that effects due to differences in the timing of the source pressure decrease are of second order by comparison to the effective yield reduction.[6]

2.4.3 Crush Response

Other constitutive models in addition to the equations of state discussed in Section 2.4.2 are required to treat the general constitutive response of porous materials. For such materials the equation of state is assumed to described only the response of material in a fully compacted or zero void condition. The response of partially crushed material is then referenced to the fully crushed state through the distention ratio, α, defined as

$$\alpha = v/v_s \geq 1.0 \tag{1}$$

where v and v_s are the specific volumes of the porous and crushed material, respectively. The pressure of the porous material is then given by

$$p = \frac{1}{\alpha} p_s (v_s, e) \tag{2}$$

where this ρ-α formulation[8] is completed by specifying the variation of α with p_s.

The functional dependence of the distention ratio, α , on pressure during loading can be derived from measured p-v response data provided that the response of a fully compacted sample is also determined over the same pressure range. The resulting crush curve has frequently been approximated in earth motion codes using a convenient function with several adjustable coefficients which are varied to give a "best fit". In our studies the crush curve is represented in tabular form with a a series of polynomial fits to accurately define the curve between tabulated values. Thus any reasonable crushup behavior can be modeled.

In principal, the unloading response can also be measured in the laboratory for a family of unloading paths from a series of points on the crush curve. In practice, this information is seldom available. As a consequence, simple models for the unloading response of α have generally been employed. In our studies release paths from pressures above the elastic limit, P_e, and below the crush pressure, P_c, were assumed to follow paths of constant α. Load paths below P_e were reversible, and material loaded above P_c was constrained to follow the solid material response with α equal to the fully crushed value of 1.0.

2.4.4 Elastic Response

At low stress levels competent rock media behave nearly elastically. In this stress regime compressive strain paths are essentially reversible, so that neither dilatation, nor permanent compaction are experienced by the material, and its response is fully described by the various elastic moduli. Thus inclusion of this low stress behavior in the numerical model is relatively straightforward, so long as care is taken to insure that discontinuities in the material response are not introduced at the juncture between states of reversible and irreversible deformation.

In general, data for relatively soft rocks such as tuff display a nonlinear response even in the elastic stress regime. In addition, static and dynamic measurements of elastic moduli usually differ. Non-linearities in the moduli are included in the numerical model when sufficient information exists to define the material behavior; however, in most cases constant moduli are sufficient to adequately

characterize the elastic response unless the test bed response is of particular interest in the low stress regime.

Our numerical models have generally utilized dynamic values of elastic moduli determined from seismic data for the test site of interest. Ultrasonic measurements conducted on small laboratory samples usually yield appreciably higher velocities than are obtained seismically for the material in situ, although values of Poisson's ratio based on ultrasonic velocity measurements have generally supported values derived from seismic velocity data.

2.4.5 Plastic Response

Plastic response in the numerical model is based on the usual formulation of plasticity theory in which the total strain rate tensor is separated into elastic and plastic components, where the elastic components of strain rate are assumed to satisfy Hooke's law. Plastic flow occurs only after the stress state reaches a critical yield surface which in general is a function of both the current state of stress and of the past incremental strain history. Thermal softening in response to deformation heating, work hardening, and changes in effective stress due to dilatation or compaction can all potentially contribute strain and strain rate dependent terms to the yield surface.

Stress deviators initially calculated on the basis of Hooke's law to exceed the yield surface are adjusted to the yield surface locus using a particular flow rule. The associative flow rule adjusts the stress deviators perpendicular to the yield surface, resulting in an increased mean stress (or equivalently, material dilatation) if plastic flow occurs in a region where the yield strength is increasing with confining pressure (such as is the case for a Mohr-Coulomb surface). Since the mean normal stress varies during the process of adjusting the stress deviators, iteration or a Taylor series approximation to the strength function is required if the associative flow rule is invoked. Alternatively, adjusting the deviators at constant pressure, the non-associative flow rule, does not alter the mean normal stress, nor does it introduce a plastic flow related dilatation.

In addition to depending on the shape of the yield surface, bulking produced

by the associative flow rule depends strongly on the value of Poisson's ratio, being a maximum for $\nu = 0$ and zero for $\nu = 0.5$. Thus we generally avoid this formulation unless sufficient material response data exists to support its use. Both pancake and chimney calculations invoked the non-associative flow rule to adjust the stress deviators during plastic deformation.

2.4.6 Fracture Model

A variety of tensile fracture models have been, or currently are in use in ground motion codes.[9] They vary in complexity from simple models to rather sophisticated time-dependent theories. Unfortunately, the data required to establish values for the constants in the more complex theories are almost entirely lacking for brittle fracture in earthen media. Although some data supporting time-dependent fracture initiation exists, they suggest that rate-dependent fracture models are not needed for ground shock calculations in which time scales of milliseconds to seconds are important.[9]

Currently, the failure criterion in STAR is based on the mean normal stress reaching a critical minimum value. In the chimney and pancake calculations discussed in this report this critical value was assumed to be zero. Whenever the mean normal stress was calculated to fall below this value, both the mean normal stress and the deviators were set to zero. If this failed material subsequently recompacted to normal density, it was assumed to be fully healed and thus able to achieve its former strength. It should be noted that this failure model will permit the material to develop some tensile strength if one or more of the principal stress components are sufficiently compressive to result in a net positive mean normal stress.

2.5 OVERLAY TECHNIQUES

In order to obtain a more accurate solution at early-times and to avoid problems with early-time distortion due to cavity growth, it has been found convenient to overlay the solution of one-dimensional shock hydrodynamic problem into the two-dimensional STAR grid. The technique for accomplishing this in a way which minimizes the perturbations due to the overlay is fairly complicated; however, an outline of the technique will be given here.

Each cell in the STAR grid is divided up into an even, but otherwise arbitrary

number of triangular subregions (72 subregions have been used for the present calculations). The areas and centers of each of these subregions are established and the interpolated velocities for the regions are computed. The following area-weighted variables for each STAR cell are then summed: density, internal energy, kinetic energy, momentum, maximum density (crushup information), three of the four stress deviators, and pressure. The fourth stress deviator is determined from the constraint that the trace of the deviatoric stress tensor must vanish. The stresses are then rotated into the proper coordinate system through the appropriate tensor transformation. The co-areas are checked to see if any STAR cell lies outside the boundaries of the SIMONE calculation and the summations are adjusted as required.

Density, mass, total energy, plastic energy, minimum cell volume and the three deviators are then calculated and the equation of state is entered with this density and energy to return a pressure. If the pressure returned is within 5% of the value overlayed from the 1D computation, it is accepted; otherwise, the density and energy are established from an iteration with the Hugoniot until the pressure returned by the equation of state is equal to the pressure from the overlay within an acceptable bound. The velocities of the STAR grid intersections are then interpolated from their location with respect to the SIMONE grid.

Unfortunately, this version of the overlay technique was established following the computation of the strong chimney material cases. The iteration utilizing the Hugoniot was not used for those cases, and as a result certain perturbations to this solution resulted. These perturbations affect the region immediately adjacent to the cavity and will be considered in the analysis in Section 3.

3. PANCAKE SIMULATION OF NEARBY CHIMNEY

3.1 CONFIGURATIONS OF PANCAKE COMPUTATIONS

3.1.1 Geometry

The region modeled in the axisymmetric computations reported here included locations extending to 1200 meters from the working point in the positive and negative axial directions, as well as in the radial direction. The sketch in Figure 1 shows this region and the coordinate system used for the computations. The entire mesh consisted of 7,938 cells. Although this number of cells would suggest relatively crude zoning, it is adequate to resolve the major features of interest regarding the interaction of the ground shock with the chimney region. Advantage has been taken of so-called "sigma zoning" wherein zone sizes are increased as a function of distance away from the origin.

The region included in the computation has been chosen large enough such that waves do not reach the boundaries during the time of interest of the computation. This completely obviates the necessity for sophisticated boundary treatments which sometimes can impact solutions adversely.

A limited region of the calculational grid which was used for analysis is shown in Figure 2. The effects of an explosion-produced chimney was modeled in these two-dimensional computations as a disk or pancake where the area of the pancake which intersects direct rays from the working point of the explosion was taken to be equal to the area subtended by the expected chimney profile for a chimney centered at a range of 152 meters (500 feet) from the working point. The thickness of the pancake was selected to give a volume equal to actual average chimney volumes.

Two chimney positions were studied: a "far" location with the chimney centered at 152 meters (500 feet) from the working point and a "near" chimney at a range of 122 meters (400 feet). The locations of the "near" and "far" chimneys are shown in Figure 2. The doubly cross-hatched region indicates an overlap of pancake volumes from one case to the next. Notice that for the disk centered at 122 meters, its interface with the tuff surrounding the cavity is only 95 meters from the working point. One set of computations was done for a chimney material which was relatively strong and another set of computations was performed for a chimney material which

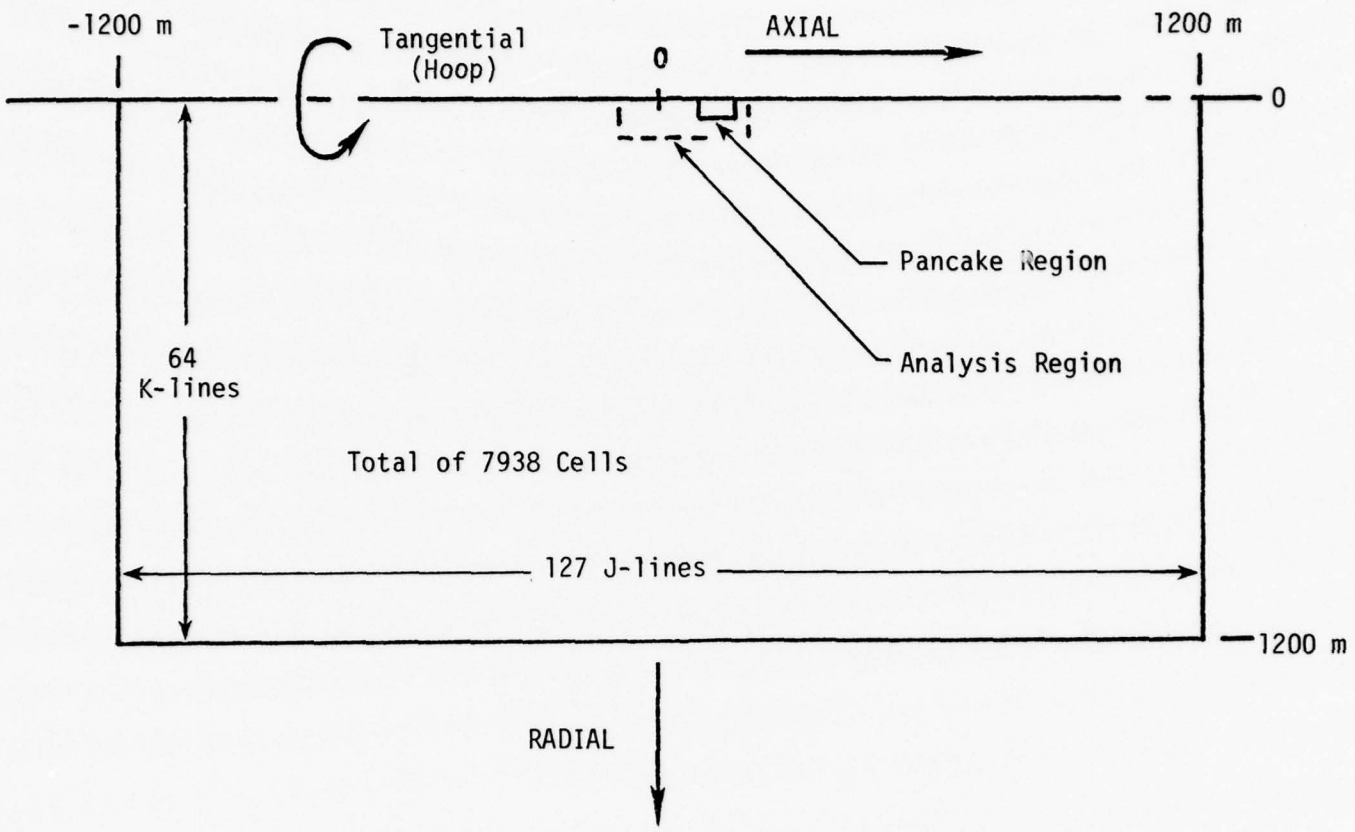

Figure 1. Coordinate system and general configuration for pancake problems.

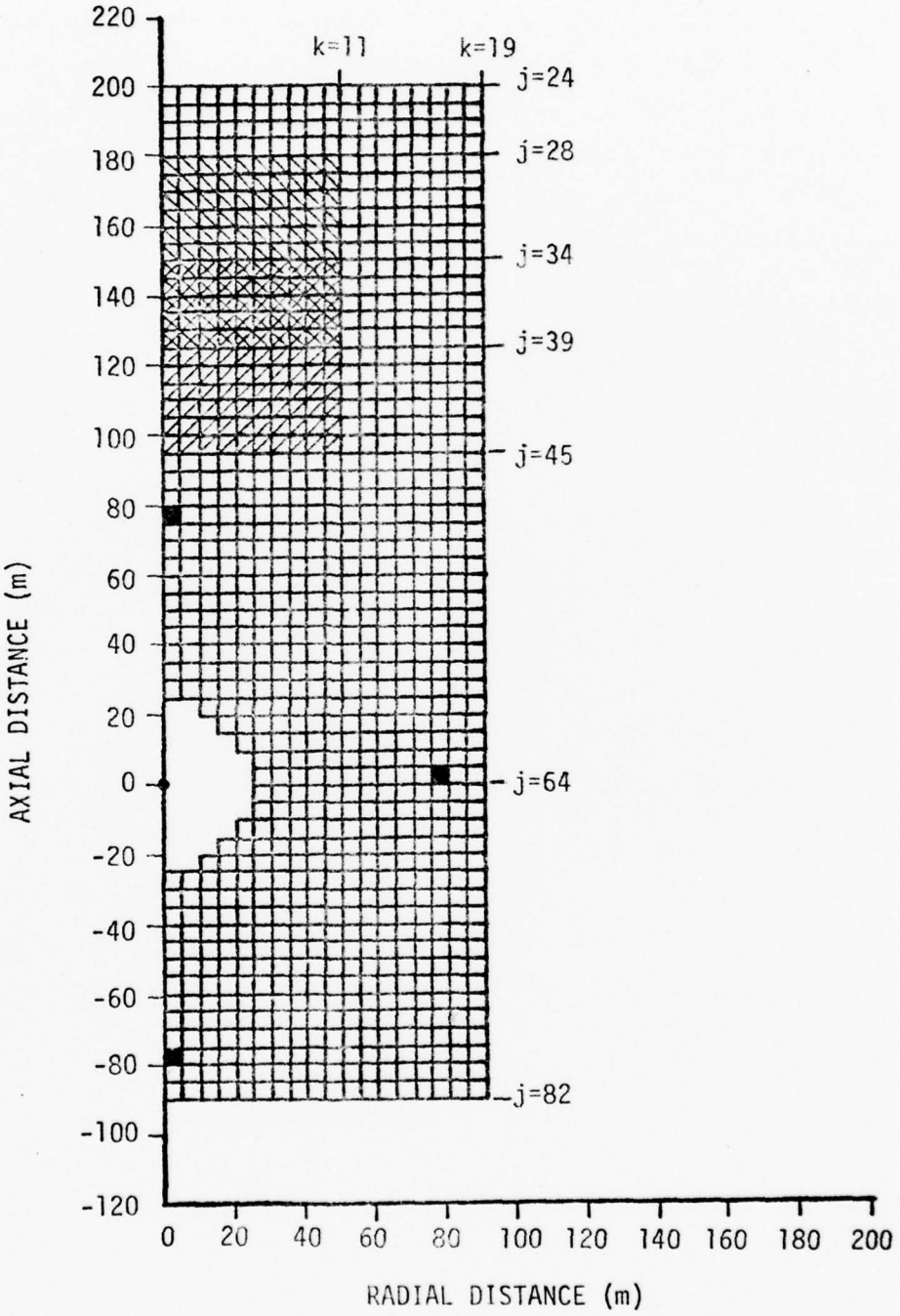

Figure 2. Small section of 2D chimney calculation grid. Cross hatched regions indicate the two chimney locations which were studied. Stress, velocity and displacement histories were obtained for the three solid cells.

supported no shear stress (weak case). Prior to the performance of the weak chimney material set of computations, a technique to distort the initial grid to reduce errors in the overlaying procedure (discussed in Section 3.1.2) was developed. This technique led to the grid shown in Figure 3 which replaced the equivalent region of the grid shown in Figure 2. Details of the material properties of the chimneys, as well as the free-field tuff, are discussed in Section 3.2 below.

The limited grid of Figure 2 will be used as the region in which certain contour and isometric plots are drawn. Also, the darkened cells at about 80 meters from the working point indicate the regions where time history data has been saved.

3.1.2 Initial Conditions

The two-dimensional STAR calculations performed were initialized using the results of a one-dimensional calculation performed with the 1D SIMONE code. The utilization of the 1D code to compute the early-time shock hydrodynamics is at once more accurate and less expensive than performing the early dynamics in the 2D code. The large distortions which occur adjacent to the expanding cavity are more easily accommodated in the 1D code. Extensive rezoning which would be required in the 2D computation is known to lead to some diffusion which may impact the solution.

The initial conditions for all four studies were taken from a SIMONE calculation of a hypothetical 10 kT explosion in the same tuff which was used as the medium for the two-dimensional calculations (see Section 3.2 for properties). Since until the wave reaches the inhomogeneity caused by the inclusion of the pancakes, the problem is that of a spherical burst, it is, in principle, possible to allow the initialization of the problems for the "far" pancakes to occur at a later time than for the "near" pancakes. A comparison of the early behavior for problems initialized at different times indicated that some differences did exist in the solution in the region which was unaffected by either chimney. As a result, all four computations were initialized at the time of 33.7 milliseconds in order to improve comparisons among the calculations.

The overlays for the two sets of computations were performed using different techniques. The two major differences in these techniques concerned one aspect of

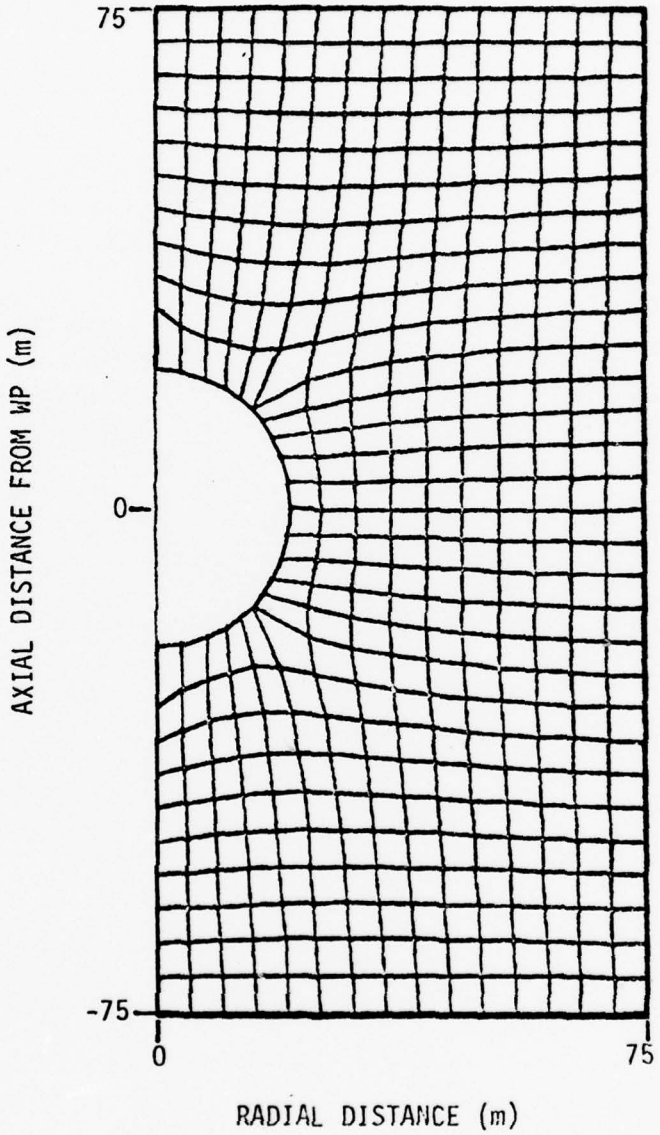

Figure 3. Rectangular grid distorted to conform to the cavity radius in the 1D calculation at the time the results are overlayed into the 2D mesh.

the overlay procedure itself and the utilization of a deformed grid in the two-dimensional problems. The original overlay procedure which was used for the strong pancake cases conserved momentum and energy very precisely, but resulted in some zones for which the overlaid variables were not consistent with the equation-of-state of the material. The weak pancake cases utilized the technique which is described in Section 2.5. The utilization of the deformed grid for the weak pancake problems allowed us to avoid certain problems in determining the co-areas for the "staircase" grid in the cavity regions shown in Figure 2.

A comparison of the velocity profiles in the 2D grids for the two sets of problems at a time of 33.73 ms is shown in Figure 4. No substantial differences are seen to exist between the two sets of problems. The axial, mean, and hoop stress profiles for the two studies are shown in Figures 5a and b. For the stresses, some differences can be observed near the cavity and at the shock front. As indicated earlier, the overlay procedure which was used reduces the perturbations in the solution from incompatabilities of overlaid conditions with the material equation-of-state.

While a number of test calculations have been done to develop the current grid distortion and overlay procedures, the extensive studies required to sort out differences in the computations due to these modifications have not been done. However, some conclusions can be drawn from the solutions at hand and these will be discussed in Section 3.3.

3.2 MATERIAL PROPERTIES FOR THE PANCAKE SIMULATIONS

3.2.1 Undisturbed Tuff

Three different material regions reside in the pancake calculations: the cavity, the disturbed chimney material, and the surrounding undisturbed tuff. As discussed in Section 2.4.2, the cavity gas was described by a simple gamma-law gas treatment. Both the disturbed chimney material and the surrounding tuff were initially assumed to be loaded hydrostatically to a uniform pressure of 6.83 MPa, a value typical of the lithostatic overburden pressure in tuff at a depth of about 400 meters. A single material response model was employed for each separate material. Thus, layering

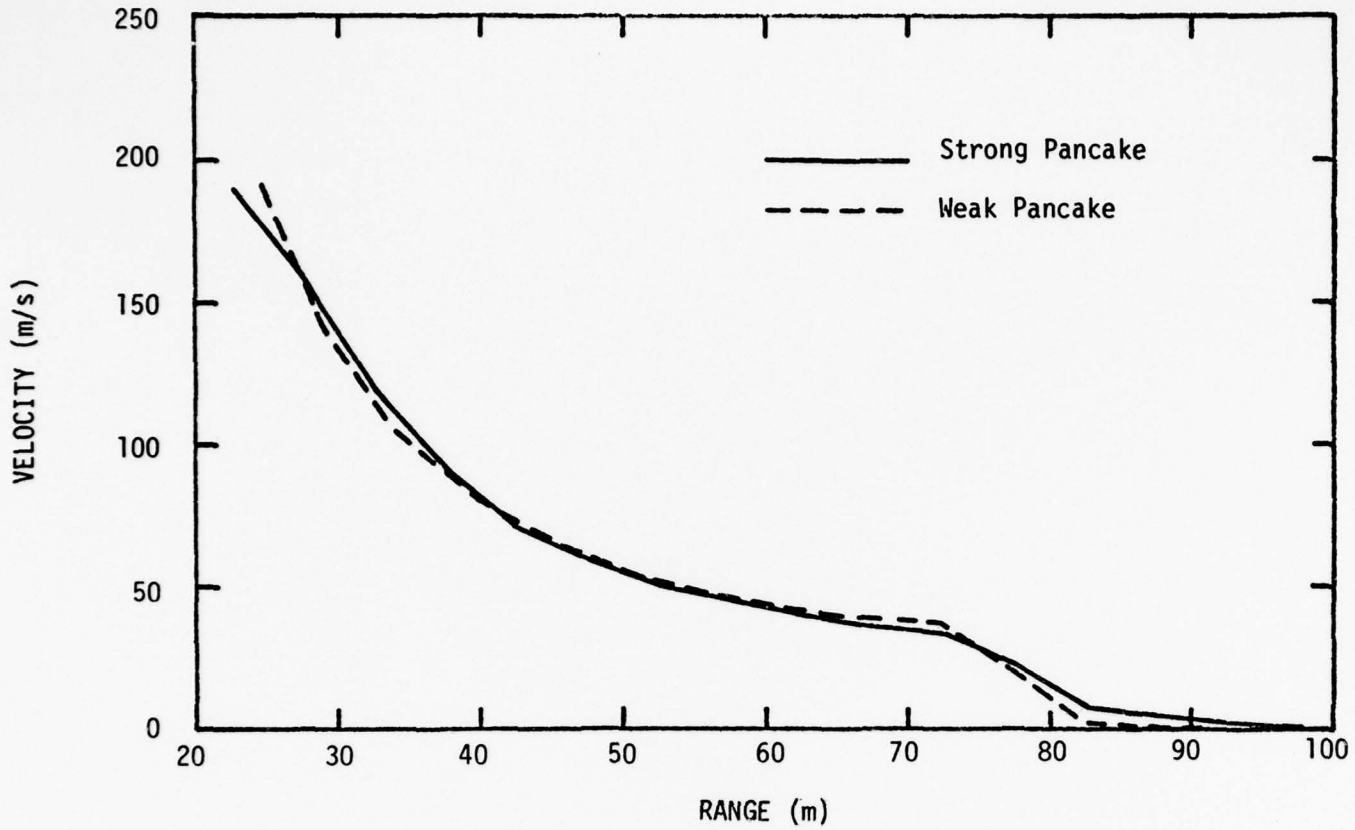

Figure 4. Velocity profile overlaid into the 2D grid at 33.73 ms for the pancake problems.

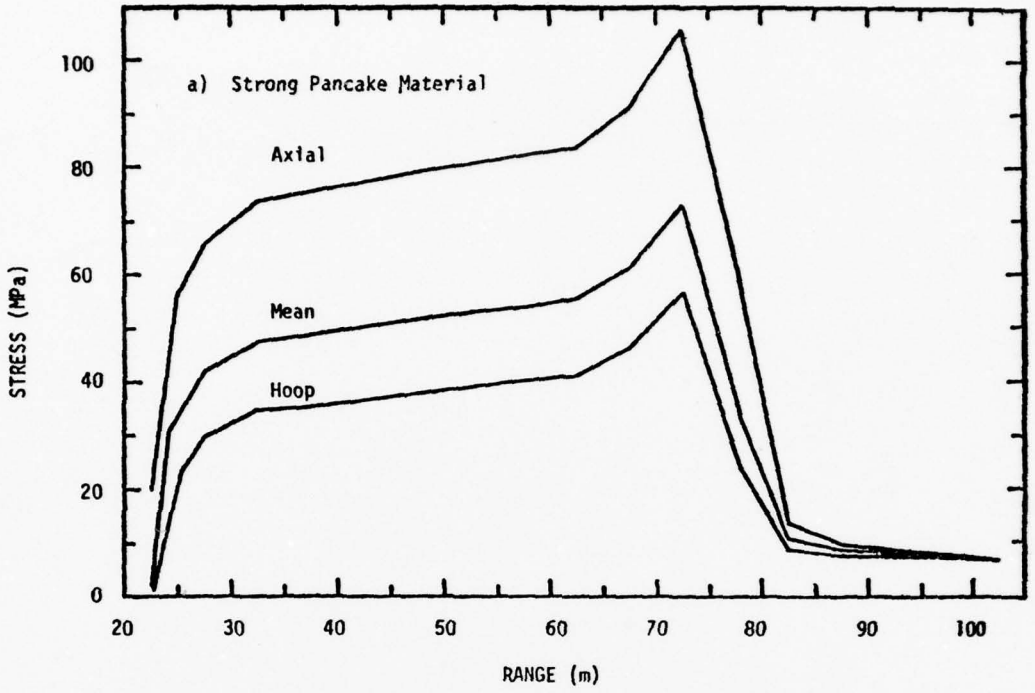

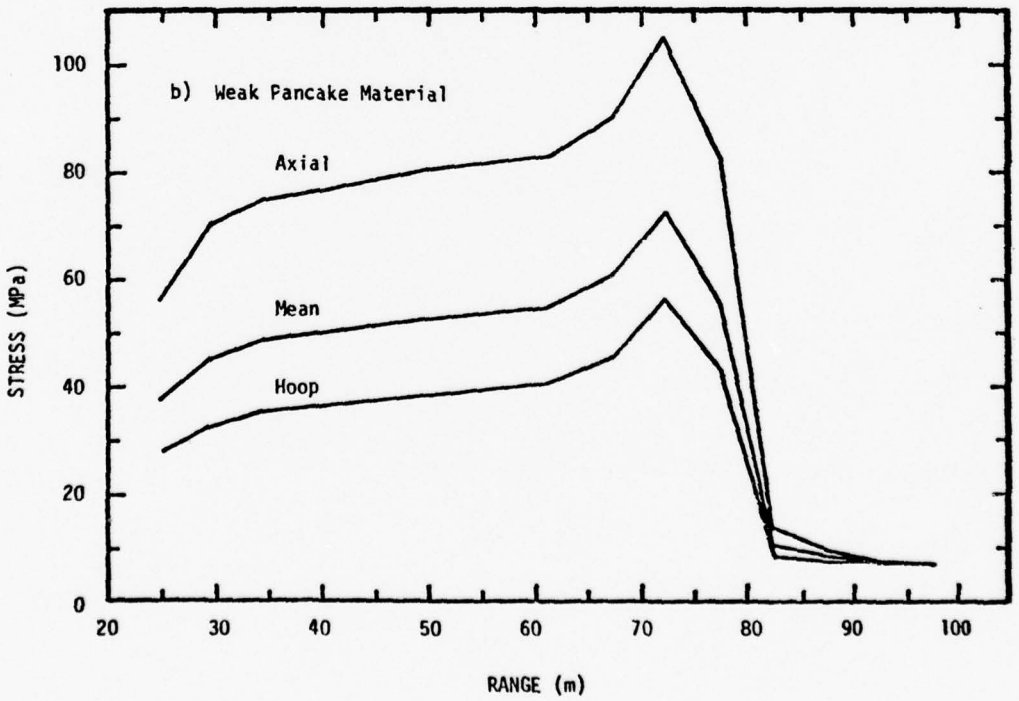

Figure 5. Stress profiles overlaid into pancake problems.

effects in either the chimney or surrounding tuff were not considered. Material properties of the undisturbed tuff were selected to be reasonably representative of the response of typical NTS tuff, although there are deviations as will be discussed. Development of the pancake material models is described in Section 3.2.2.

Material models used to described the response of the undisturbed tuff were developed from laboratory test data obtained for samples taken from various locations in the Mighty Epic test bed.[10] Elastic properties, listed in Table 1, are based on USGS seismic log data obtained in exploratory hole U12n.10 UG#7[11] in addition to the laboratory response data contained in Reference 12. The resulting longitudinal velocity, V_p, of 2286 m/s is not unusually low, although it is about 270 m/s less than the average value derived from seismic data for other test sites in competent tuff. Density of the undisturbed tuff prior to shock compression, 1.920 Mg/m^3, is typical of values measured for NTS tuff.

Response of the fully compacted material was represented in the code by a tabular equation of state generated using the techniques discussed in Section 2.4.2, assuming a water content of 17% by weight, with dry rock comprising the balance of the material. The equation of state for dry rock was calculated using a Mie-Gruneisen representation

$$p = G_o \rho_o e + p_H(v)\left[1 - \frac{G_o \rho_o}{2}(v_o - v)\right] \tag{3}$$

where $G_o = 0.33$ is the Gruneisen ratio, $v_o = 1/\rho_o = 0.4219$ m^3/Mg is the ambient specific volume, and p_H is the Hugoniot shock pressure derived from a quadratic fit of shock velocity to measured particle velocity data given by

$$u_s = A + B\,u_p + C\,u_p^2 \tag{4}$$

for constants A, B and C equal to 350.25 m/s, 0.70476 and 1.0055 x 10^{-4} s/m, respectively.

Table 1

Low Pressure Properties Materials in Pancake Simulations

Material Property	Undisturbed Tuff	Strong Pancake	Weak Pancake
Density, ρ_o (Mg/m^3)	1.920	1.470	1.470
Young's Modulus, E_o(GPa)	6.78	1.54	0
Bulk Modulus, K_o (GPa)	6.64	0.214	0.214
Rigidity Modulus, G_o (GPa)	2.55	2.55	0
Compressional Wave Speed, C_p(m/s)	2286	1568	382
Shear Wave Speed, C_s (m/s)	1152	1317	0
Water Content by Weight, M_w(%)	17	17	17

Irreversible void collapse at pressures in excess of the elastic limit was modeled using the crush response illustrated in Figure 6, where the void collapse for the pancake rubble is also shown for comparison. The initial 2% void content for the undisturbed tuff is somewhat higher than average values measured for recent tests (other than Mighty Epic) which have ranged from about 1.2 to 1.6%. However, a value of 2% air voids is well within the normal spread of individual sample values which range from less than 1% to over 5%, and 2% is far less than average values obtained for some older tests conducted in unsaturated media. The procedure described in Section 2.4.3 was used to specify release paths from the crush curves of Figure 6. Constants used to specify the shape of the crush curve are summarized in Table 2.

The pressure and energy dependent yield function, Y, employed in the calculations is

$$
\begin{aligned}
Y &= \left[Y_o + Y_m \frac{p}{p_m}\left(2 - \frac{p}{p_m}\right)\right]\left(1 - \frac{e}{e_m}\right) \quad ; \quad p<p_m \\
Y &= \left(Y_o + Y_m\right)\left(1 - \frac{e}{e_m}\right); \qquad\qquad p\geq p_m \\
Y &= 0 \qquad\qquad\qquad\qquad\qquad\qquad e\geq e_m
\end{aligned}
\tag{5}
$$

where Y_o is the unconfined yield, Y_m is the maximum increase in yield strength, P_m is the pressure at which maximum strength is attained, and e_m is the melt energy of the material, taken to be 1.91×10^3 J. Values of P_m, Y_o and Y_m are summarized in Table 2 for the various pancake simulation materials, and the resulting yield surface is illustrated in Figure 7.

3.2.2 Chimney Materials

At the time these studies were initiated very little data other than qualitative

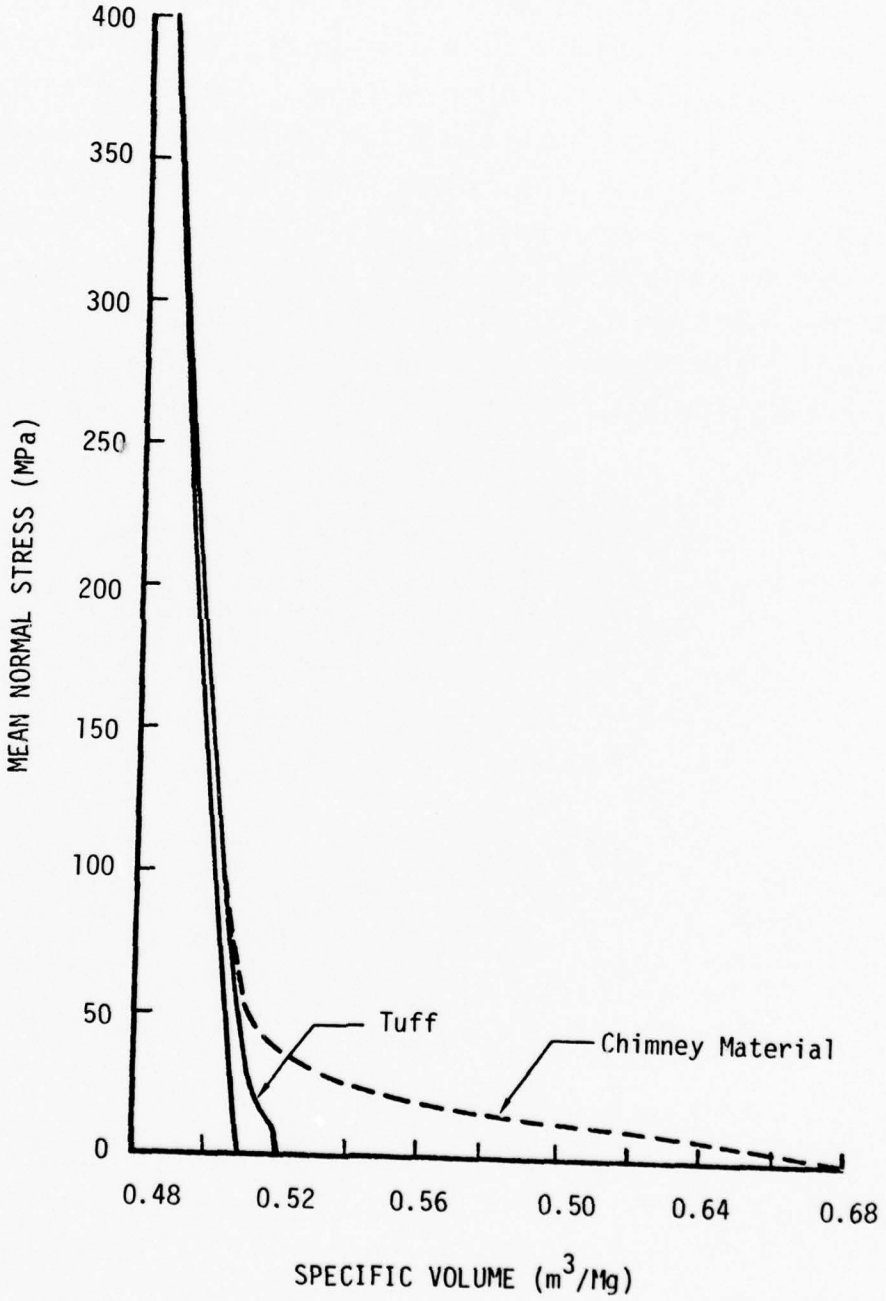

Figure 6. Porous crushup behavior for undisturbed tuff and chimney material in pancake computaions.

Table 2

Crush Curve and Yield Surface Constants in Pancake Simulations

Material Property	Undisturbed Tuff	Strong Pancake	Weak Pancake
Ambient Density, ρ_o(Mg/m^3)	1.92	1.47	1.47
Ambient Solid Density, ρ_s(Mg/m^3)	1.96	1.96	1.96
Air Void Content, V_a (%)	2.0	25.0	25.0
Elastic Pressure, p_e (MPa)	10	10	10
Crush Pressure, p_c (MPa)	400	400	400
Unconfined Yield, Y_o (MPa)	18.0	18.0	0
Yield Strength Increase, Y_m (MPa)	52.0	52.0	0
Maximum Yield Increase Pressure, p_m (MPa)	200	200	0

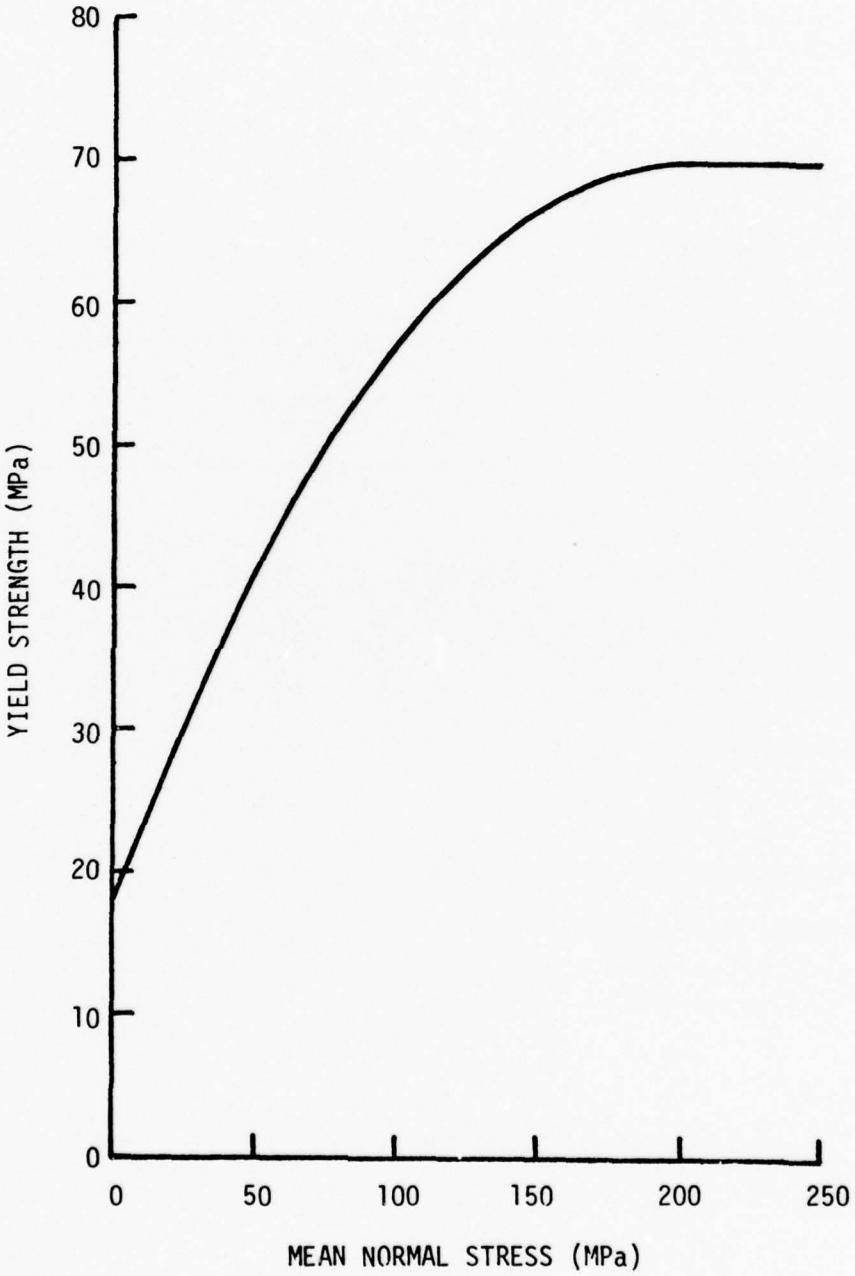

Figure 7. Yield surface for strong pancake and surrounding tuff. Weak pancake chimney material strength is zero.

observations of chimney rubble were available to characterize the response of such materials to ground shock loads. This difficulty led to the two sets of bounding calculations which assume rather extreme limits for the strength of the chimney material.

In the pancake simulations the chimney rubble was assumed to have the same composition as surrounding tuff. Thus, the tabular equation of state described in Section 3.2.1 was also utilized to specify the response of the chimney material in the fully crushed state. Of course, the initial air void content and crush curve response of the pancake material were much different from that of the surrounding tuff (see Table 2 and Figure 6). The initial air void content of the chimney material was derived by assuming that the cavity volume produced by a nominal 10 kt explosion would subsequently be distributed uniformly throughout the chimney rubble following chimney collapse. The chimney volume used was based on limited drill-back data which suggest an average chimney radius of 1.1 times the final cavity radius, R_c, and total height of 5.13 times R_c. A cylindrical chimney shape with hemispherical ends was assumed since little data were available regarding shape of the chimney above tunnel level.

The crush curve shown in Figure 6 for pancake material is relatively uncertain. It was derived from uniaxial test data obtained in exploratory hole UE12n10#9.[13] The crush response determined for the sample having the highest air void content, 10.3%, was scaled linearly in specific volume to reflect the 25% void content required by distributing the chimney volume throughout the chimney material (see Figure 6). The initial, elastic bulk modulus was chosen to be compatible with the zero pressure slope of the crush curve; whereas, in the strong chimney case the rigidity modulus was assumed to be the same as the undisturbed tuff, in keeping with the assumption that the failure response was unaltered. For the zero strength pancake simulation the rigidity modulus was set to zero since deviatoric stresses could not be supported.

3.3 RESULTS

3.3.1 Strong Chimney Material

The ground shock from the detonation propagates outward toward the pancake

regions until rarefactions are produced at about 42 ms from the near pancake; however, the wave does not reach the far pancake until 55 ms. By 60 ms the rarefaction from the near pancake has propagated back to a range of 50 meters from the detonation point producing very little effect at that range, but causing about a 50 percent reduction in axial stress near the chimney boundary itself (Figure 8). At this time, the effects due to the far pancake are nil.

The rarefaction from the near pancake continues to impact the axial stress as time goes on, but at 50 meters at a time of 80 ms the difference between the free-field and the near pancake axial stress is down to about 20 percent (Figure 9). By 80 ms the effect of the far pancake has propagated back to a range of 100 meters, but its effect is seen to be less than 20 percent at about 120 meters which is immediately in front of the far chimney.

The displacements of points initially 80 meters from the working point are shown in Figure 10. The displacement response for the far pancake problem is essentially the same as that for the free-field. It is seen that the maximum difference in displacement for the near pancake occurs at about 125 ms and is only 0.22 meters. This displacement difference endures until 250 ms when the solution was ended. At this time velocities were approximately zero throughout the region of interest with only a small elastic wave propagated to the far field.

As indicated above, axial stress has been considered in order to evaluate the propensity for dynamic cracking to occur between the chimney and the detonation point as a result of the rarefaction wave emanating from the chimney. High values of hoop and radial stresses are believed to be responsible for preventing the late-time hydrofracture of the site medium by cavity gases. A hoop stress time history for the field point at 80 meters is shown in Figure 11. The far pancake history is very close to that of the free-field, whereas at 50 ms, the close pancake solution diverges from the free-field response, exhibiting tension at around 60 ms. Recall that the axial stress was also depressed with respect to the free-field values at this time and at a range of 80 meters (See Figure 8). By 90 ms, however, the near pancake

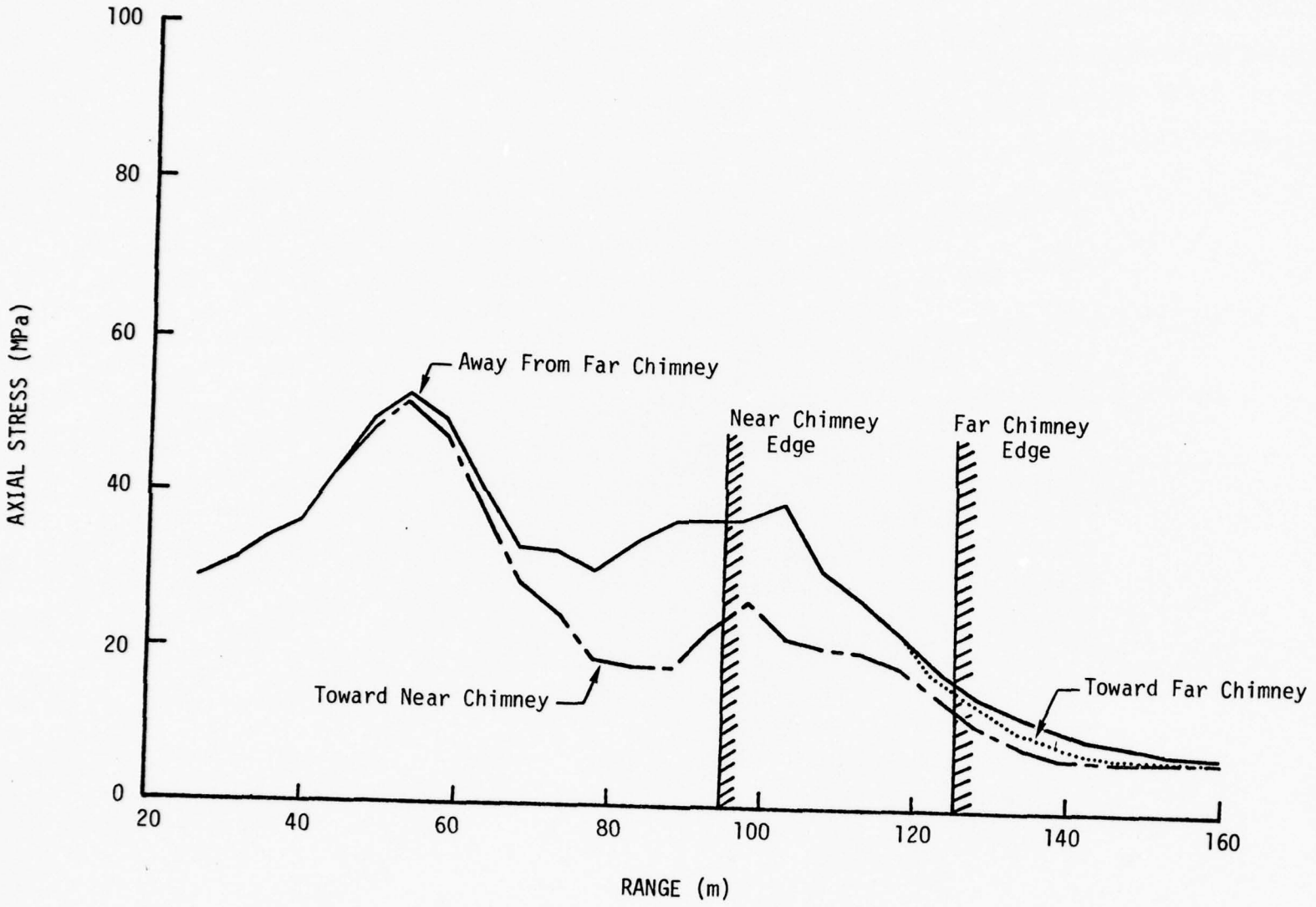

Figure 8. Axial stress at 60 ms in strong pancake calculations. (Note suppressed zero on the abscissa.)

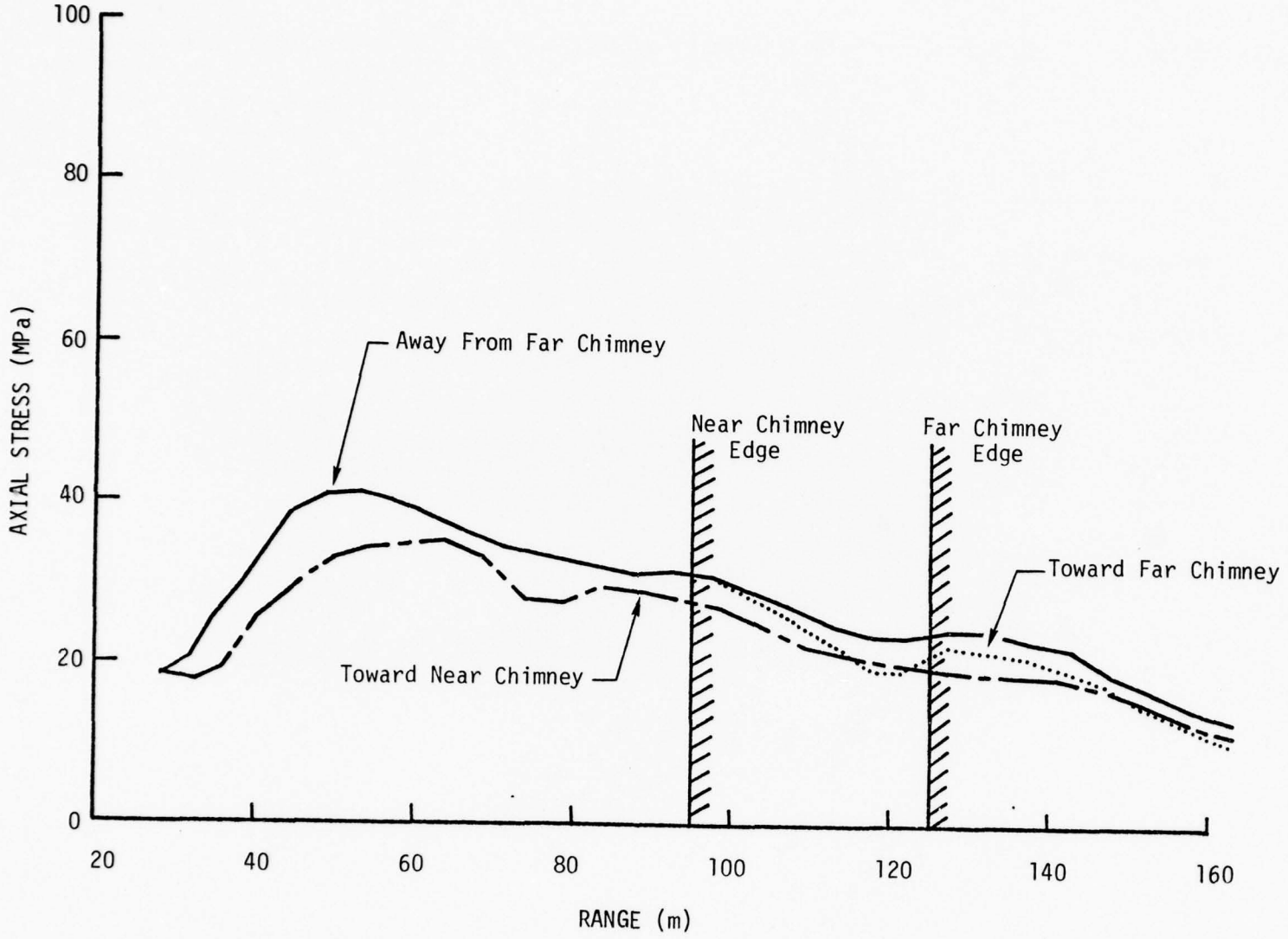

Figure 9. Axial stress at 80 ms in strong pancake calculations. (Note suppressed zero on the abscissa.)

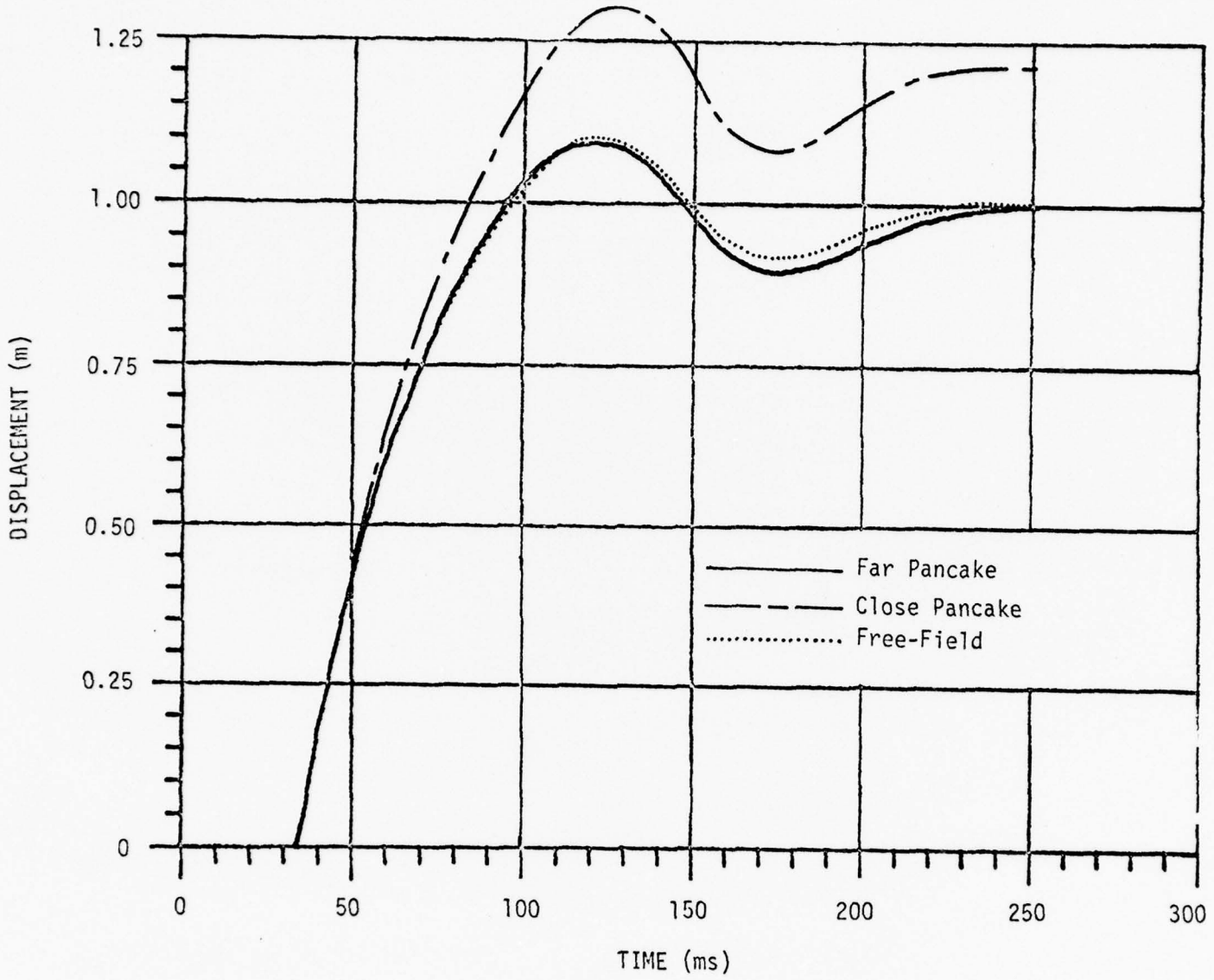

Figure 10. Displacement of a point initially 80 m from the WP.

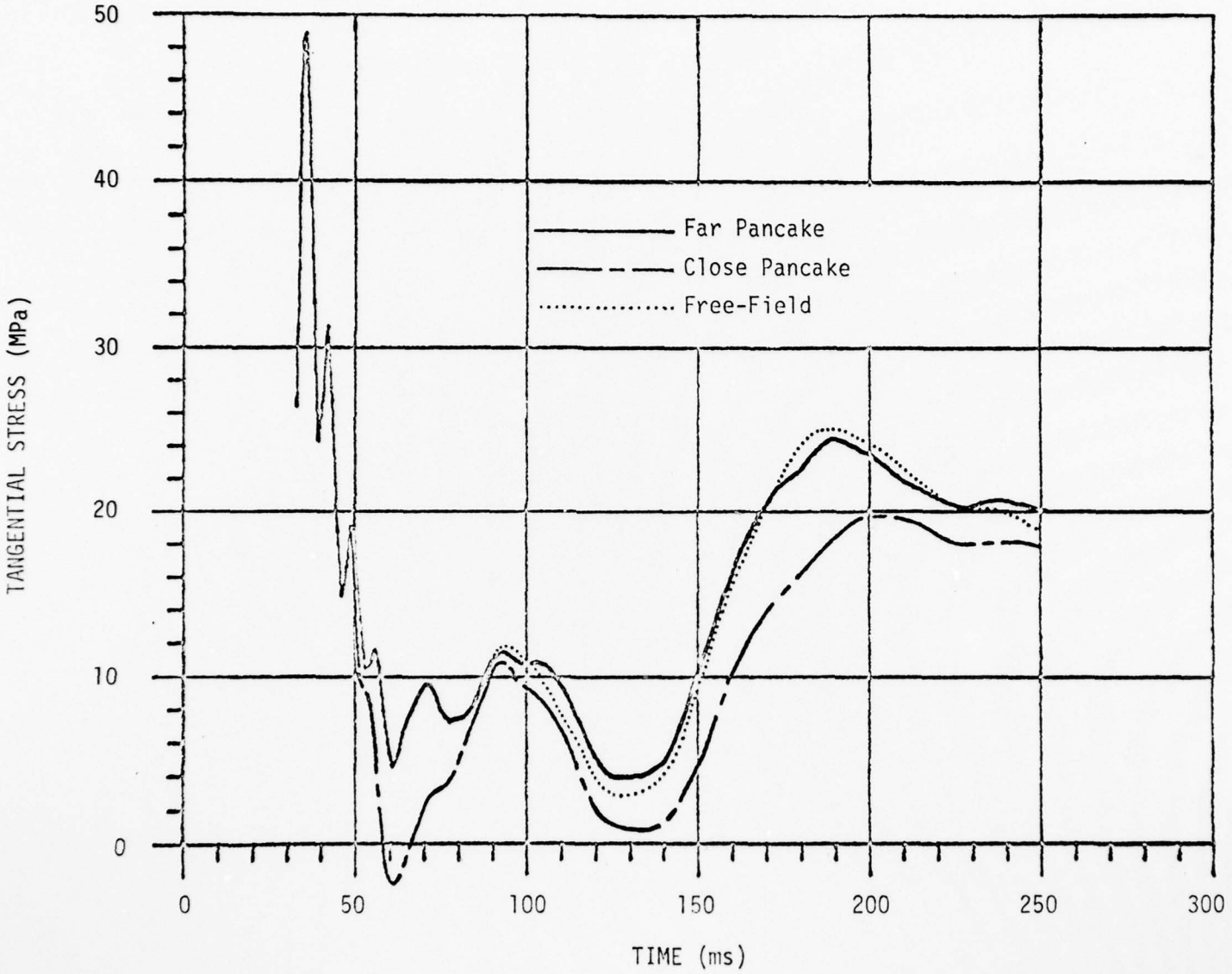

Figure 11. Tangential (hoop) stress at a point initially 80 m from the WP.

tangential stress is very close to that of the free-field. During the next reverberation it becomes depressed once again, however, the rebound which commences at about 130 ms drives the tangential stresses for all cases upward to the rebound values before the residual stresses establish themselves. The residual tangential stresses for the two pancake problems are each within about 5 percent of that for the free-field. Considering that the edge of the chimney is only about 15 meters from the field point being considered it appears that the inclusion of the pancake for both cases has produced relatively small effects in the late-time stress fields.

The residual hoop stress about the cavity at a time of 250 ms is shown in Figure 12 for the near pancake computation. The predominant influence is seen to be confined to a region relatively close to the pancake itself and outside the region of high residual stress around the cavity. A much better feeling for the influence of the chimney on the stress field can be obtained from Figure 13, in which the contour plot of the close chimney hoop stress field (dashed lines) has been superimposed on the results obtained for the farther chimney location (solid contour lines). Although the stress field is modified slightly near the cavity in the two cases, the region in which the stress field is significantly affected is seen to lie well beyond the peak in the residual stress field. It is interesting to note that the closer chimney location appears to increase the peak hoop stress very slightly rather than to degrade it in this region as one might expect. Of course, in the vicinity of the chimney the residual hoop stress is reduced appreciably by the stress relief in the weak rubble material.

The tangential stresses for both cases are shown for the ray connecting the detonation point with the center of the pancake in Figure 14. The influence of even the close chimney is seen to be negligible at ranges less than 70 meters. Even out to the edge of the near chimney, the differences are not substantial, being a maximum of about 15 percent.

The residual stress fields for the far pancake problem are shown in Figure 15. In this important region, adjacent to the cavity, the shape of the stress fields do not show any unusual characteristics when compared with results from other studies.

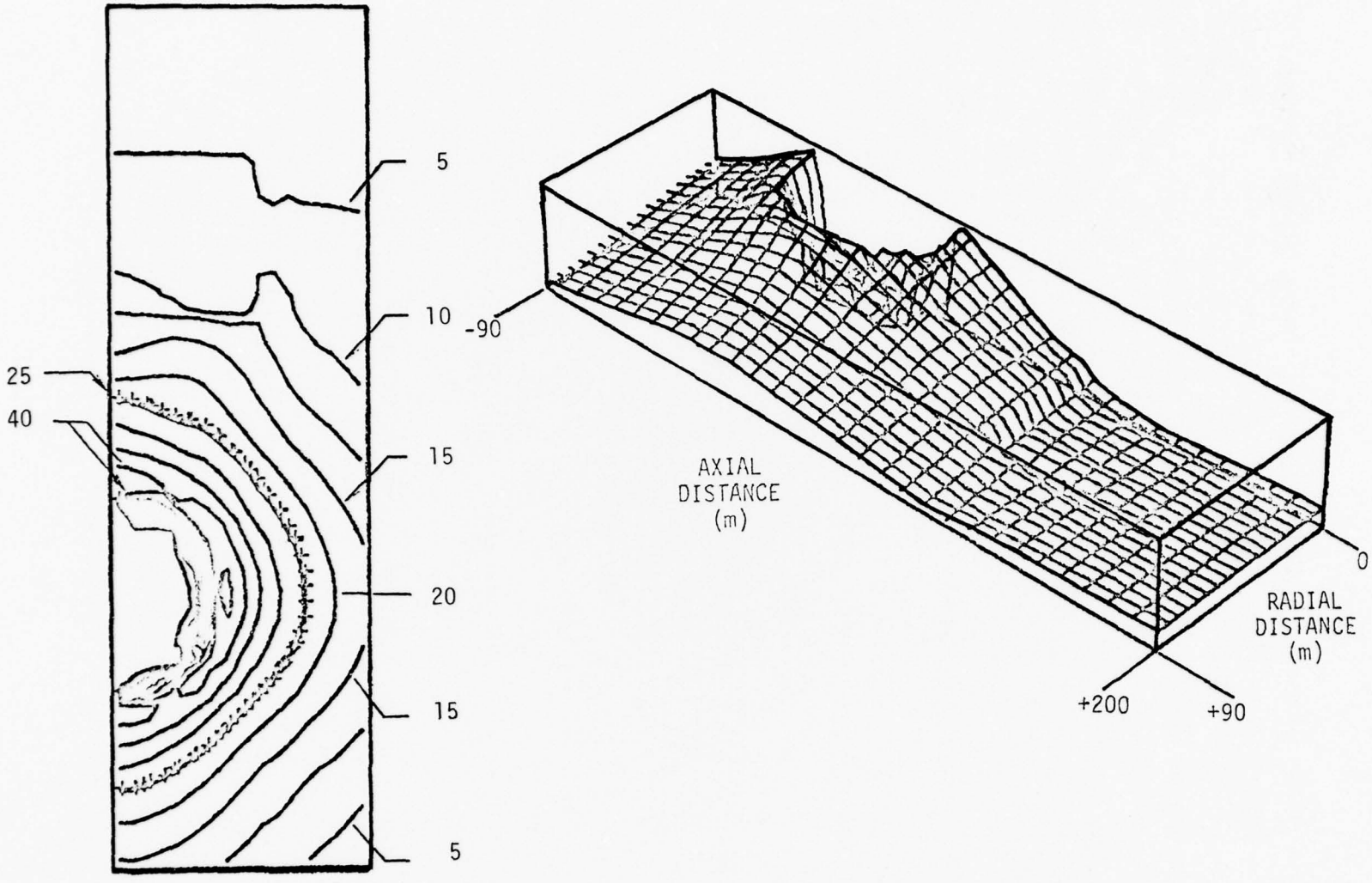

Figure 12. Contour and isometric plots of tangential stress at 250 ms for pancake centered at 122.5 m (402 ft). Contour interval is 5 MPa; peak stress is 46.2 MPa.

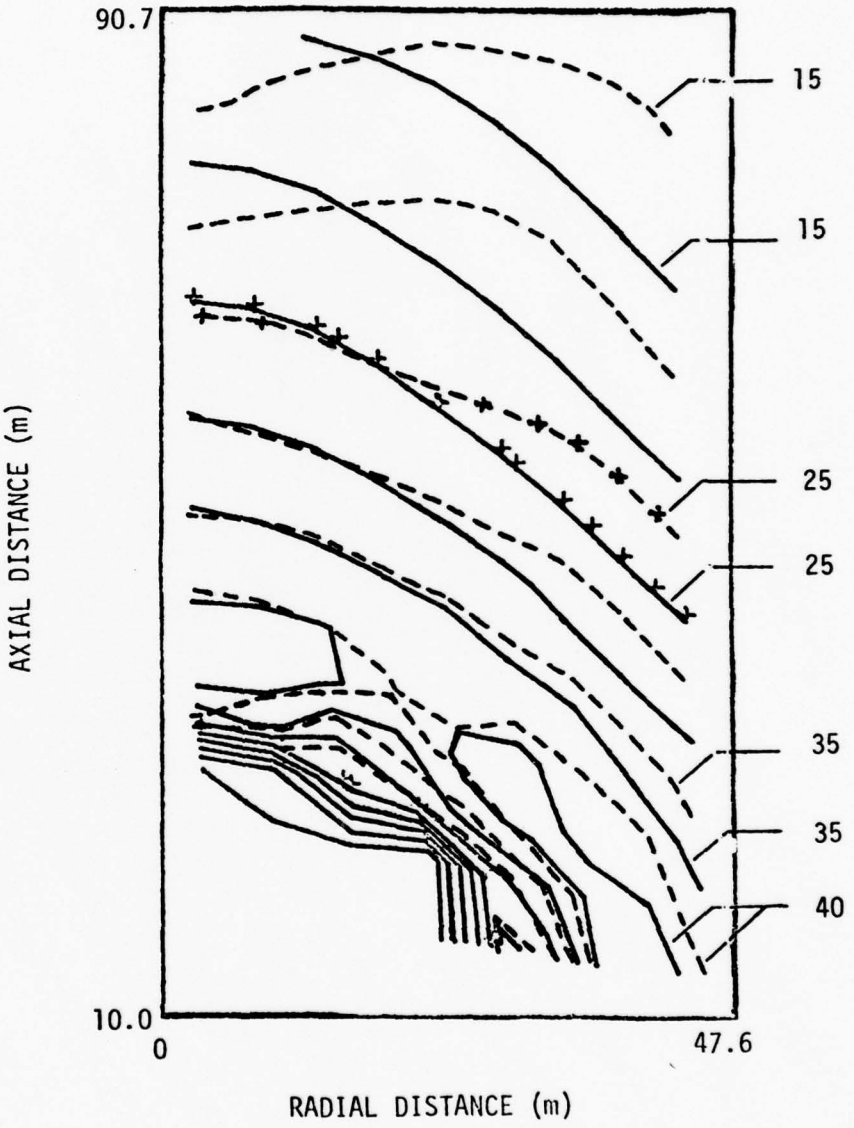

Figure 13. Comparison of tangential stress near the cavity for the two pancake problems at 250 ms. Contour interval is 5 MPa; solid contours are for far chimney, dashed contours denote results for close chimney location. Plus symbol marks every fifth contour.

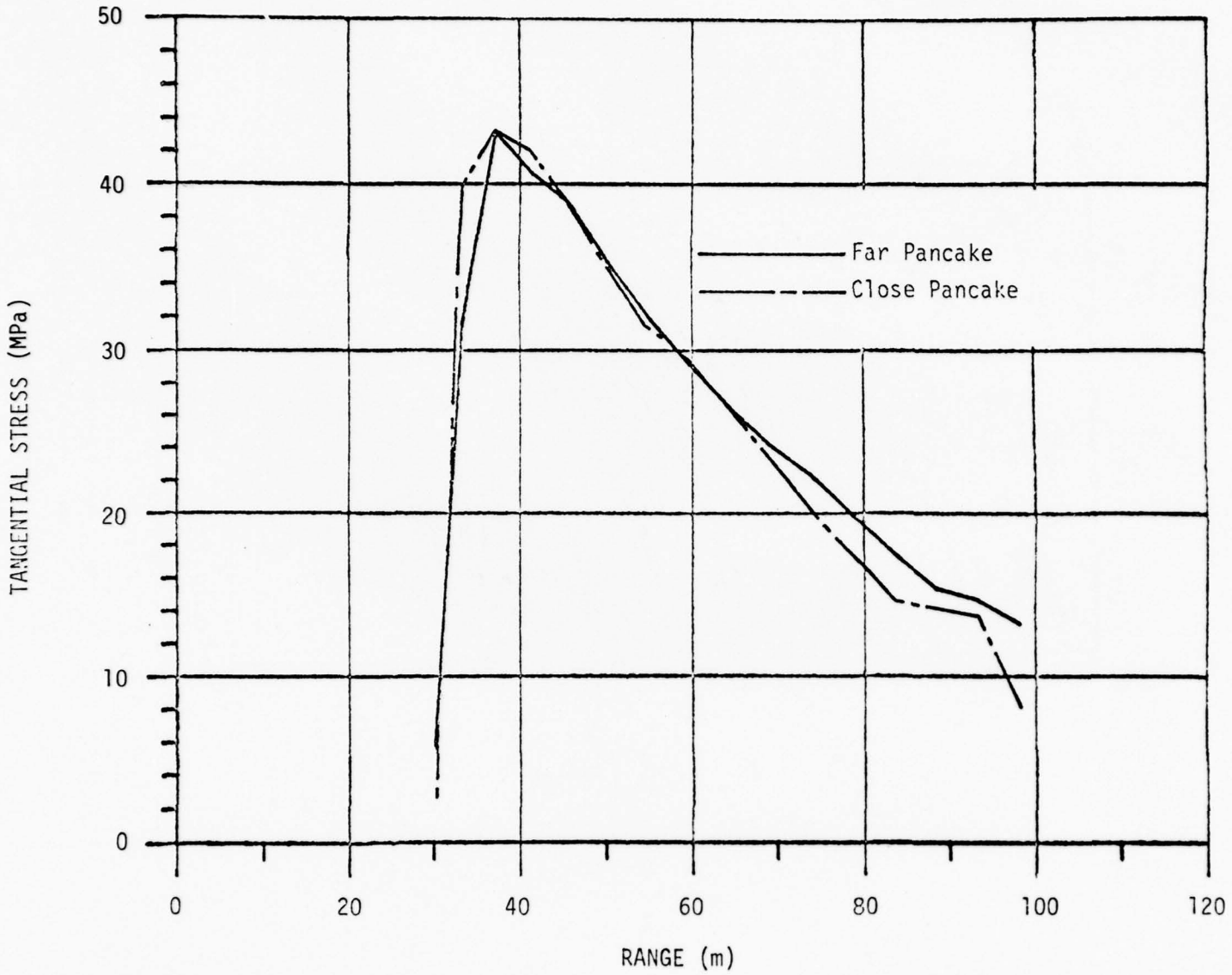

Figure 14. Comparison of tangential stresses calculated along the axis of symmetry for the two pancake locations studied at 250 ms.

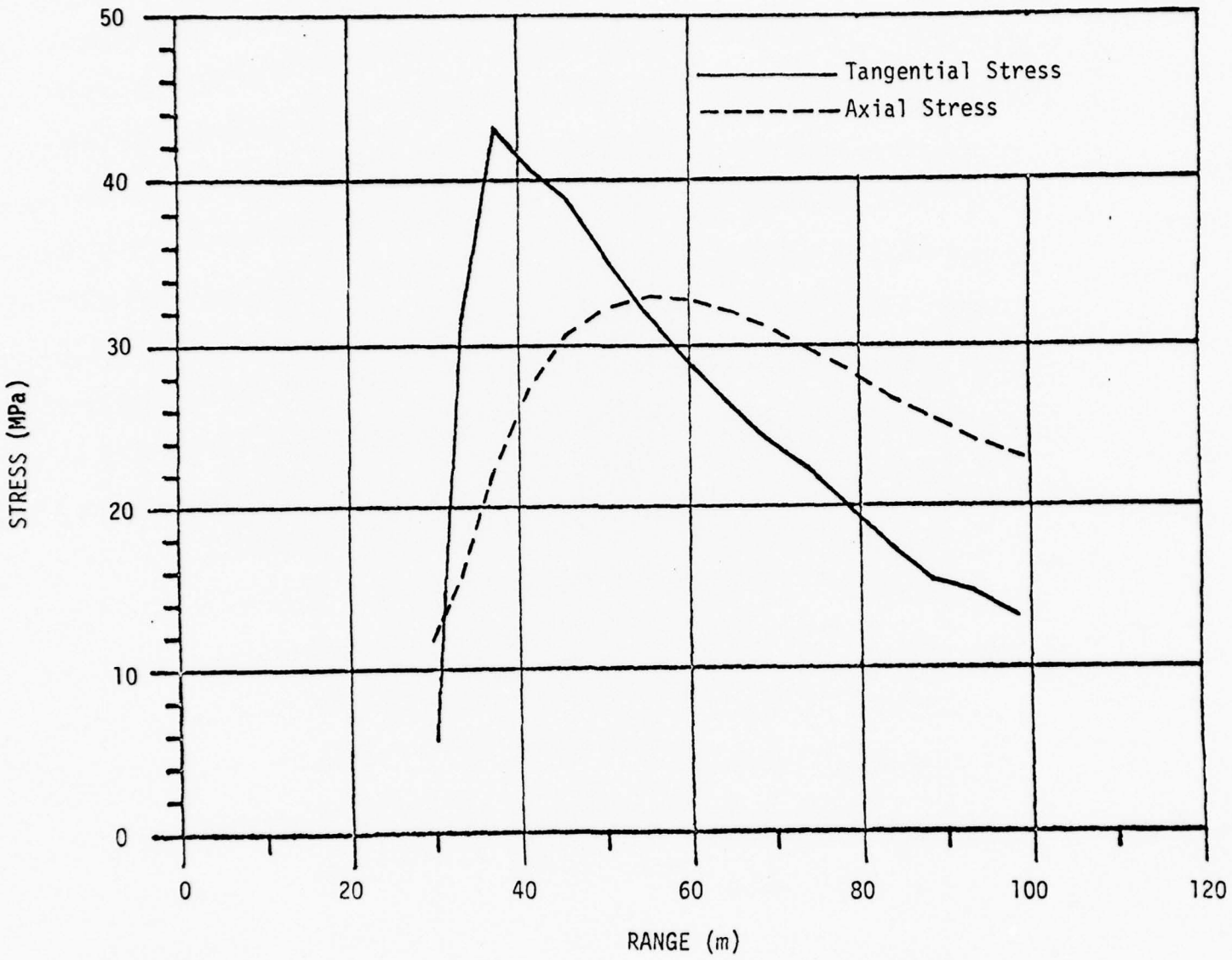

Figure 15. Tangential and axial stress at 250 ms calculated along the axis of symmetry for the pancake located 152.5 m (500 ft) from the WP.

3.3.2 Weak Chimney Material

The results from the strong chimney compuations discussed above indicated that the far chimney had very little influence on the stress field around the cavity at any time. The near chimney (centered at 122 meters) produced a rarefaction wave which was strong enough to result in a modest and temporary reduction of the stresses in the vicinity of the cavity at a time of about 80 ms. Neither chimney location produced more than a slight change in the residual stress field around the cavity.

There was concern that the material model for the chimney rubble used in these first results might have been too strong; thus, underestimating the possible effect on the shock wave interaction and residual stress field. In order to establish some bound on the effects of this uncertainty, the strength of the rubble was reduced to zero in the calculations here. This is clearly overly conservative, particularly at shot level in the chimney where drill-back indicates that the strength of the material within the chimney is comparable to that of the surrounding tuff.

The effect of the rarefaction from the chimney region on the axial stress profiles at times of 60, 80 and 100 ms is shown in Figures 16 through 18, respectively. The rarefaction has reached a range of approximately 45 meters at 60 ms (Figure 16) in the near chimney calculation. The dramatic reduction of axial stress adjacent to the weak pancake is already apparent at this time. An effective spall into the chimney reduces the axial stress immediately in front of the chimney to zero. This type of separation is also apparent in stemming computations at interfaces between a rock and weak stemming material.[6]

At 60 ms the wave is just reaching the close edge of the far pancake; hence, the axial stresses in the problem are not yet perturbed by its presence. The far chimney axial stress profile is identical to that of the free-field (taken as the ray away from the near chimney.)

The hoop stress profile at 60 ms (Figure 19) shows that the rarefaction leads to tension in this component from the pancake edge at 95 meters back to 65 meters from the detonation point. The radial stress component is also tensile in this region,

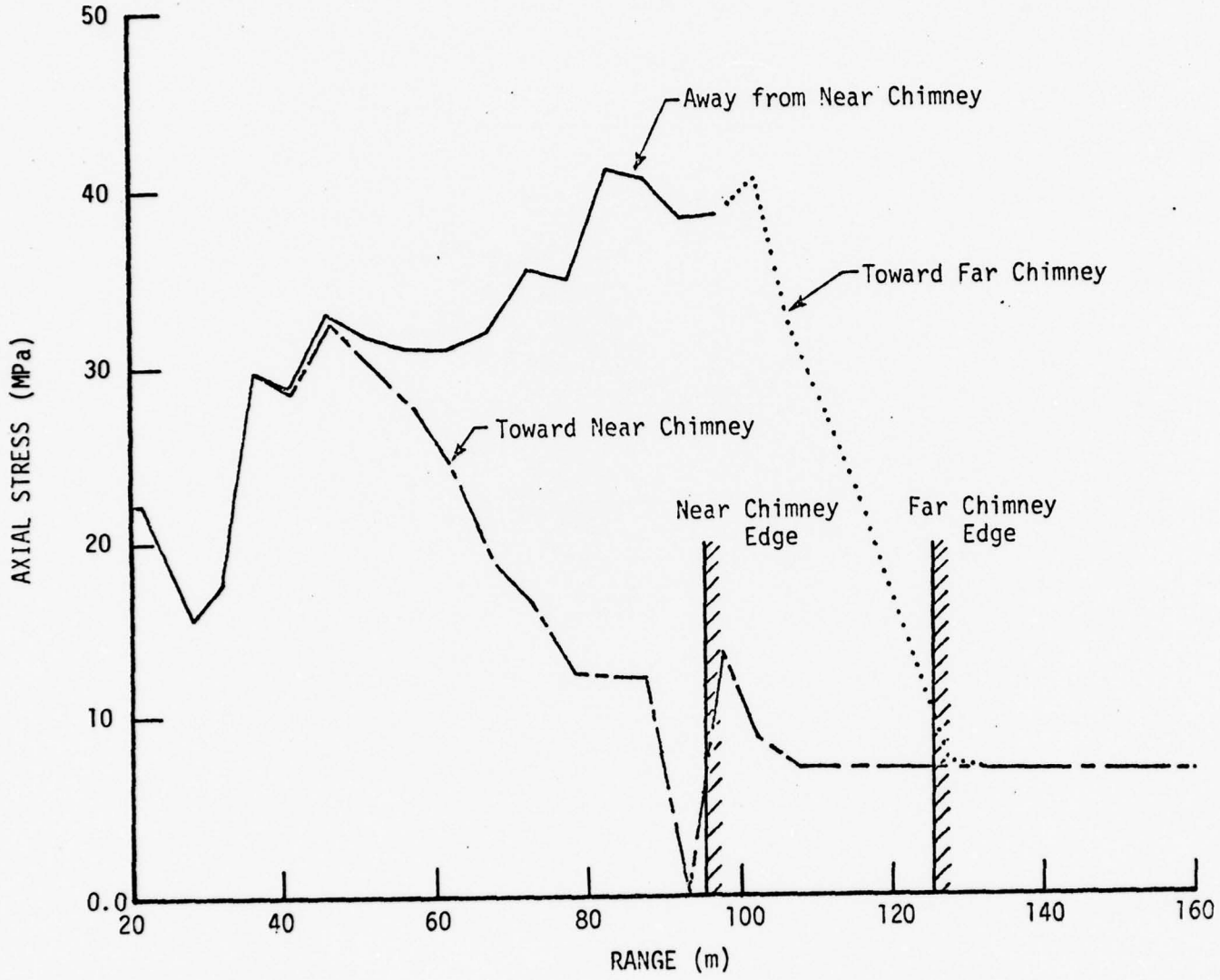

Figure 16. Comparison of axial stress profiles at 60.2 ms in weak pancake calculations. (Note suppressed zero on the abscissa.)

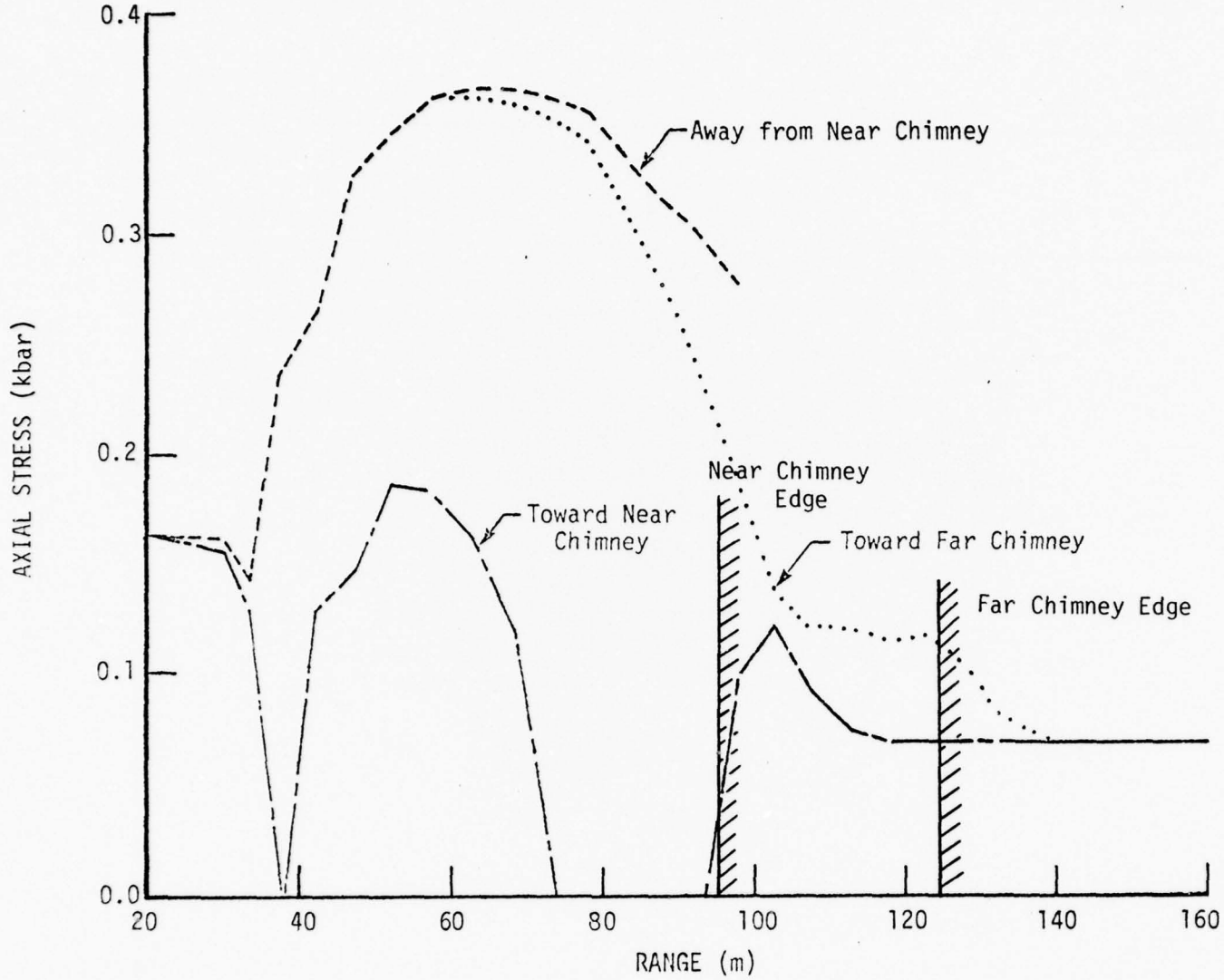

Figure 17. Comparison of axial stress profiles at 80.4 ms in weak pancake calculations. (Note suppressed zero on the abscissa.)

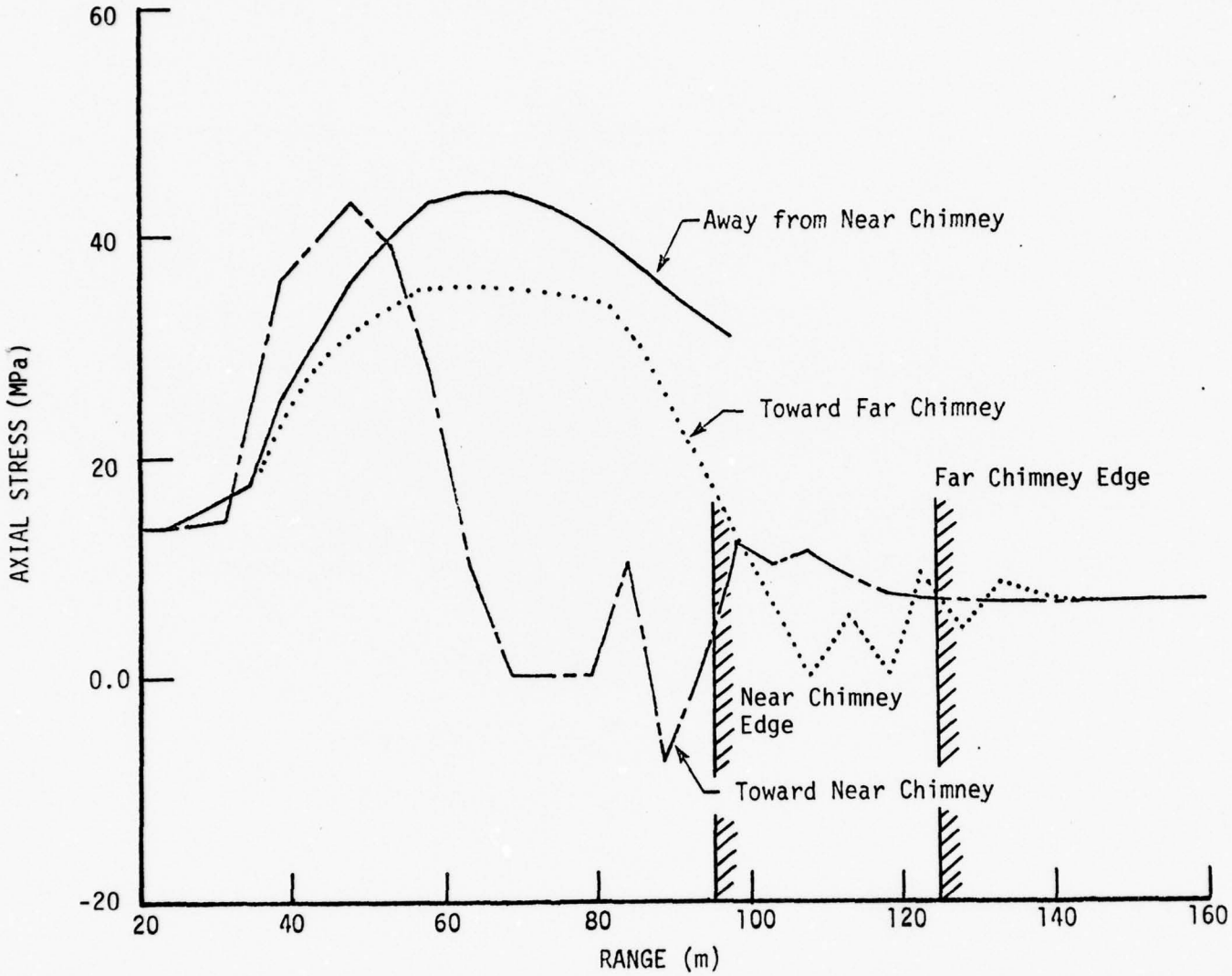

Figure 18. Comparison of axial stress profiles at 100.5 ms in the weak pancake calculations. (Note suppressed zero on the abscissa.)

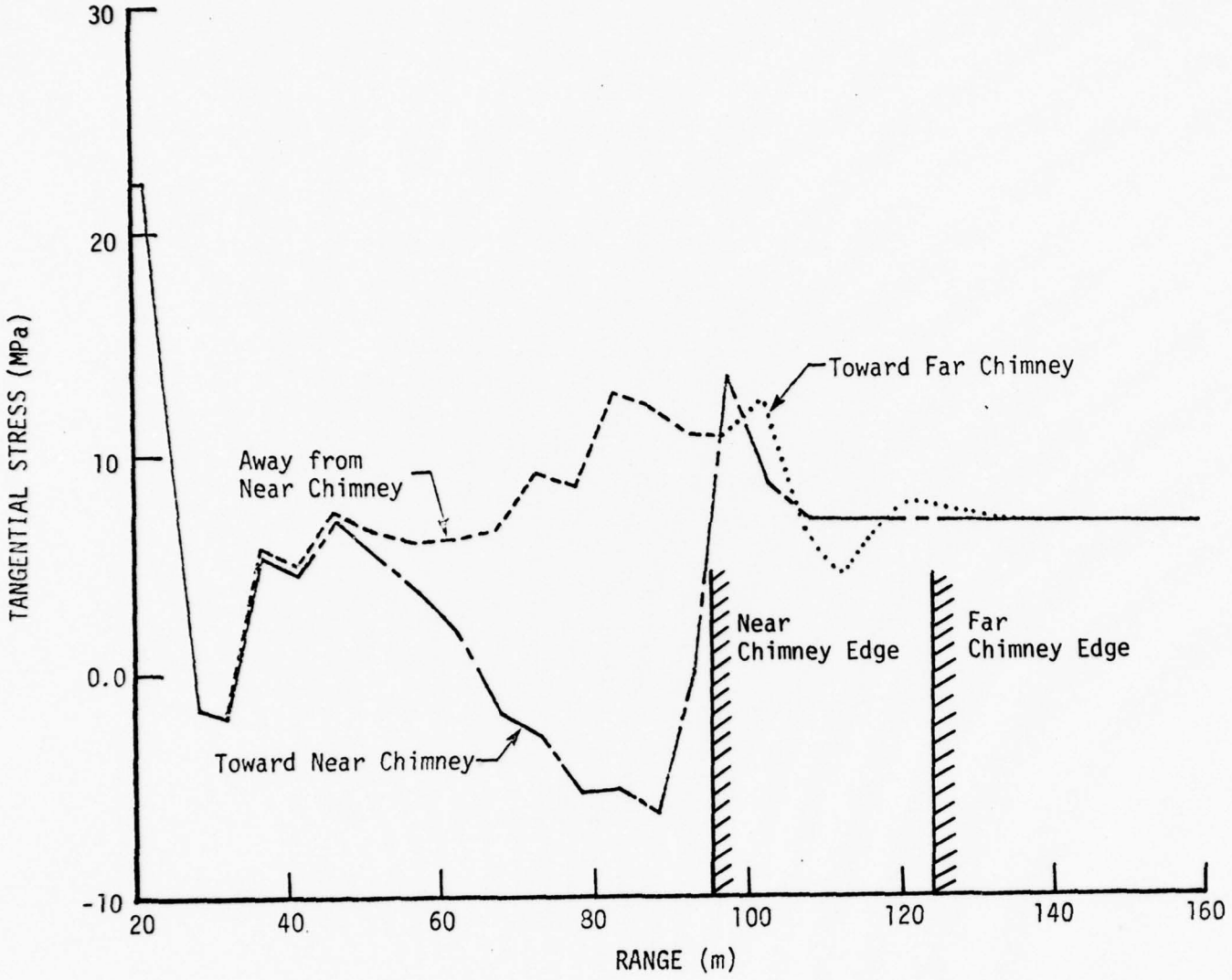

Figure 19. Comparison of tangential stress profiles at 60.2 ms in weak pancake calculations. (Note suppressed zero on the abscissa.)

but is not identical to the hoop stress due to the asymmetry produced by the disk. At times prior to the rarefaction, the hoop and radial stresses are essentially identical. The far pancake profile is unperturbed at this time.

By 80 ms a large region has been fractured between 75 meters, and the pancake edge and the peak axial stress is reduced by nearly a factor of two by the presence of the near chimney (Figure 17). Also, the combination of the rarefaction from the cavity and that from the pancake have caused the unloading of the tuff adjacent to the cavity. The far chimney has caused a rarefaction which has propagated back to 60 meters. This wave has not yet influenced the peak axial stress near the cavity, but has created a 35 percent drop in stress at about 100 meters.

The region in the near pancake problem which was fractured at 80 ms has started to reload by 100 ms (Figure 18). The rock located between 69 and 79 meters is fractured (in the sense that this material is below normal density and mean stress is zero) while rock closer to the chimney edge is alternately in tension and compression. While it is believed that reloading is probable back to the overburden level it should be borne in mind that the numerical treatment of fracture may play a role in establishing the stress state, especially in the immediate vicinity of a fractured region.

The tangential stress profile for the near pancake at 100 ms shows the fractured region between 69 and 79 meters (Figure 20). The peak hoop stress is about the same as the free-field value as was the case for the axial stress, however the region over which high stress acts is about one half of that for the free-field case. The reloading of the hoop stress near the chimney to levels above overburden is credible as an arching mechanism around the weak chimney. Similar effects have been noted in computations of shock interactions with weak sand columns.[6]

For the far chimney at 100 ms no region of fracture exists. The axial stresses for the 10 meters in front of the pancake are seen to be approaching zero (Figure 18). The rarefaction has influenced the axial stress back to the cavity by this time reducing the peak stress by only about 20 percent. The hoop stresses of this time are tensile near the pancake and the peak is down by approximately 40 percent

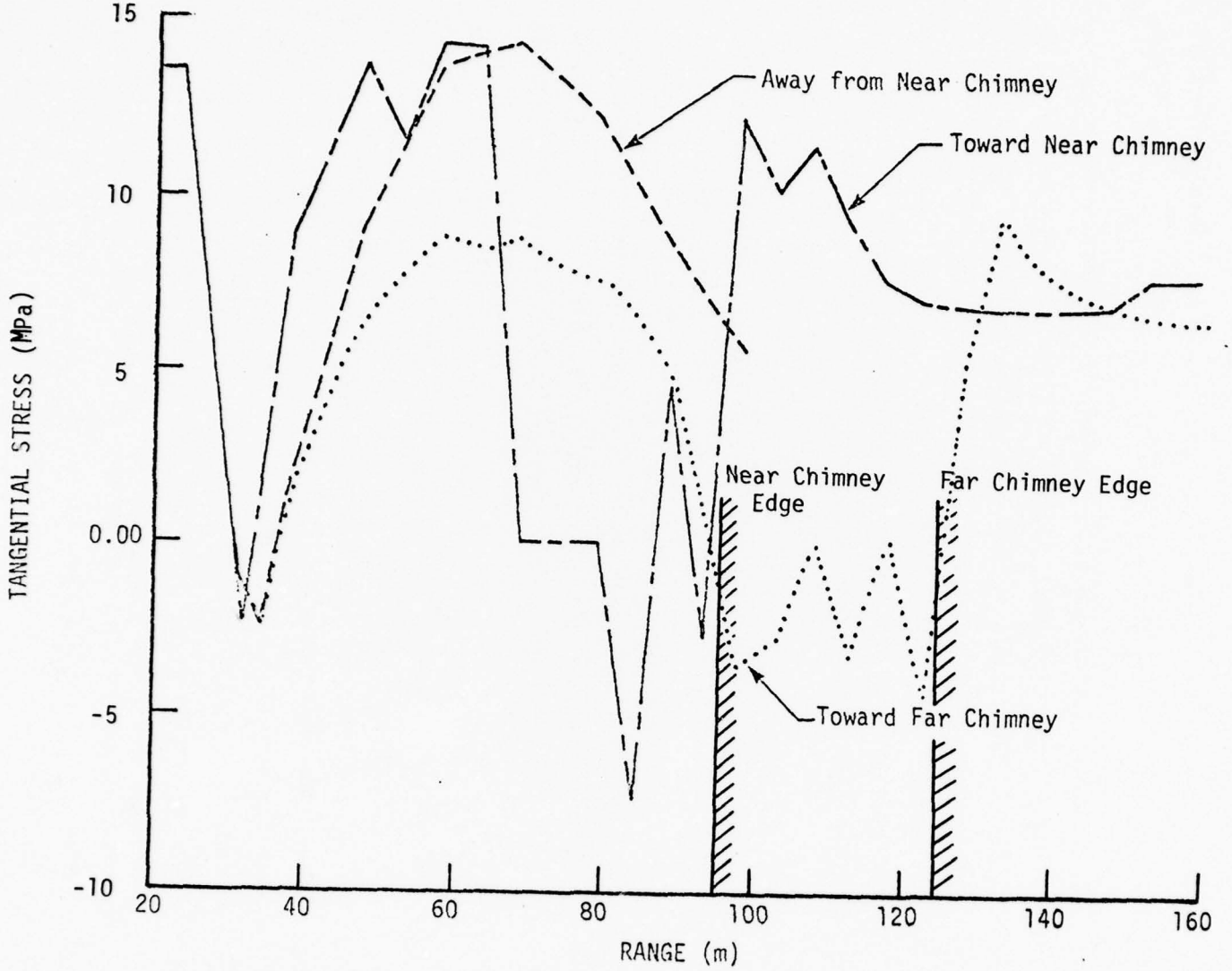

Figure 20. Comparison of tangential stress profiles at 100.5 ms in the weak pancake calculation. (Note suppressed zero in the abscissa.)

(Figure 20). Arching around the far pancake is also evident in the figure.

The influence of the chimney at a point initially located between the chimney and the WP at a range of 80 meters from the WP is illustrated in Figures 21 and 22. The more distant chimney produces a relatively small change in displacement (~20 percent) and peak hoop stress. The close chimney location increases the final displacement by nearly a factor of three and the hoop stress is reduced to zero. The large displacements are consistent with the unloading of this region in the near pancake problem. For the distant chimney location, neither the dynamic, nor residual stresses are appreciably influenced (Figure 22); however, the perturbation at this 80 meter range which results from the presence of the near chimney is evident. In this case, the material fractures shortly after the initial shock passage as the tuff at the chimney edge spalls into the weak chimney region.

Residual stresses are established after rebound when only small amplitude elastic oscillations continue out far from the source. The axial stress profiles (Figure 23) show the effects of the zero strength pancakes dramatically. The near pancake has reduced the peak axial residual stress by 30 percent and narrowed the region near the cavity over which this stress is compressive by more than a factor of three. The far chimney produces only a 15 percent reduction of peak stress with compressive stresses enduring out to 87 meters.

Both chimneys leave fractured regions on axis. These regions are 12 meters long for the near and 15 meters for the far pancake. The near pancake fracture zone starts as close as 69 meters from the detonation point while that for the far pancake starts at 87 meters. The hoop stresses (Figure 24) do not show a reduction of the peaks as dramatically as that for the axial stress components, but the steep gradients to the fractured regions are similar. One does not expect as large a reduction in the hoop stresses as in the axial stresses near the cavity since the rarefaction from the finite diameter pancakes suffers geometric attenuation as it propagates back toward the cavity.

3.3.3 Strong Versus Weak Cases

As indicated in Section 3.1.2, the two sets of problems were initialized

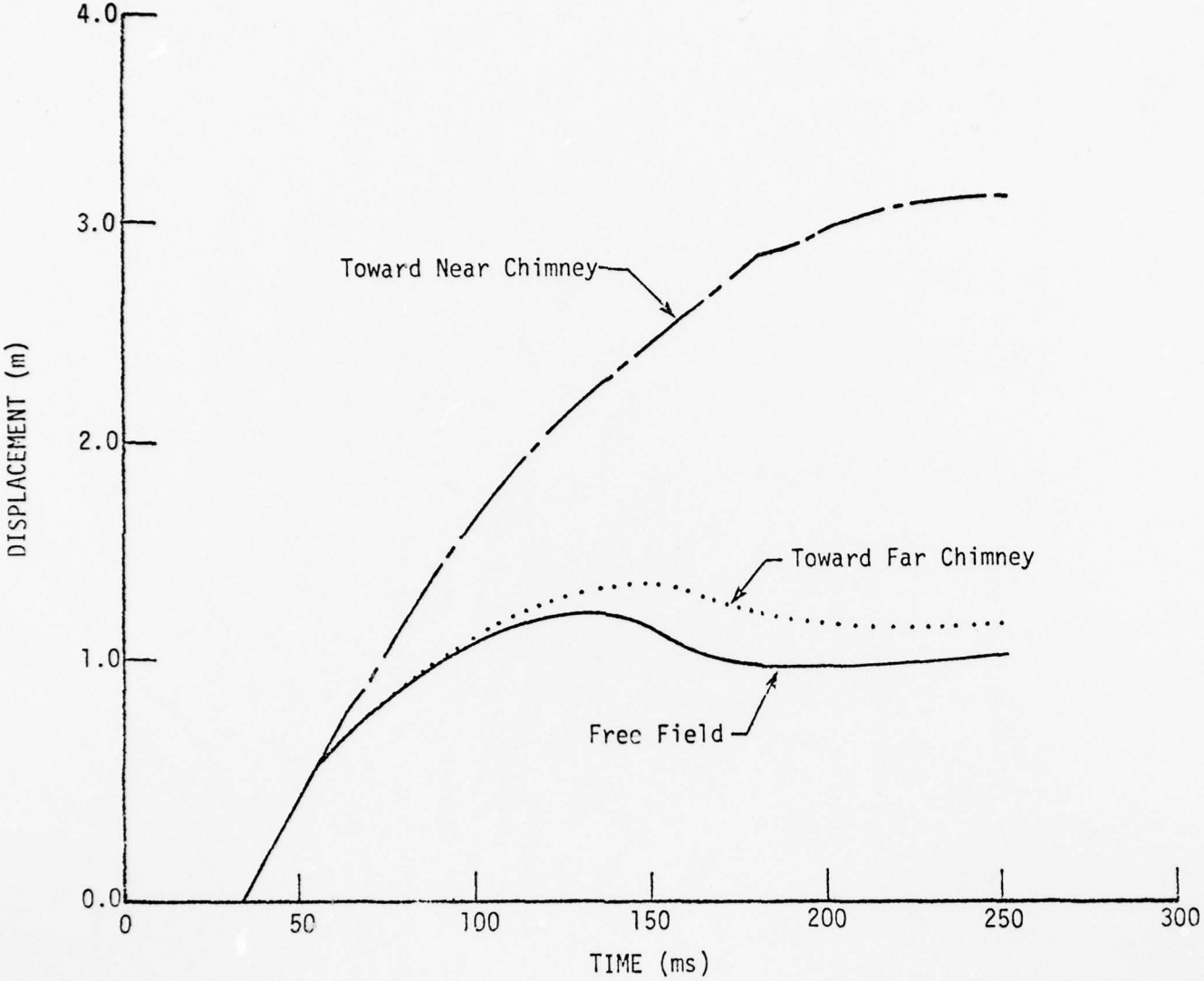

Figure 21. Comparison of displacement of points initially 80 meters from WP.

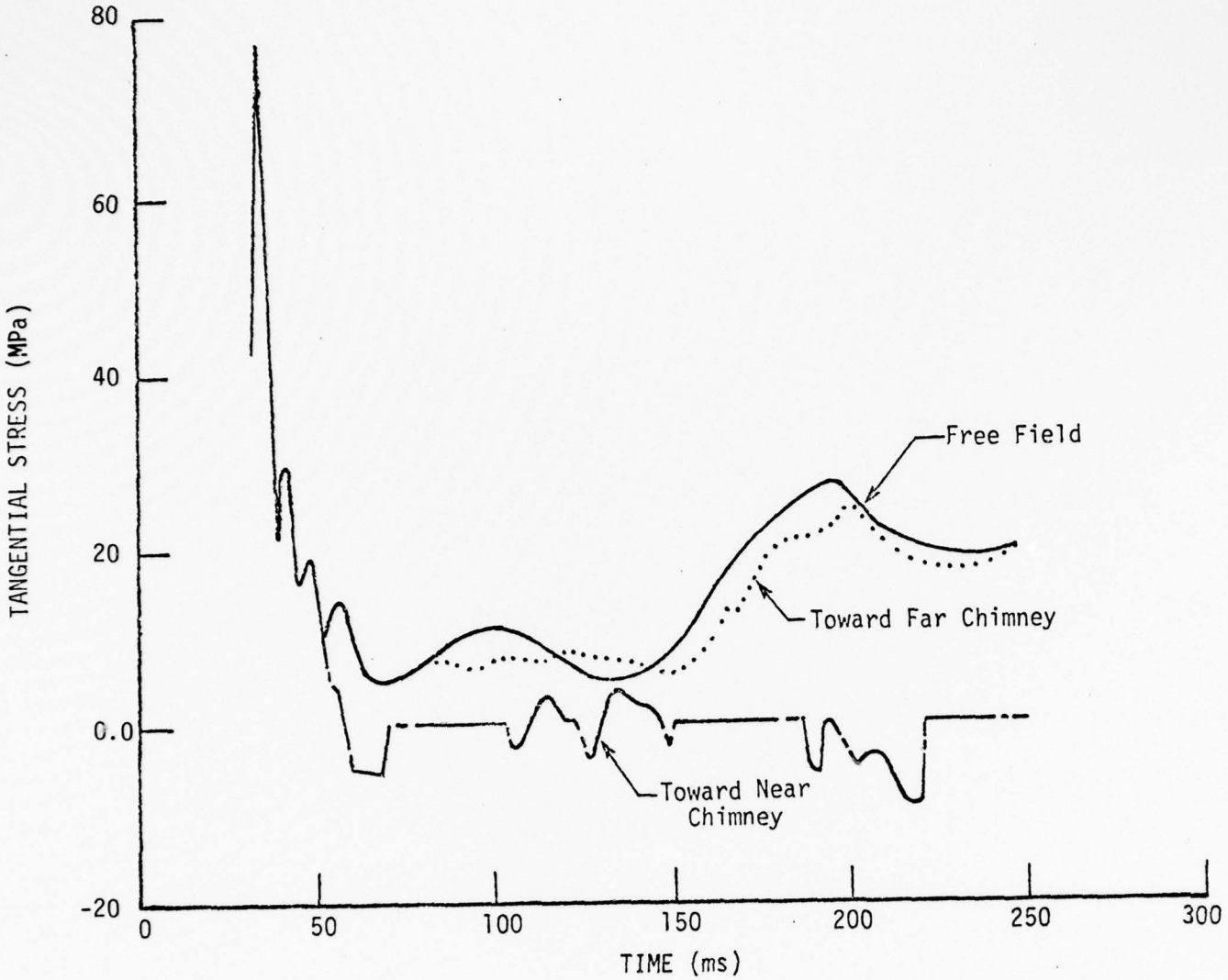

Figure 22. Tangential (hoop) stress at points initially 80 meters from the WP.

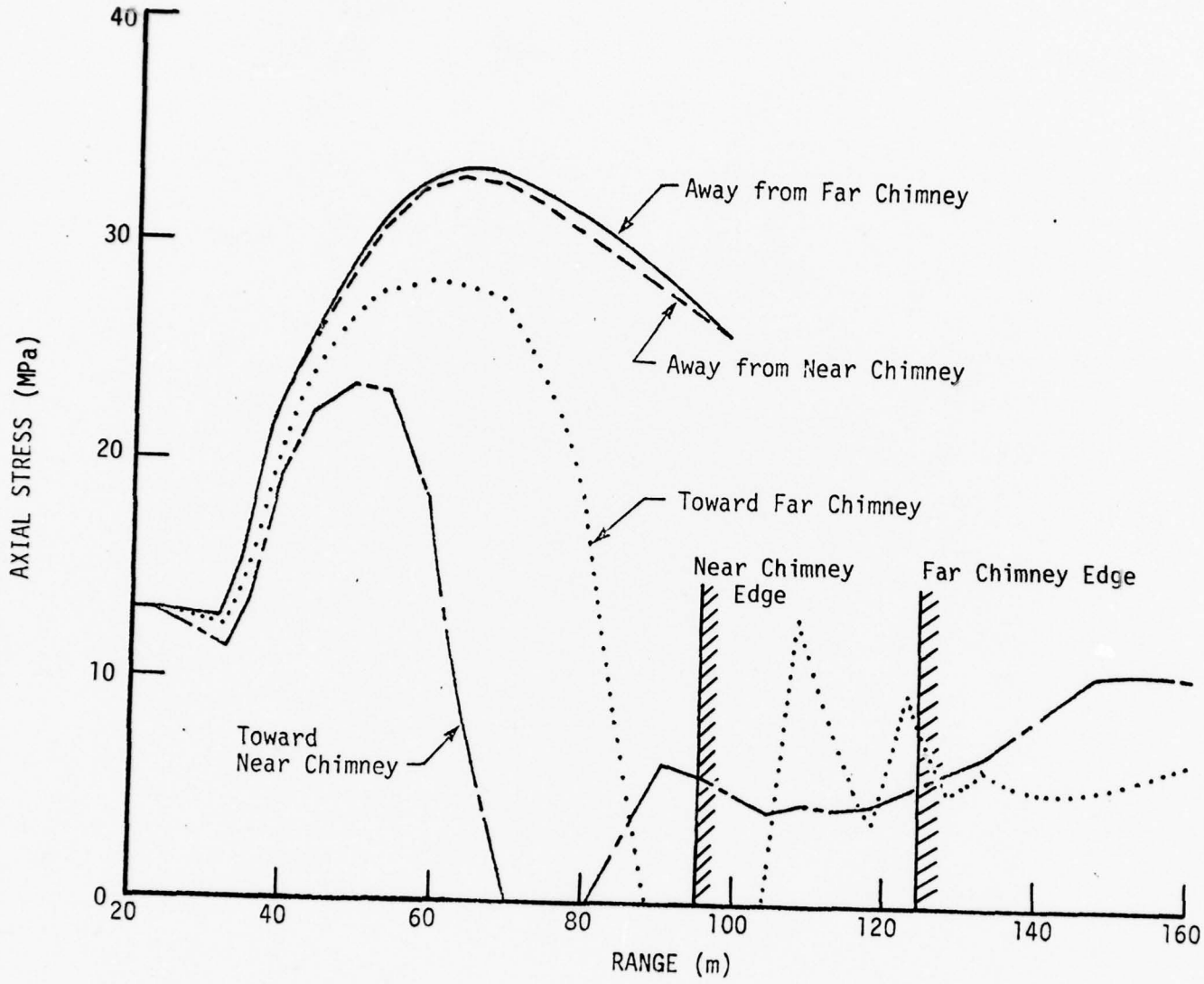

Figure 23. Comparison of axial stress profiles at 241 ms in weak pancake calculations. (Note suppressed zero in the abscissa.)

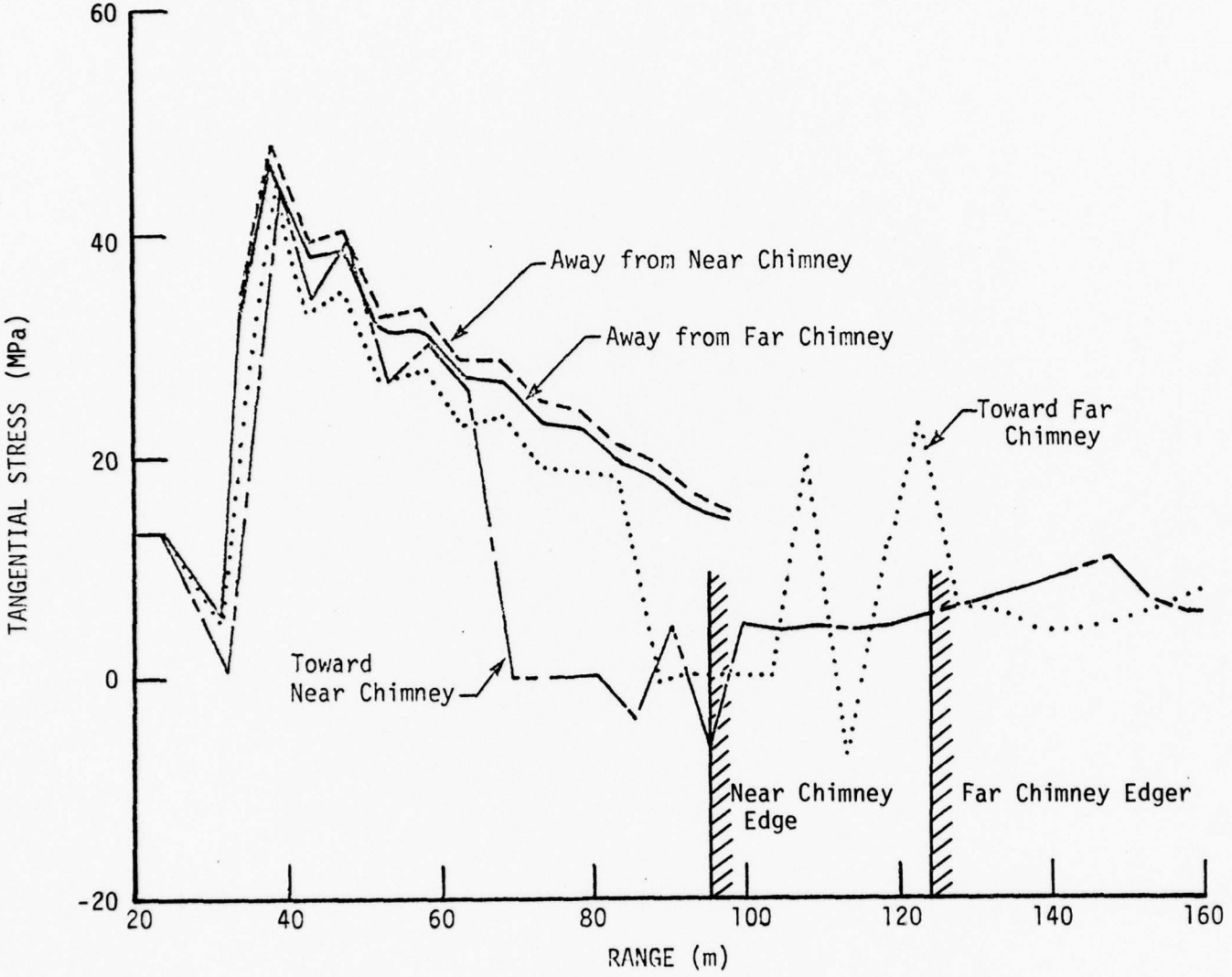

Figure 24. Comparison of tangential stress profiles at 241 ms in the weak chimney calculations. (Note suppressed zero in the abscissa.)

differently. The differences were in the utilization of a deformed grid (Figure 3) in the vicinity of the cavity and an overlay technique which produced self-consistent field variables for the weak cases. The results indicate that at times before about 80 ms it is not possible to directly compare the two sets of problems. For example, the axial stress profiles at 60 ms for the differing material cases (Figures 8 and 16) show a region from 45 to 65 meters for which the axial stress in the strong chimney material cases is higher than that for the weak cases. Considering just the far pancake problems which have not been influenced by the rarefaction from the pancake at this early time, it is clear that this difference must be due to the initialization of the problems.

While it's difficult to sort out the precise cause for the difference, the likely source of this effect is due to the difference between the staircase cavity boundary utilized in the strong cases from the more spherical cavity boundary afforded by the utilization of the deformed grid shown in Figure 3. Because of the flattened region of cavity along the axis of the problem where most of our comparisons have been made, a plane wave is driven into the 2D grid when in fact it should be a spherical wave. The difference in geometric attenuation then, seems to be responsible for this effect. Comparison of the axial stress profiles at 80 ms (Figures 9 and 17) shows that the difference between the peaks located at about 50 meters from the detonation point is only about 10 percent at this time. A comparison with one-dimensional computations in similar materials which have been run out to later times shows that the stress profile for the weak pancake material problems is the more correct one at 60 ms.

The most dramatic difference between the two sets of problems is clearly the generation of significantly reduced stresses and regions of fracture by the weak pancake material.

The residual stress fields which were established for the two cases are remarkably similar considering the fact that the weak pancake material problems are considered to be extreme bound. The residual hoop stresses for all four computations are very similar out to the region where the weak pancake material cases drop off into the zones of fracture (Figure 24). A similar statement can be

made for the axial residual stress which, of course, unloads to a greater extent due to the geometry of the problem.

The bounding computations including the zero strength material in the pancakes were performed because no information was available regarding the properties of chimney material. Data obtained more recently[14] suggest that the reduction in the strength of chimney material is only about 25 percent at confining pressures above 1 kbar along with a reduction of the cohesion to zero. This reduction, which under confinement is within the variation of the strength of the rock from place to place in situ, is more compatible with the strong pancake material problems than the zero strength problems.

Additional effects which lead one to believe that all of these computations are conservative are the placement of the pancake with respect to the axis and the distribution of the cavity void volume uniformly throughout the pancake. The former effect is conservative because in an actual configuration, the rarefaction would not be focused back along the axis since the chimney volume is distributed upwards and at increasing ranges from the detonation point. This means that considerably more geometric attenuation can be expected regarding the propagation of the rarefaction back towards the vicinity of the cavity. The latter effect has the result of increasing the strength of the rarefaction close to the cavity. This is unrealistic since the region of the chimney closest to the cavity is known to be recompacted to nearly normal densities. A third difference between the real world and the computations reported here is that the pancake configuration includes a plane surface from which a nearly plane wave rarefaction results. In the real world, the chimney looks more like a cylinder whose axis is perpendicular to the axis of symmetry in the computations; a configuration which would also produce significant geometric attenuation of the rarefaction as it moved back towards the cavity region.

4. IN-CHIMNEY DETONATION

4.1 CONFIGURATIONS OF IN-CHIMNEY COMPUTATIONS

4.1.1 Geometry

Two two-dimensional computations were performed for the in-chimney detonations study. The biggest differences between these two calculations was in the presumed shape of the chimney region and the material properties as discussed below in Section 4.2. One computation considered a chimney which was cylindrical having hemispherical top and bottom. The second calculation included a conoidal-shaped chimney as shown in Figure 25. The natural symmetry axis for these problems lies in the vertical direction. Other than the inclusion of a uniform and hydrostatic overburden pressure, the effects of gravity were not modeled in these computations. Also, for purposes of these exploratory computations, the incorporation of layering of the material properties as a function of elevation was not included. The computational grid included a total of 7200 cells for each problem and covered distances of 1060 meters and 530 meters in axial and radial extent, respectively. One-dimensional calculations were used to initialize both of the two-dimensional problems (see Subsection 4.1.2 below). For comparative purposes a one-dimensional calculation was run to late-times.

The shape of the cylindrical chimney shown in Figure 25 was originally thought to be characteristic of many of the chimneys explored in tuff. The diameter was chosen based on a survey of measured chimney dimensions.[15] These data suggest that the chimney radius at the working point level averages 5 to 15 percent larger than the initial cavity radius. Likewise, the height of the chimney was specified as 5.13 times the cavity radius based on Reference 15. The volume utilized for the cylindrical chimney is consistent with that used in the pancake studies discussed in Section 3.

The conoidal shape shown in Figure 25 was developed based on new data coming from exploration in progress at about the time these calculations were performed.[16] By way of comparison, the lower hemispheres for both computations are essentially the same as is the overall height from the very top of the chimney to the bottom of the cavity. The major difference then is the additional volume

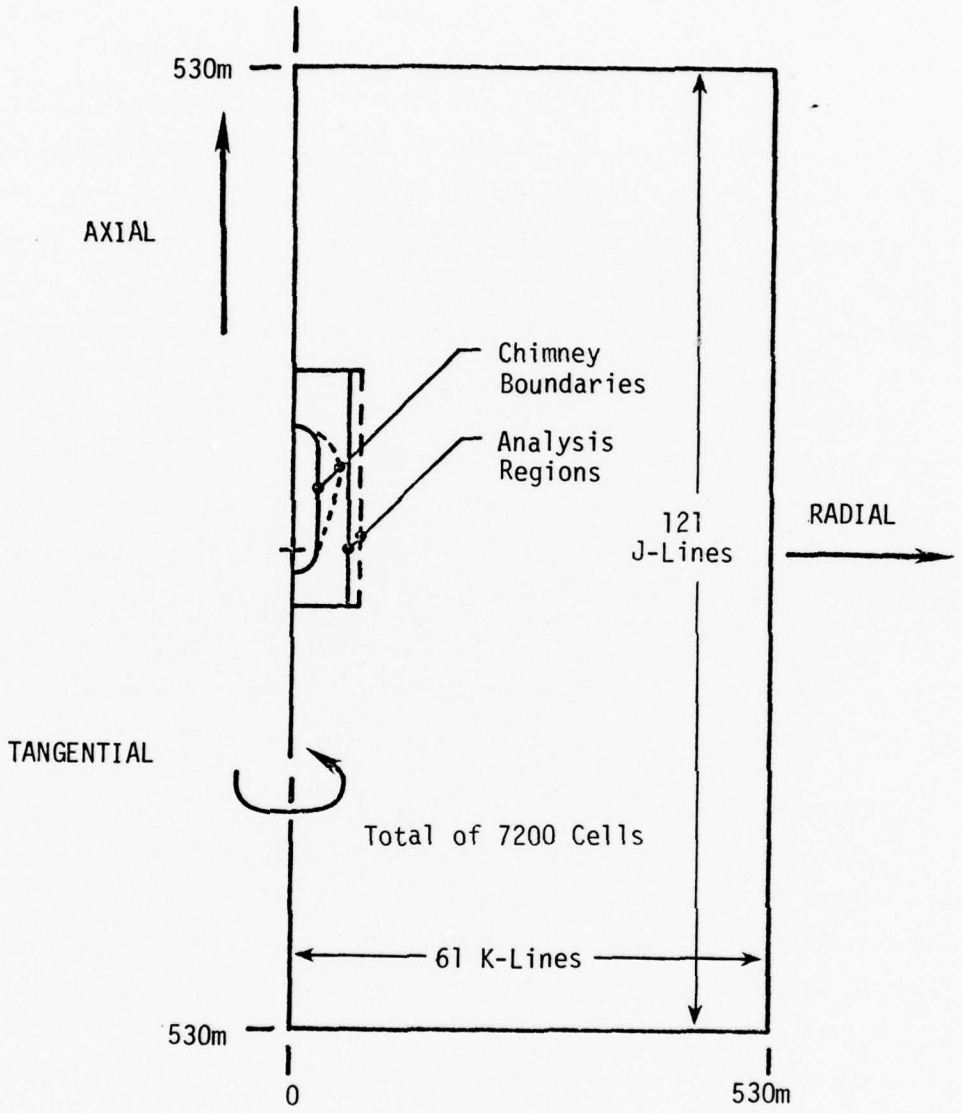

Figure 25. Coordinate system and general configuration for in-chimney problems.

due to the flared side walls of the chimney. This volume amounts to $4.87 \times 10^5 m^3$ of additional volume compared with a volume of $4.57 \times 10^5 m^3$ for the cylindrical chimney. This volume difference will have an effect on the distribution of air voids, as discussed in Section 4.2.

Regions of the computational mesh are shown for each of the problems in Figure 26. Notice that the deformed grid technique discussed in Section 3 has been utilized for both problems in the vicinity of the cavity. No attempt has been made to deform the grid to match the shape of the chimney itself. Since the overlay occurs well inside this boundary, the impact of the staircase grid at the chimney boundary should have only minimal effect upon the results.

4.1.2 Initial Conditions

Initial conditions for the in-chimney study were obtained from two one-dimensional SIMONE computations. While the initial conditions for pancake problems (Subsection 3.1.2) were all taken from one SIMONE calculation, this was not possible for the in-chimney studies due to the material differences in the chimney region. As a result, the *initialization process was* performed when the shock in each of the one-dimensional calculations reached a range of 29.3 meters. This corresponded to a time of 12.84 ms for the cylindrical chimney, but only 7.69 ms for the conoidal chimney due to the higher propagation velocity in that material.

The velocity profiles overlaid to the two problems are shown in Figure 27. The steep wave front which is calculated in the fine zone one-dimensional calculation must of necessity be smeared out in the two-dimensional calculations due to the larger zone size employed. The overlaid stresses for the cylindrical chimney problem are shown in Figure 28. The peaks of the stress wave which occur at about 26 meters have been clipped by the overlay routine in order to make the intra-cell thermodynamic conditions consistent. A similar situation exists for the stresses overlaid into the conoidal chimney problem (Figure 29).

4.2 MATERIAL PROPERTIES FOR THE IN-CHIMNEY DETONATION

4.2.1 Undisturbed Tuff

The constitutive model described in Section 3.2.1 was used to specify the

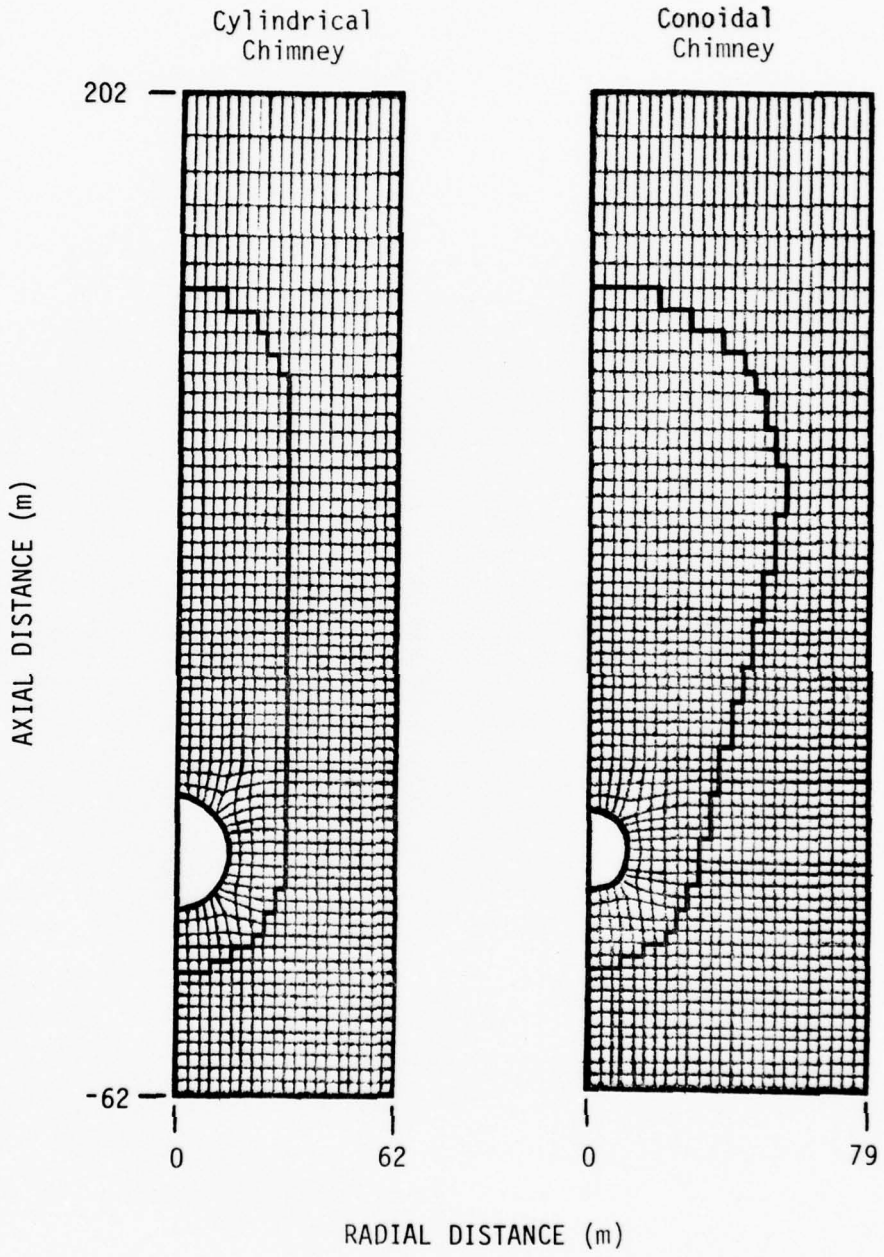

Figure 26. Interior sections of computational grids for the in-chimney problems.

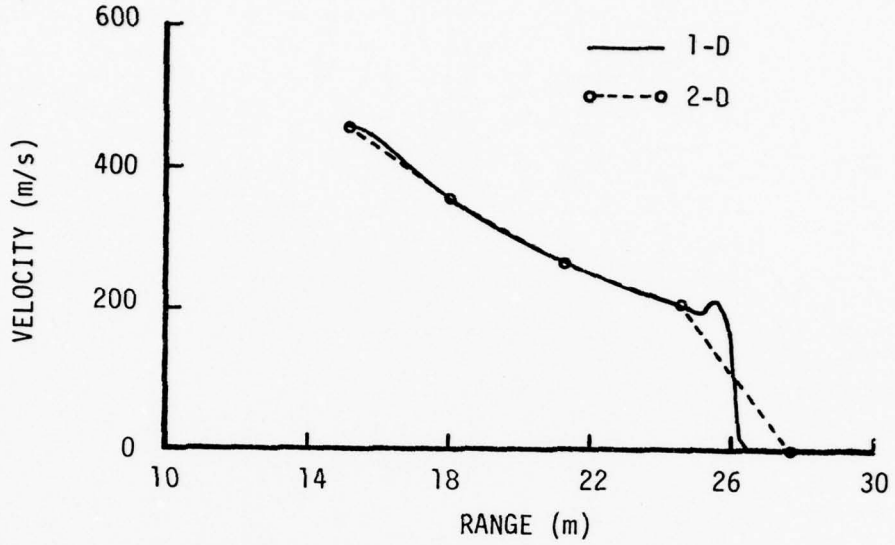

a) Cylindrical Chimney, t = 12.84 ms

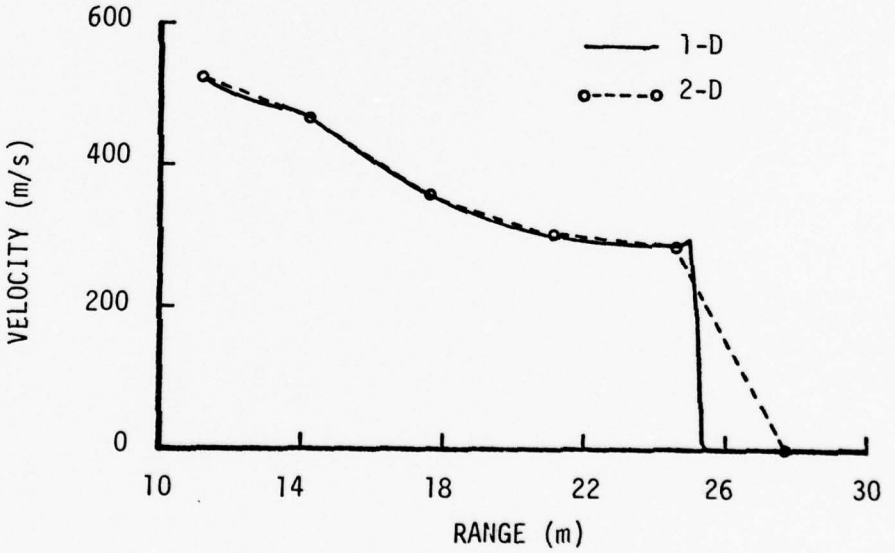

b) Conoidal Chimney, t = 7.69 ms

Figure 27. Velocity profiles overlaid into the two-dimensional grid for the in-chimney problems.

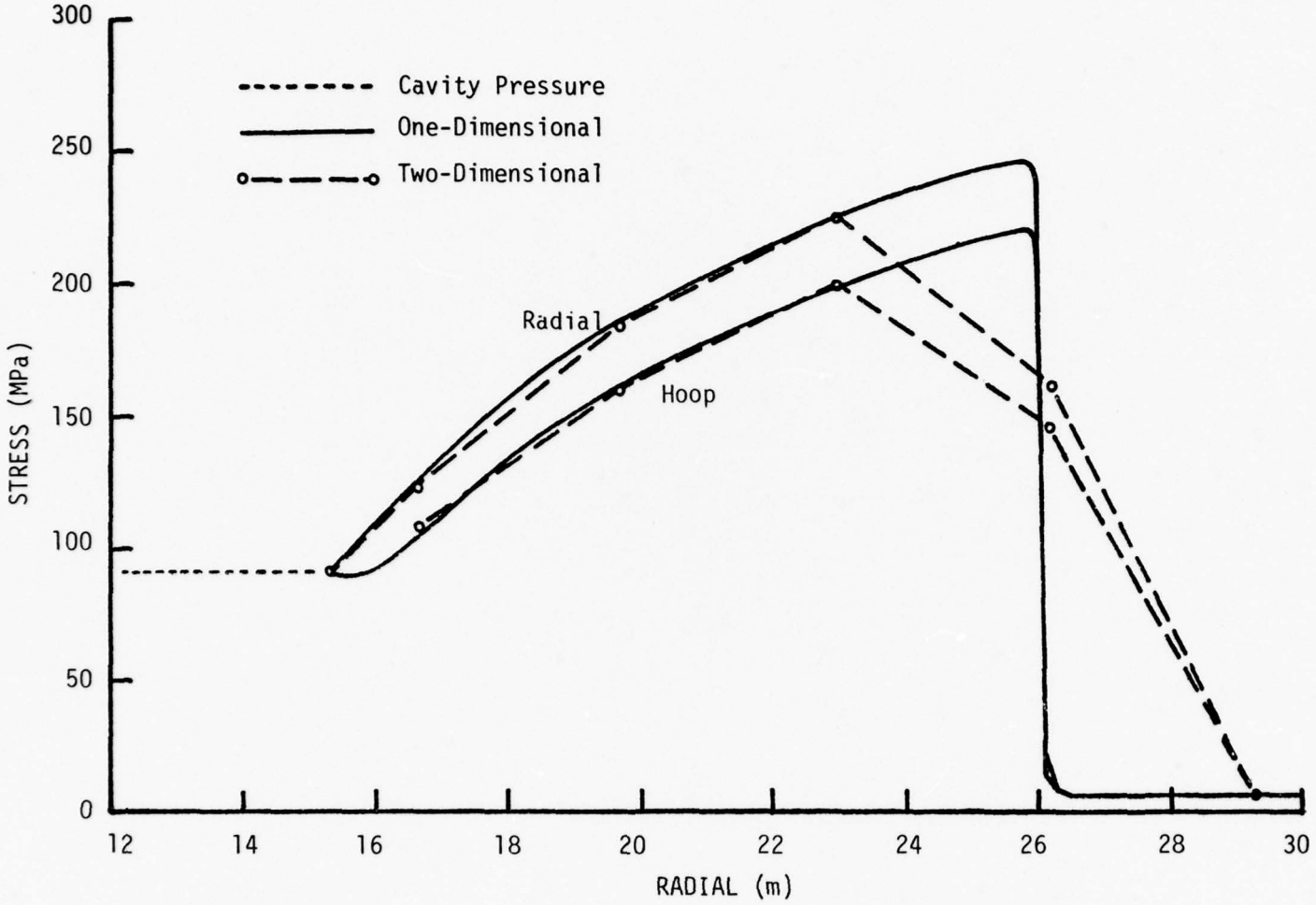

Figure 28. Stress profiles overlaid into the cylindrical chimney problem at 12.84 ms. Radial stress in the outward direction from the WP.

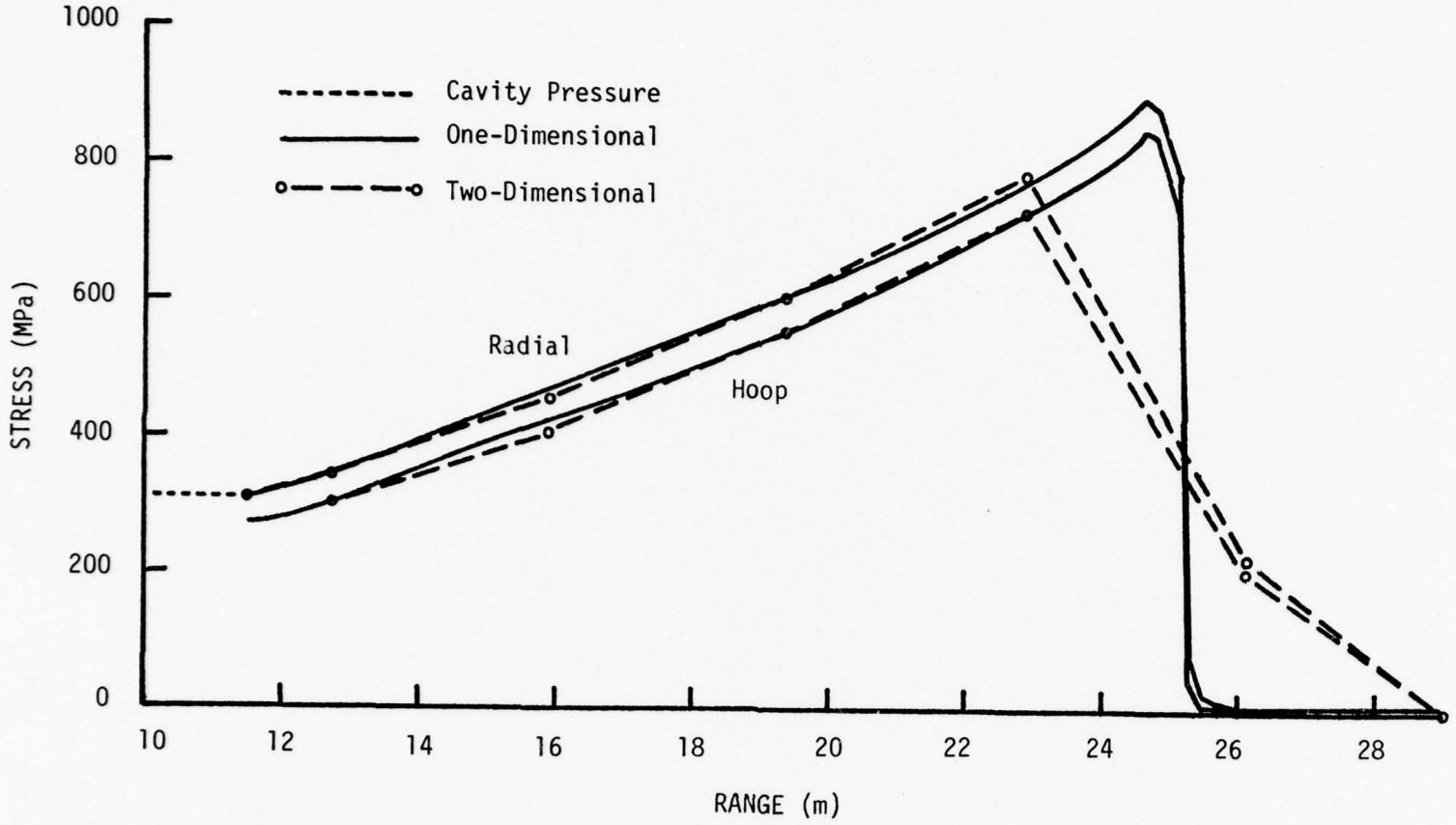

Figure 29. Stress profiles overlaid into the conoidal chimney problem 7.69 ms. Radial stress is in the outward direction from the WP.

response of the undisturbed tuff in the pancake problems. Thus differences between the ground motion calculated for the pancake and the in-chimney studies are not due to differences in the site material properties. As discussed in Section 3.2.1, the undisturbed tuff properties are reasonably representative of the average response measured for core samples of Area 12 tuff at tunnel level. Air void content and strength in the calculational model are somewhat higher than average values for sites other than Mighty Epic, while compressional and shear wave velocities are slightly lower. However, the assumed values fall well within the range of data measured at virtually all sites in competent tuff.

4.2.2 Chimney Materials

In the interim between initiating the pancake and the in-chimney calculations, additional material response data became available for chimney and "chimney-like" materials. Also, drill back and chimney gas flow data were acquired during the course of the in-chimney study which assisted in locating the boundary of the conoidal-shaped chimney. Thus in some cases, the material properties and chimney volumes assumed in the in chimney computations differ in several important respects from the values assumed in the pancake studies discussed in Section 3.

4.2.2.1 Cylindrical Chimney. As discussed in Section 4.1.1, chimneys in tuff originally were thought to be cylindrical, and this assumption was made in computing the chimney volume assumed in the pancake studies (Section 3.2.2). This geometry was also adopted for the first in-chimney calculation. Distributing the cavity volume throughout the available chimney material again led to an initial air void content of 25% in the chimney rubble. Thus, for this chimney configuration the crush curve utilized in the pancake simulations was adopted (Figure 6, Section 3.2.2). In accord with our previous assumption that the composition of the chimney rubble would be the same as the surrounding tuff, the water content of the rubble was taken to be 17%, and the tabular equation of state discussed in Section 3.2.1 was used to specify the p-v response of fully crushed rubble.

Particular concern was given to modeling the strength of the chimney material in view of the results of the pancake studies which amply demonstrated the sensitivity of the calculated stress fields to this property. Unfortunately, no data were available

to directly determine the strength of the chimney material for events conducted in Area 12 tuff. As a consequence, we were forced to model the rubble strength based on data obtained from rubble manufactured by crushing samples of Tonopah tuff, reconstituting them under a confining pressure and then measuring the strength of this "chimney simulant".[17] These data were then compared to the response of the virgin material to deduce the degradation in strength which would result from preexisting fractures. However, the failure surface determined in this fashion could not be used directly, since Tonopah tuff is a welded tuff which is far stronger than tunnel bed tuff in Area 12. Instead, we utilized an average failure surface for Area 12 tuff as reported in Reference 18 scaled down as a function of pressure by the same ratio as was determined in the Tonopah tuff tests. The resulting yield surface is compared in Figure 30 with those developed for the surrounding tuff and for the chimney rubble in the conoidal-shaped chimney computation.

A limited number of tests have since been conducted on virgin, reconstituted, and pulverized samples of tuff from drill hole UE12e.1.[14] These data qualitatively support the strength reduction estimate developed above from the Tonophah data, at least for the 7 MPa confining stress level at which data was obtained. More recent average tuff yield data in n-tunnel[19] generally have given somewhat greater values for the material strength than was the case for the average strength reported in Reference 18 (see Figure 30.). This suggests that the assumed rubble strength in the cylindrical chimney calculations may be too low, particularly for rubble at and below the tunnel horizon where considerable compaction by the weight of overlying material seems certain.

4.2.2.2 Conoidal Chimney. The rather dramatic earth motion and residual stress field obtained in the first in-chimney shot calculation suggested that establishing a satisfactory residual stress field about the detonation point might not be possible within the limits of plausible material response models for the chimney rubble. To address this question, at least in part, a final calculation was accomplished which incorporated new chimney shape and properties data which had just become available. Rubble properties were assumed to be the same as those measured for the layer of tuff which resides above the Might Epic test bed tuff, and the numerical response model was based on seismic data and laboratory measurement on core samples

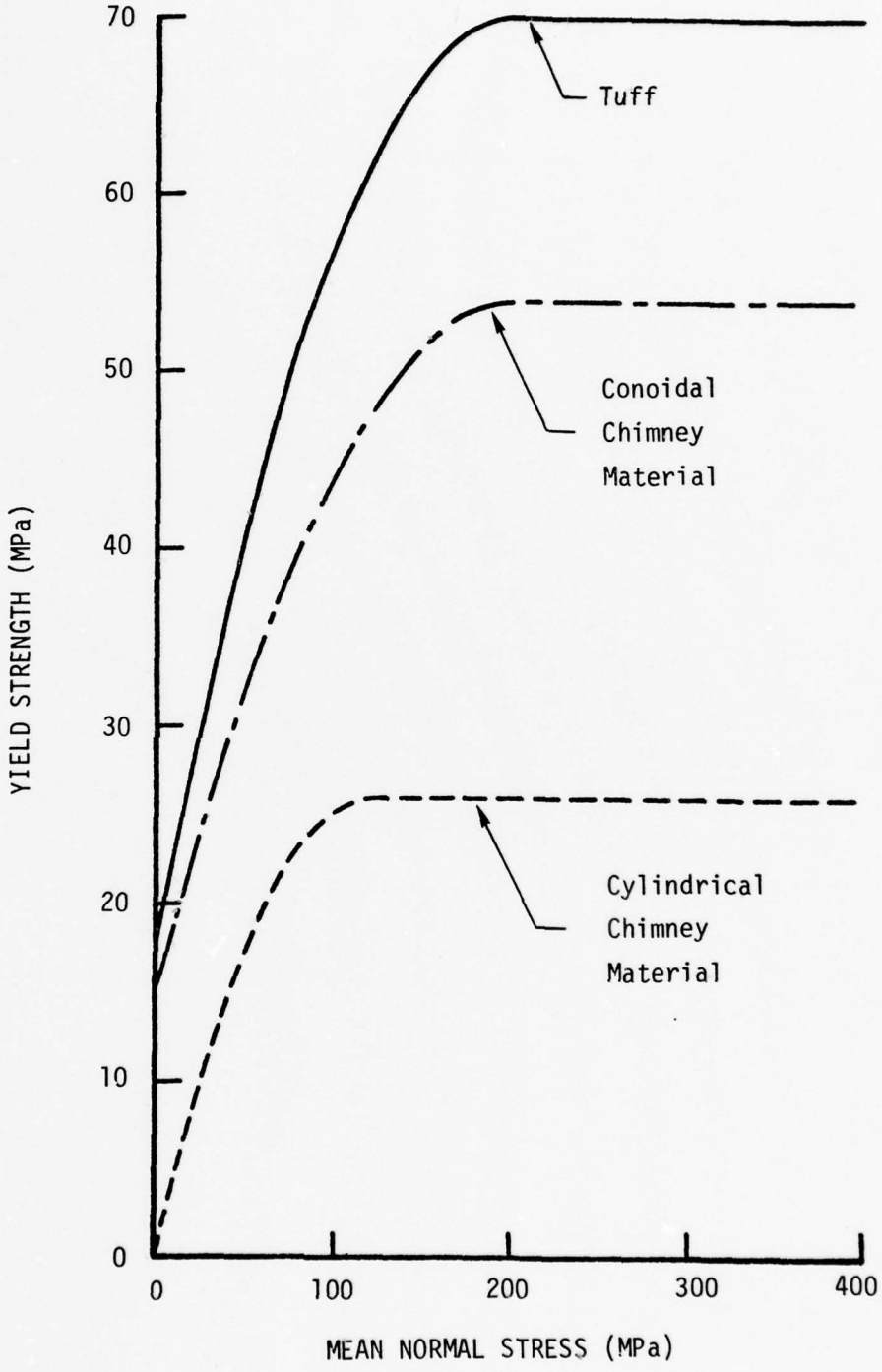

Figure 30. Yield surfaces for in-chimney computations.

obtained from this region.[12] The equation of state for this material has the form

$$p_s = \Gamma\rho e + A\mu_s + \beta\mu_s^2 \qquad (6)$$

where μ, A and B are constants listed in Table 3, and $\mu_s=\rho/\rho_s-1$, with $\rho_s=1.88$ Mg/m^3.

An average air void volume of 7.0% was used for the initial air void content and the resulting porous crush response is compared in Figure 31 to that of the surrounding tuff and the crush response assumed in the cylindrical chimney calculation. In assuming an initial void content of 7.0%, the bulking effects of the chimney collapse process have been neglected. Core data and reentry observations suggest that this approximation may be quite reasonable in the lower levels of the chimney. Indeed, more recent chimney gas flow tests suggest that the average air-filled porosity of the chimney as a whole lies in the range of 7.5 to 13 percent.[20] Thus any tendency for increased compaction to occur at lower levels in the chimney must result in air-filled void volumes at or near the assumed 7% value. These average chimney void volume measurements are also consistent with the drill back data[16] which suggest the conoidal shape assumed in the calculations, with its greatly increased volume in comparison to the cylindrical chimney geometry.

As indicated in Figure 30, the yield surface for the conoidal chimney material is approximately a factor of two stronger than that of the cylindrical chimney rubble at the same confining pressure. Again the form of the yield surface is that given by Equation (5) with constants listed in Table 3. Actually the difference in the effective strengths of the two chimney materials is much greater than is suggested by Figure 30, due to the coupling between the porous crushup and yield response models. The constitutive model used to represent the response of the cylindrical chimney material is extremely dissipative due to the high air void content and low pressure required for void collapse (Figure 31). As a consequence, in this material the stress induced by ground shock drops very rapidly with time. Thus, most of the motion of this chimney material occurs at very low pressure levels where the allowable stress difference is quite small (see Figure 30). In the much more competent

Table 3

Material Properties Used to Describe
Tuff and Chimney Rubble Response in In-Chimney Simulations

Material Property	Undisturbed Tuff	Cylindrical Chimney Rubble	Conoidal Chimney Rubble
Ambient Density, ρ_o (Mg/m^3)	1.920	1.470	1.750
Poisson's Ratio , ν	0.33	0.50	0.33
Bulk Modulus, K_o (GPa)	6.64	0.214	4.83
Rigidity Modulus, G_o (GPa)	2.55	0 to 1.04[(a)]	1.85
Compressional Wave Speed, Cp (m/s)	2286	382	2043
Shear Wave Speed, C_s (m/s)	1152	0	1028
Elastic Pressure, p_e (MPa)	10	10	10
Crush Pressure, p_c (MPa)	400	400	370
Air Void Content, V_a (%)	2.0	25.0	7.0
Unconfined Yield, Y_o (MPa)	18.0	0	15.0
Strength Increase, Y_m (MPa)	52.0	26.0	39.0
Maximum Pressure, p_m (MPa)	200	120	200
Γ	-	-	1.80
A (GPa)	-	-	5.0
B (GPa)	-	-	18.0

(a) Rigidity modulus varies quadratically with distention ratio, α; ranging from 0 to 1.04 GPa as pressure increases from 0 to 400 MPa, respectively.

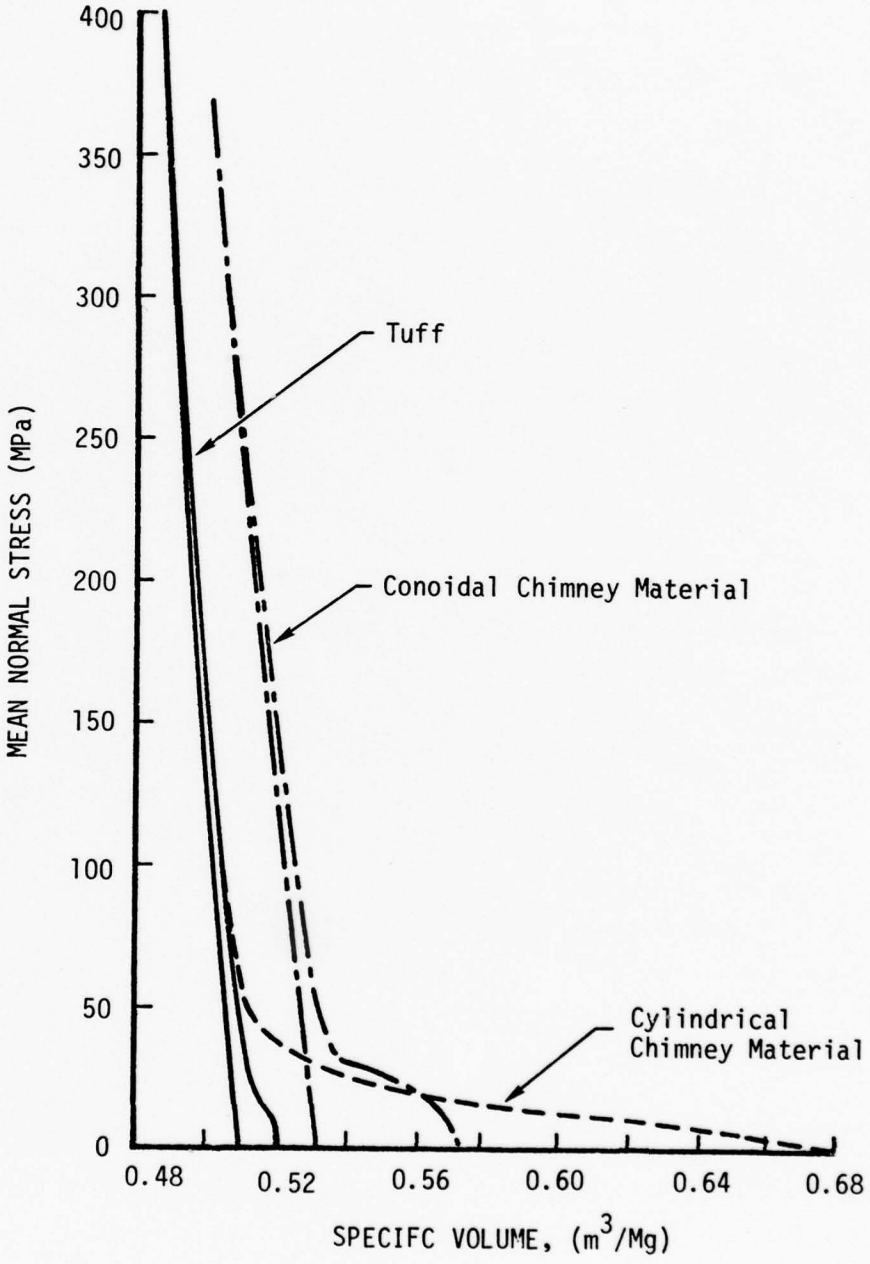

Figure 31. Porous crushup behavior for undisturbed tuff and chimney materials in in-chimney computations.

conoidal chimney material, however, stress wave attentuation is much less severe due to the lower void content of this material, and consequently, the effective strength of this material is relatively high during the time most of its shock-induced motion occurs.

4.3 IN-CHIMNEY STUDY RESULTS

4.3.1 Cylindrical Chimney

The most striking feature in the results from the cylindrical chimney computation involved the development and persistence of velocities in the chimney region. To a lesser extent, the focusing which is produced by the difference in material along a "preferred direction" in the chimney is also evident. The description of some of the field variables will be illustrated through the use of isometric plots. The field variables are plotted up vertically from the spatial plane which includes the axis of symmetry of the problem. The ranges included in that plane will be noted on the figures, as will the scale of the field variable axis. The reader should note that since these plots are self-scaling, the amplitudes on the field variable axis will in general be different from plot to plot which requires some "mental scaling" to be performed. In considering the velocity isometrics, the reader should note that these values are actually the speed and regions of negative velocity (towards the detonation point) will be pointed out to the reader where they are significant.

A comparison of the velocity fields at 15 and 35 ms (Figure 32) shows the shock wave developing in the undisturbed tuff region, as well as in the chimney material. The difference between the velocity field at 15 ms and that at the overlaid time of almost 13 ms is some additional propagation in range along with a drop in the peak velocity from 455 meters per second to 400 meters per second. By 35 ms, it is clear that the chimney material has been accelerated to significantly higher velocity than the undisturbed material. A cusp in the wave front at the cavity boundary is caused by the relatively slow propagation velocity of the shock in the chimney material. By 50 ms (Figure 33), the velocity in the tuff outside the chimney is only about one-tenth of that inside the chimney. At 100 ms, the only significant velocities in the problem are those in the chimney material. The peak velocity in the chimney has gone down by more than a factor of 2 from that at

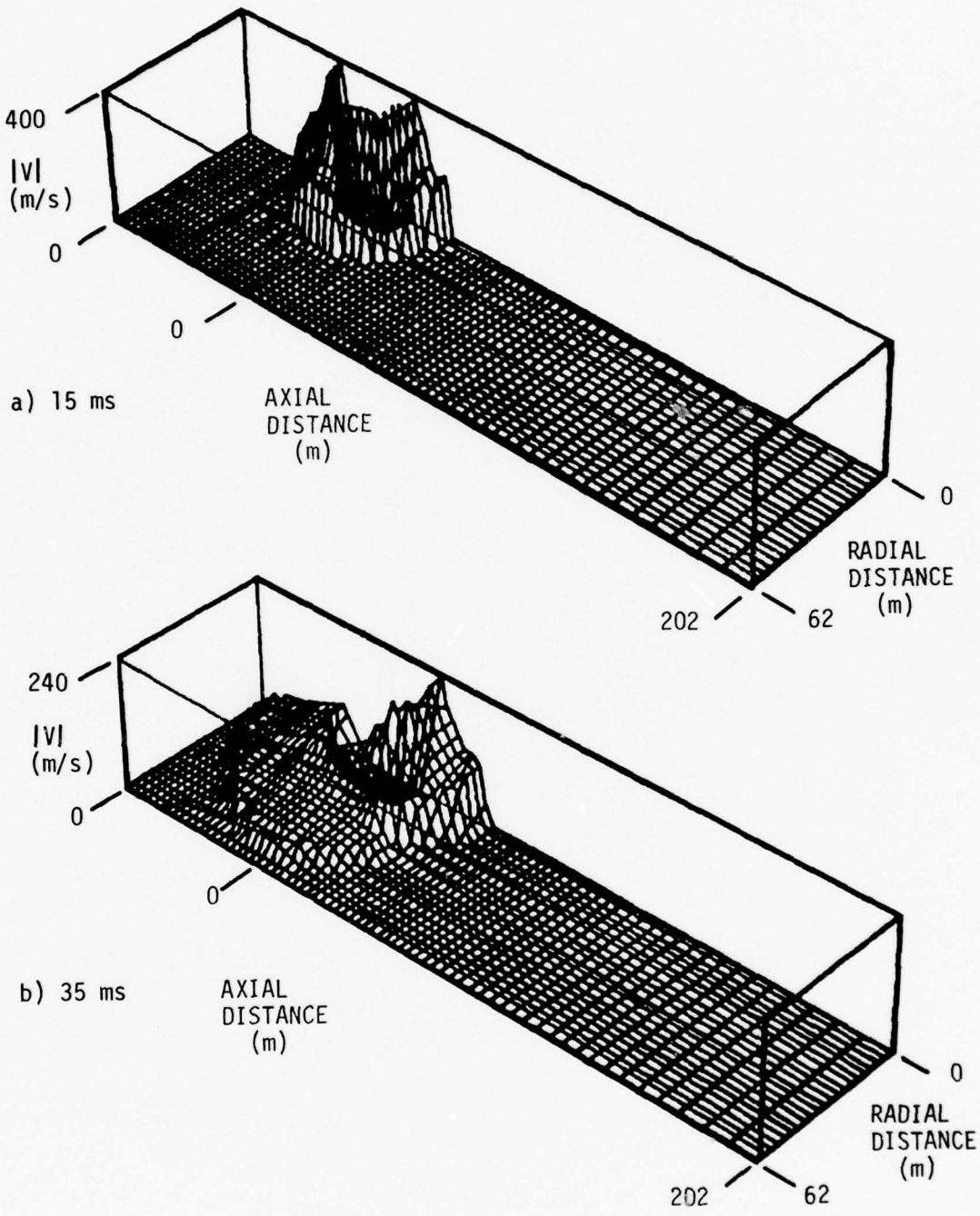

Figure 32. Isometric plots of speed fields for the cylindrical chimney computation at 15 and 35 ms.

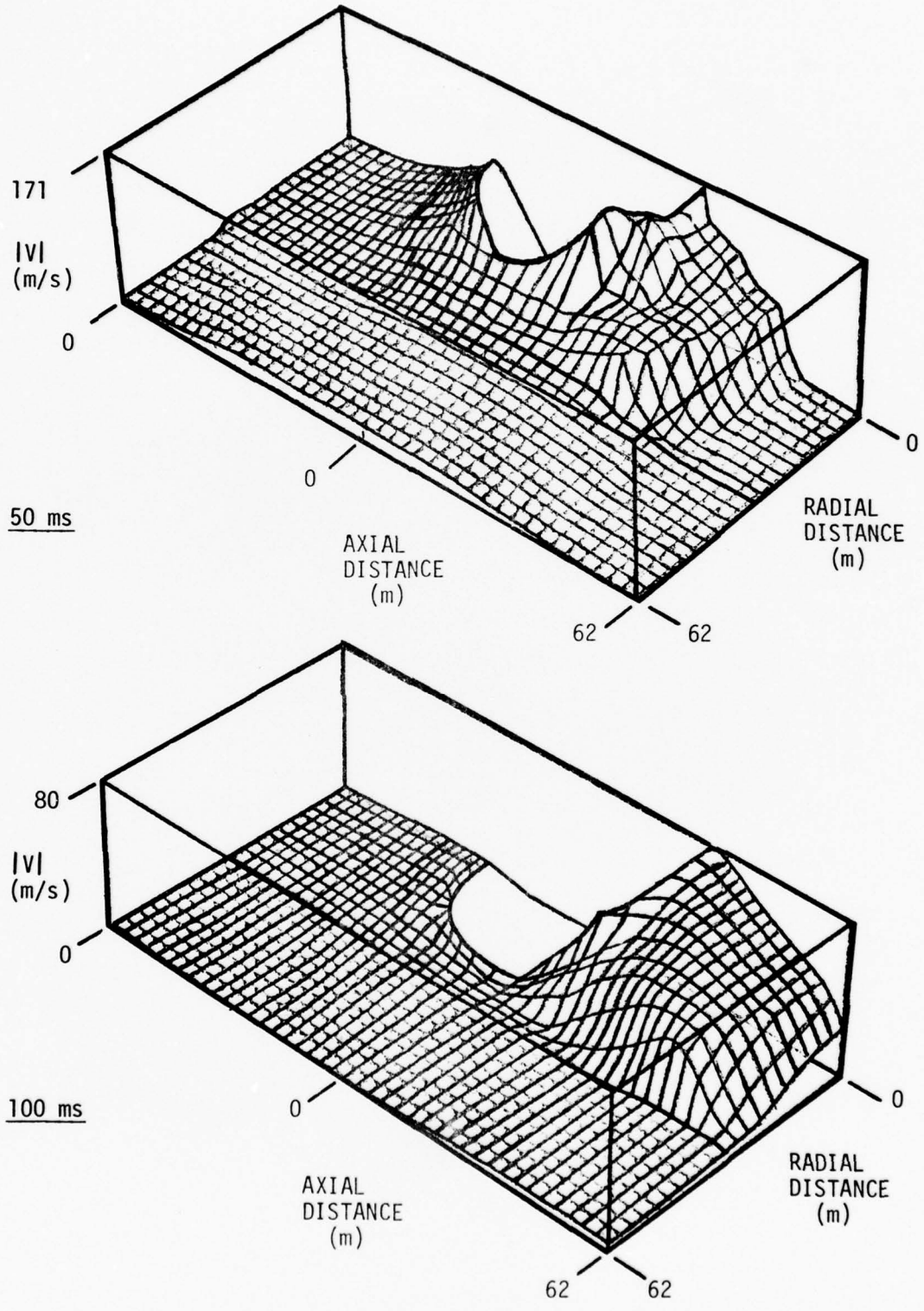

Figure 33. Isometric plots of speed fields for the cylindrical chimney at 50 and 100 ms.

50 ms. By 100 ms, the rebound has begun and the region next to the cavity in the hemisphere below the working point level is moving back towards the detonation point.

Figure 34 shows a profile of the velocities near the axis of symmetry, also indicating the rebound velocities. A comparison of the one-dimensional spherical solution conducted entirely in chimney material with the two-dimensional solution suggests the beginning of a focusing effect. In the one-dimensional solution since the entire sphere is expanding at the same rate, the cavity pressure drops faster than in the two-dimensional problem where strong tuff lies outside the chimney region in the lower hemisphere. This leads to a sustained pressure by comparison which continues to drive the chimney material. It is already clear that the residual stress fields formed at later times will be grossly affected in this region since chimney material is not rebounding with the surrounding tuff.

For an explosion of this yield in the undisturbed medium, the motions would ordinarily be minimal at about 190 ms. After that time, relatively small oscillations around zero endure in velocity. The half period for such oscillations in this calculation is about 60 ms. However, the chimney region material continues to move outward from the detonation point as shown in Figure 35. At 200 ms, the motion in the free-field is predominantly back towards the detonation point, but the motion in the chimney region is outward. Owing to the faster propagation velocity in the surrounding tuff, the wave, by coupling through to the region at the top of the chimney, has actually produced motions of chimney material back towards the cavity (Figure 36). It is also seen in the figure that a large region of the chimney continues to move outward at 250 ms with a maximum velocity of about 20 meters per second.

By 300 ms, the material at the top of the chimney moving inwards has stacked up against the enormous mass of material still moving away from the detonation point. The peak velocity, which is relatively uniform in the chimney region, is now close to 9 meters per second. The chimney material continues to slow down with the majority of it moving at about 3 meters per second, but with a peak velocity of 6 meters per second near its leading edge (Figure 37). By 350 ms, the material is starting to meet resistance from the surrounding tuff at the top of the chimney region. The computation was ended at this time. A more quantitative illustration

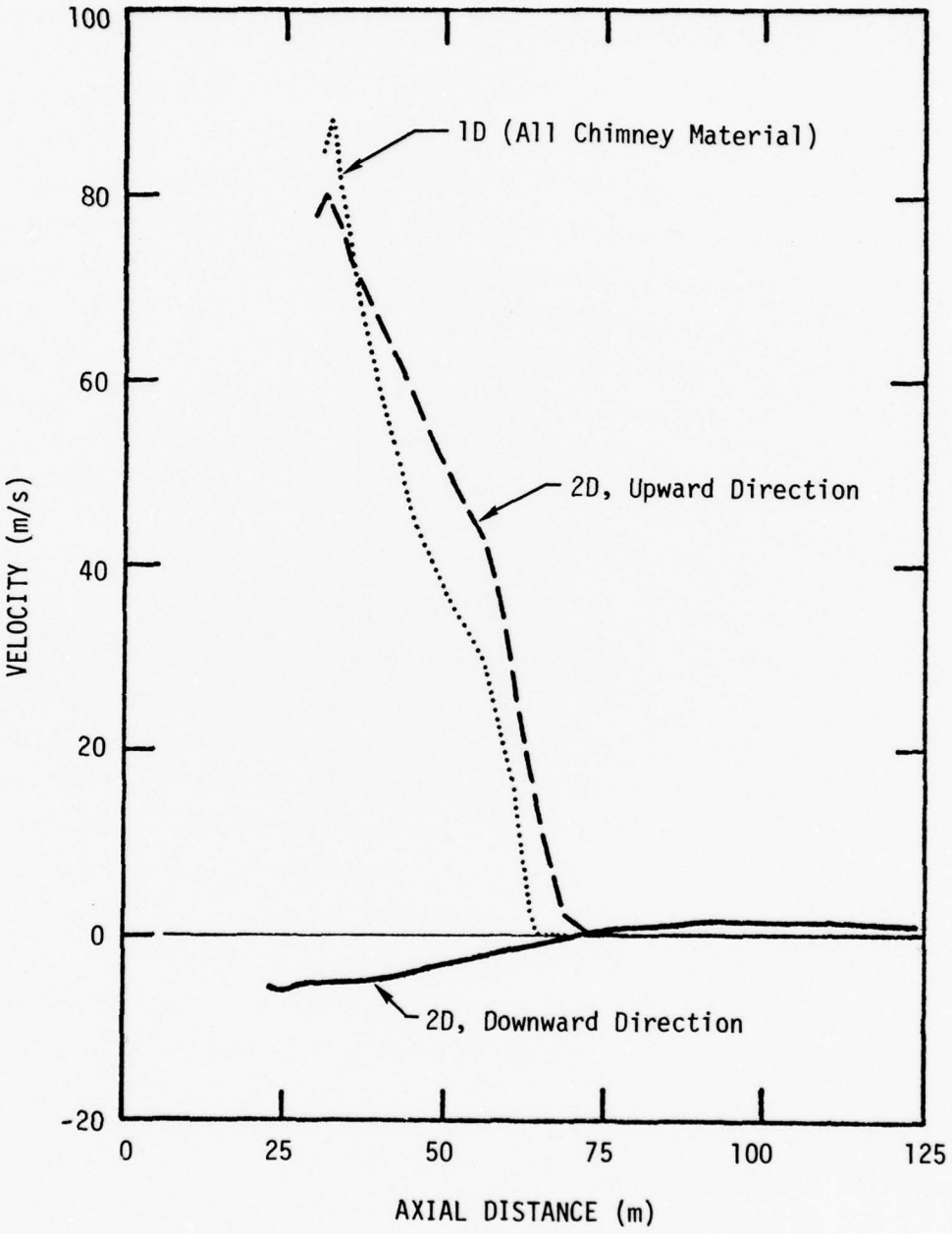

Figure 34. Velocity profiles at 100 ms.

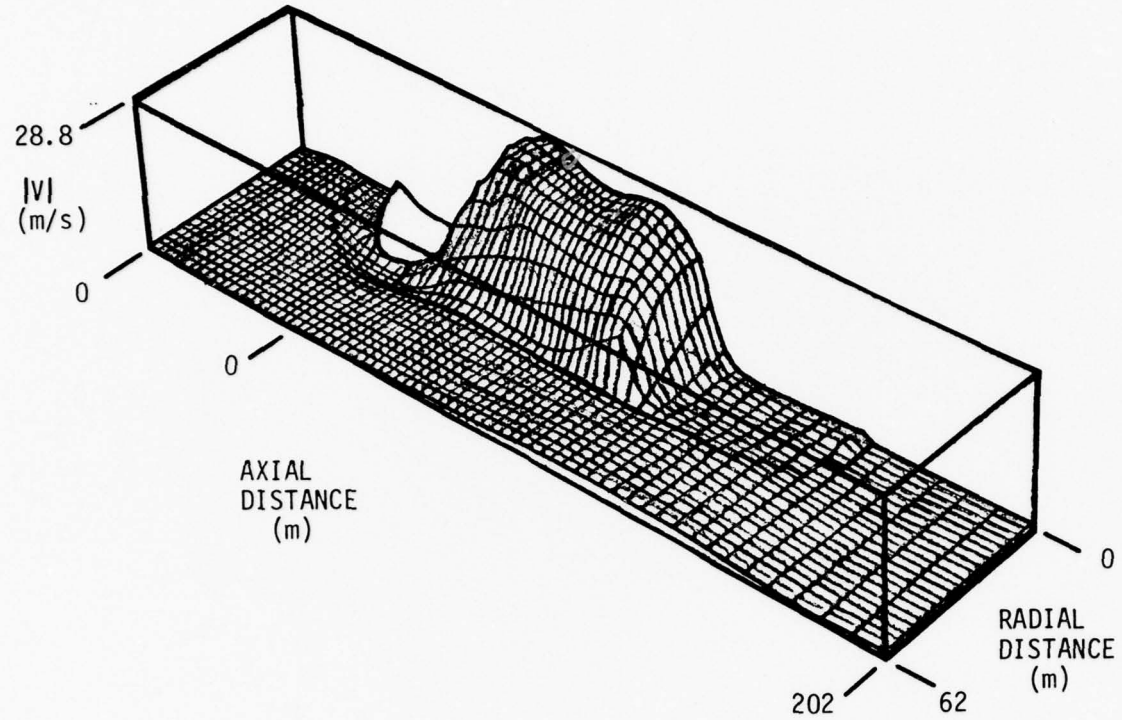

Figure 35. Isometric speed plot at 200 ms for cylindrical chimney.

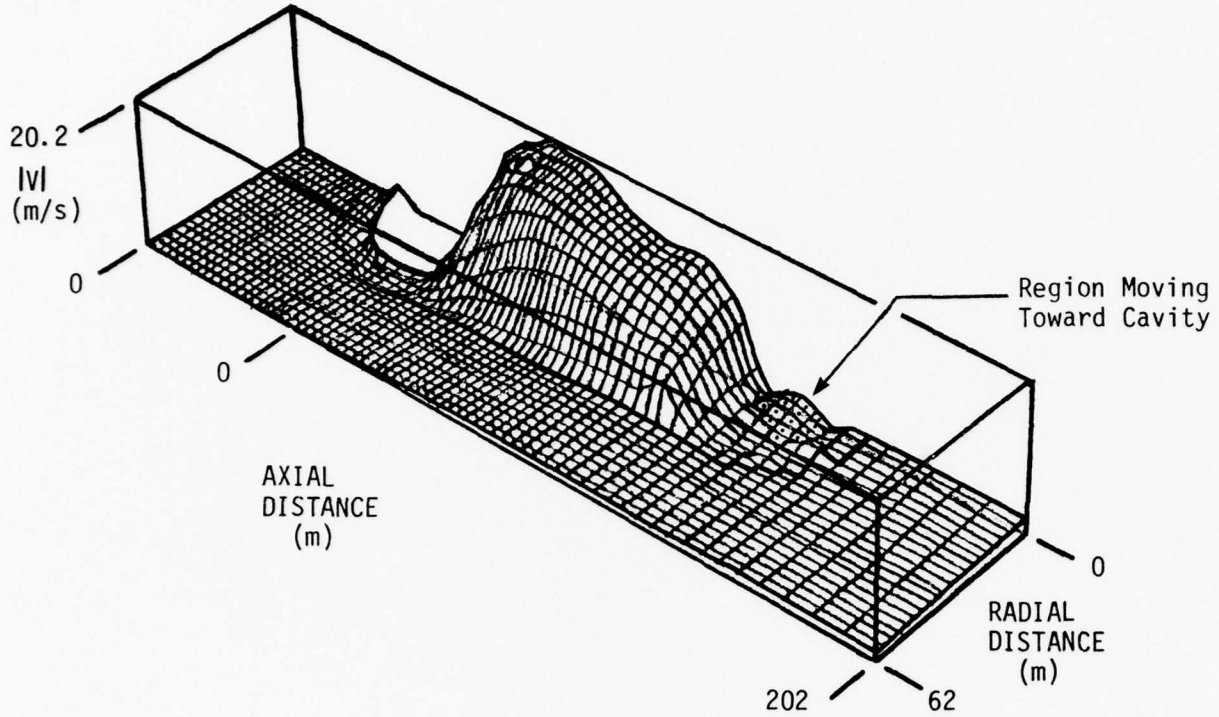

Figure 36. Isometric speed plot at 250 ms for cylindrical chimney.

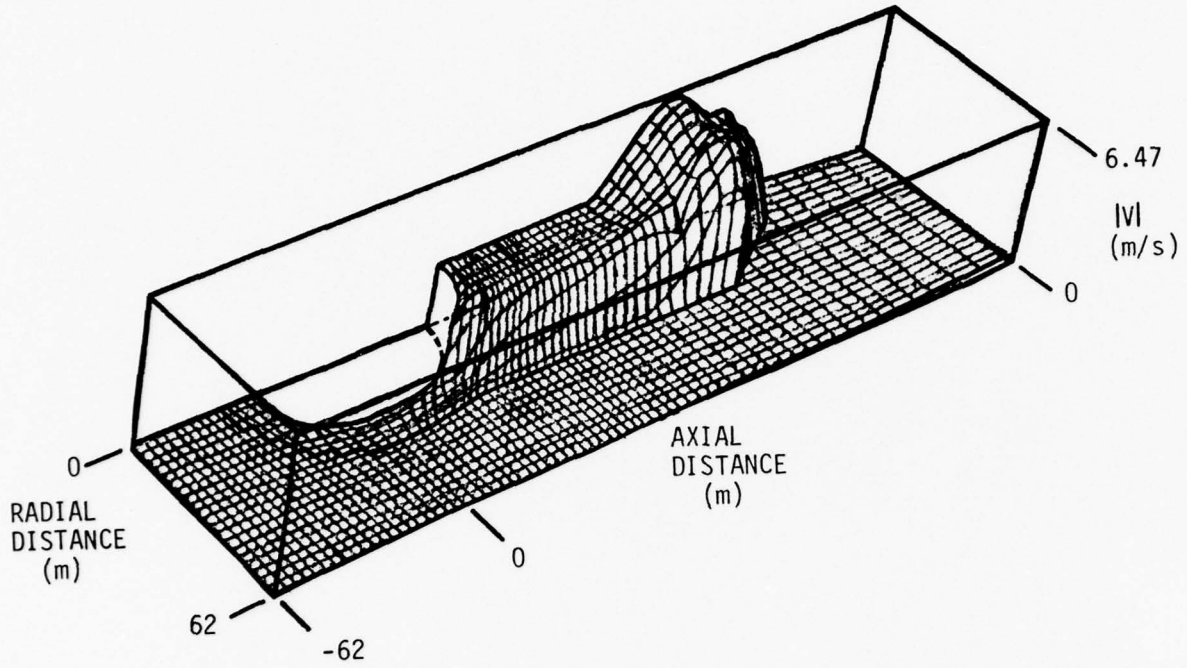

Figure 37. Isometric speed plot at 350 ms for cylindrical chimney.

of the outward velocity in the chimney at 350 ms is given in Figure 38. Notice that the steep part of the wave has just reached the top of the chimney at a range of 150 meters. It is clear that the stagnation of the chimney material at the top of the chimney will produce high stresses there which will propagate back toward the cavity. The extent of these "water-hammer" like oscillations will depend on the ability of the undisturbed material adjacent to the chimney to constrain the lateral motion, as well as the boundary condition provided by the cavity pressure.

The residual stress field in the vicinity of the chimney is still changing at 350 ms when the computation was terminated. However, in the region adjacent to the detonation-produced cavity, the residual stresses have eventually established themselves by 200 ms. The evolution of the hoop stress component from 200 ms to 350 ms is illustrated in the contour plots shown in Figure 39. A region of stress below that of the original overburden of 70 bars is seen to grow in extent even producing tensile regions within it. This region, adjacent to the chimney, would ordinarily be of low residual stress and it appears that the relief into the chimney region has further reduced that stress producing a valley through the ordinarily high residual stress field around the cavity. This valley seems to be directed back toward the detonation point level. This would clearly unacceptable for the safety for HLOS tests in which a tunnel would ordinarily be placed at working point level. The valley in stress would be a possible path of communication around the region which is ordinarily stemmed. An isometric plot of the hoop stress at 250 ms is shown in Figure 40. This shows that the magnitude of the average hoop stress in the chimney region is below that of the cavity pressure. The valley in the hoop stress referred to above is seen to be well below the chimney hoop stress and directed back towards the detonation point elevation.

The reduction of stress due to the presence of the chimney is shown by the profiles in Figure 41. These profiles are taken along lines perpendicular to the axis of symmetry at different distances above and below the detonation point level. The hoop stress profiles plotted below the working point level are very similar to those computed for the pancake problems discussed in Section 3 (see Figure 24) when the factor of two in yield is considered. At only 12 meters above the detonation point level, a 30 percent reduction is noted in the peak stress.

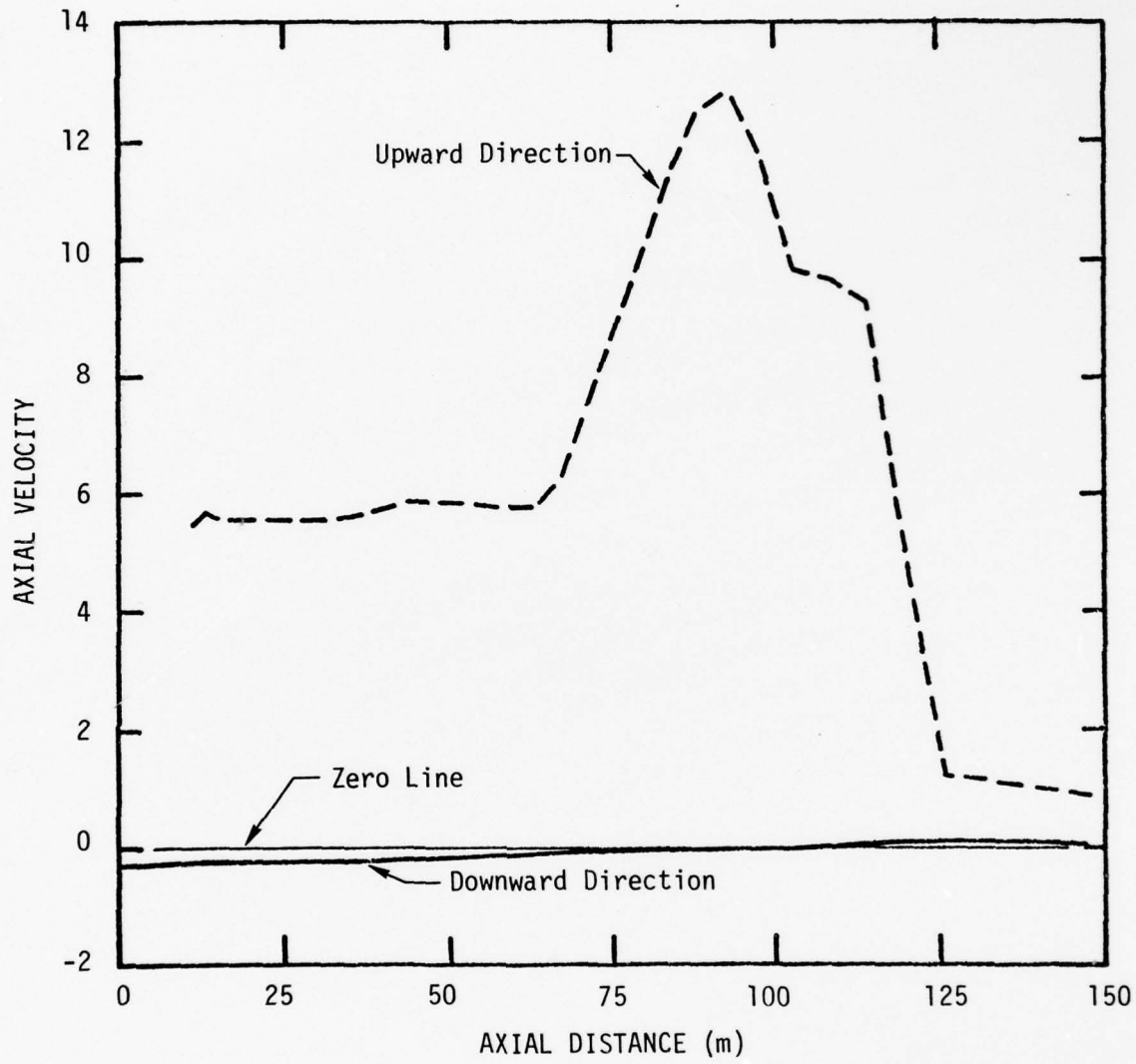

Figure 38. Axial velocity near the axis of symmetry at 350 ms for cylindrical chimney.

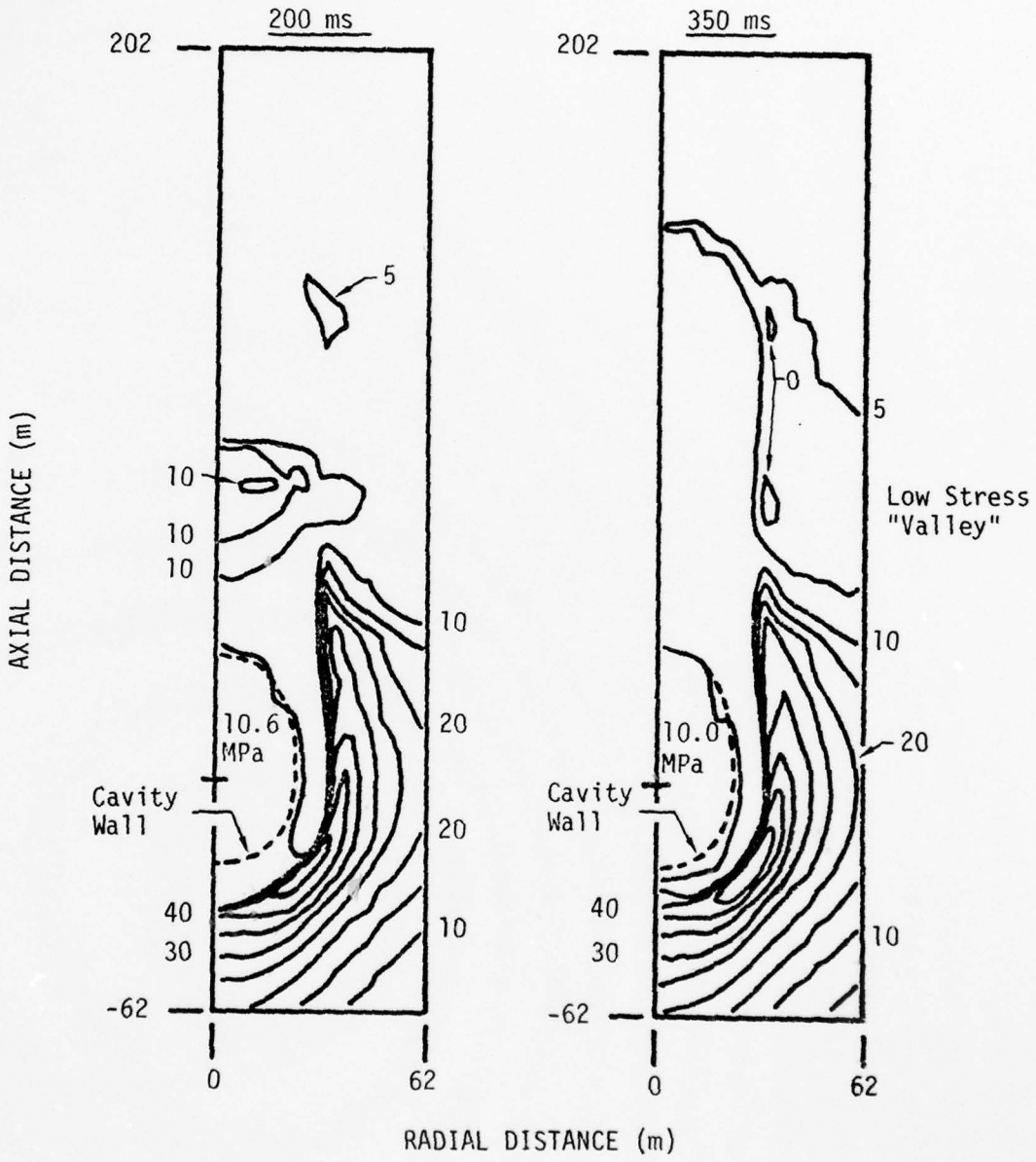

Figure 39. Comparison of hoop stress contours at 200 and 350 ms for the cylindrical chimney. Units of contours are MPa.

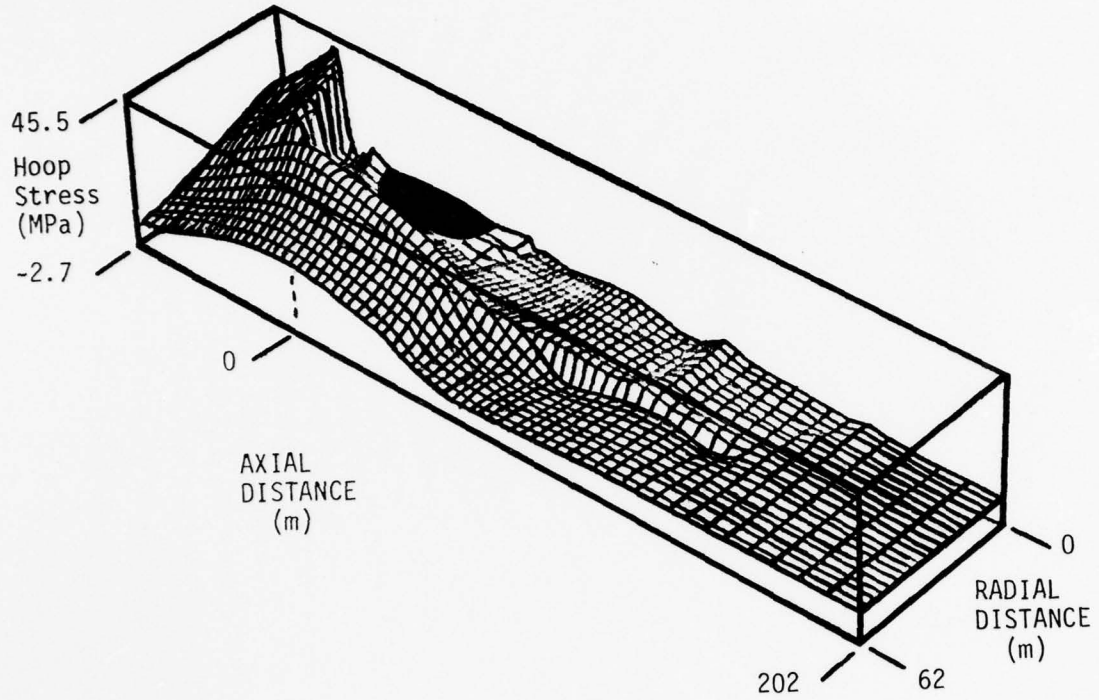

Figure 40. Isometric hoop stress plot at 250 ms for cylindrical chimney.

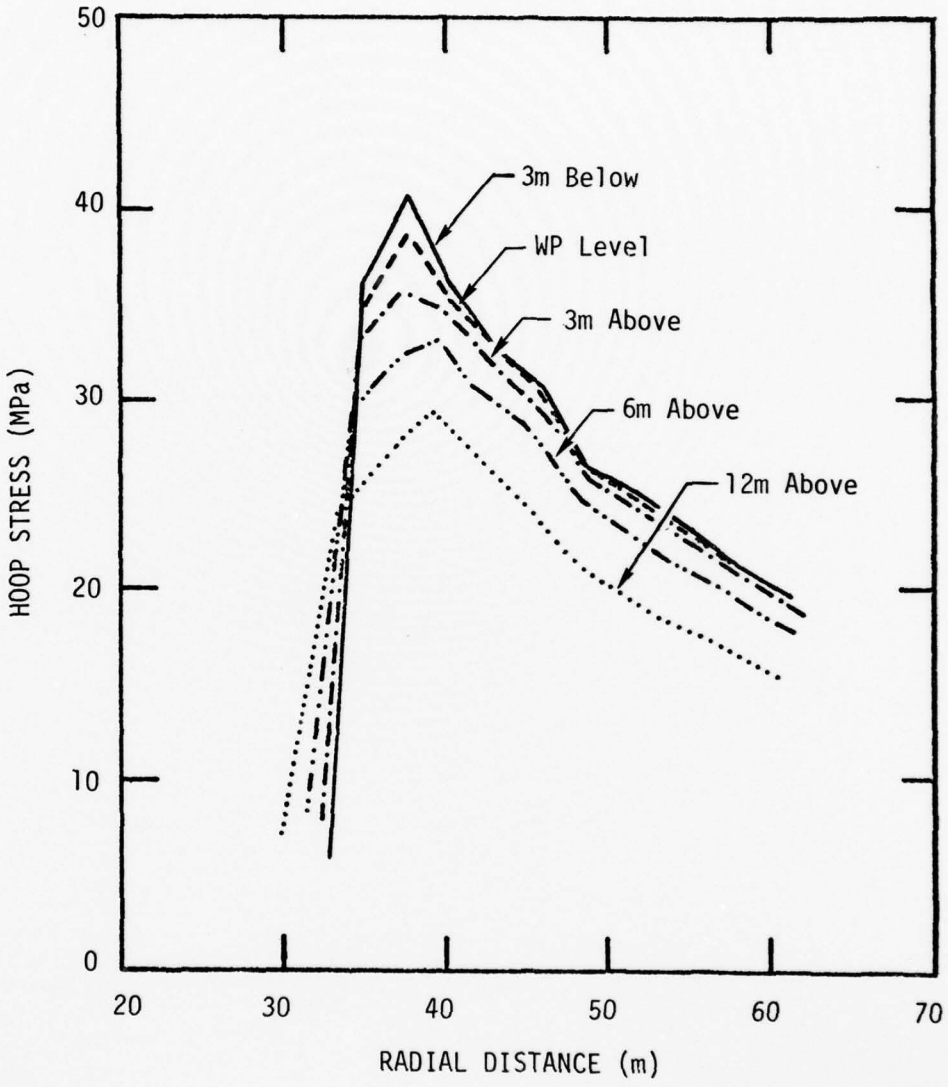

Figure 41. Hoop stress profiles perpendicular to the axis of symmetry for cylindrical chimney.

4.3.2 Conoidal Chimney and Comparison

The major differences between the two in-chimney computations concern the chimney geometries and the properties of the chimney material (Section 4.2). In terms of conducting parameter studies, this is somewhat unfortunate since in general, it is difficult to identify differences caused by the various changes. However, after reviewing the results it became clear that the substantive differences in the computations were caused by the differences in material properties, as opposed to those in geometry. These differences are discussed in what follows.

The conoidal chimney problem was initialized from the one-dimensional computation at 7.69 ms. It will be remembered that the cylindrical chimney problem was initialized at a time of 12.84 ms, the difference being due to the propagation velocity in the two different chimney materials. By 50 ms, the ground shock has established itself well out into the undisturbed tuff, as well as up into the chimney material (Figure 42). By comparison with Figure 33, it is seen that the velocity surface for the conoidal chimney is significantly more symmetric about the detonation point than was the case for the cylindrical chimney. The cylindrical chimney showed peak velocities above the cavity which were more than a factor of 2 greater than those below the cavity, and also on the axis of symmetry.

At a time of 100 ms when the rebound in the region adjacent to the lower hemisphere of the cavity is establishing itself, the chimney material has been accelerated to a peak velocity of about 17 meters per second (Figure 43). The form of the velocity profile on axis is similar to the cylindrical chimney case; however, the peak velocity for the cylindrical chimney was more than four times greater at 80 meters per second. By 200 ms, the highest velocity in the conoidal chimney case is almost an order of magnitude down from that of the cylindrical case (compare Figure 44 with Figure 35). The shape of the profile in the conoidal chimney also exhibits a dip at the center at that region which is significantly less well developed in the cylindrical chimney case. Some additional wave structure is evident for the conidal chimney (Figure 44). Some of this appears to be real and has been caused by the greater coupling between the chimney material and the undisturbed material for this case. The structure is more difficult to see on Figure 35 since the scaling for the isometric plot has been chosen to accommodate the very high peak velocity

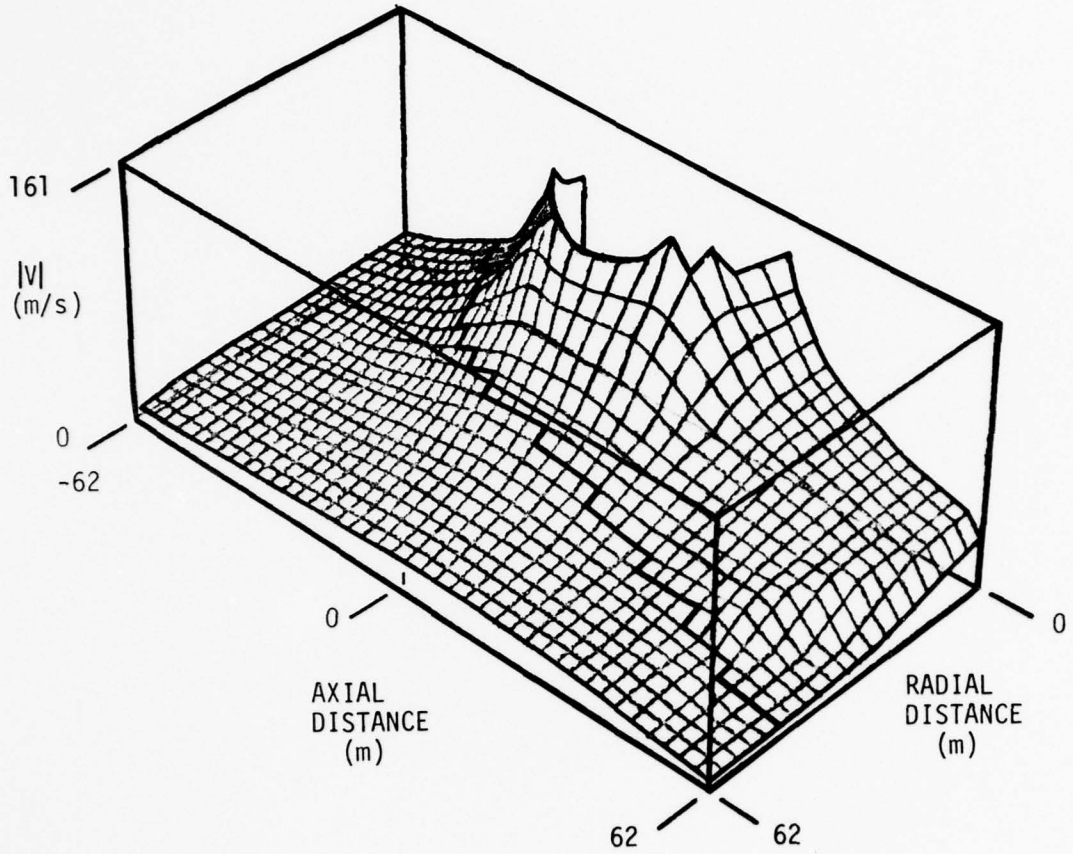

Figure 42. Isometric speed plot at 50 ms for conoidal chimney problem.

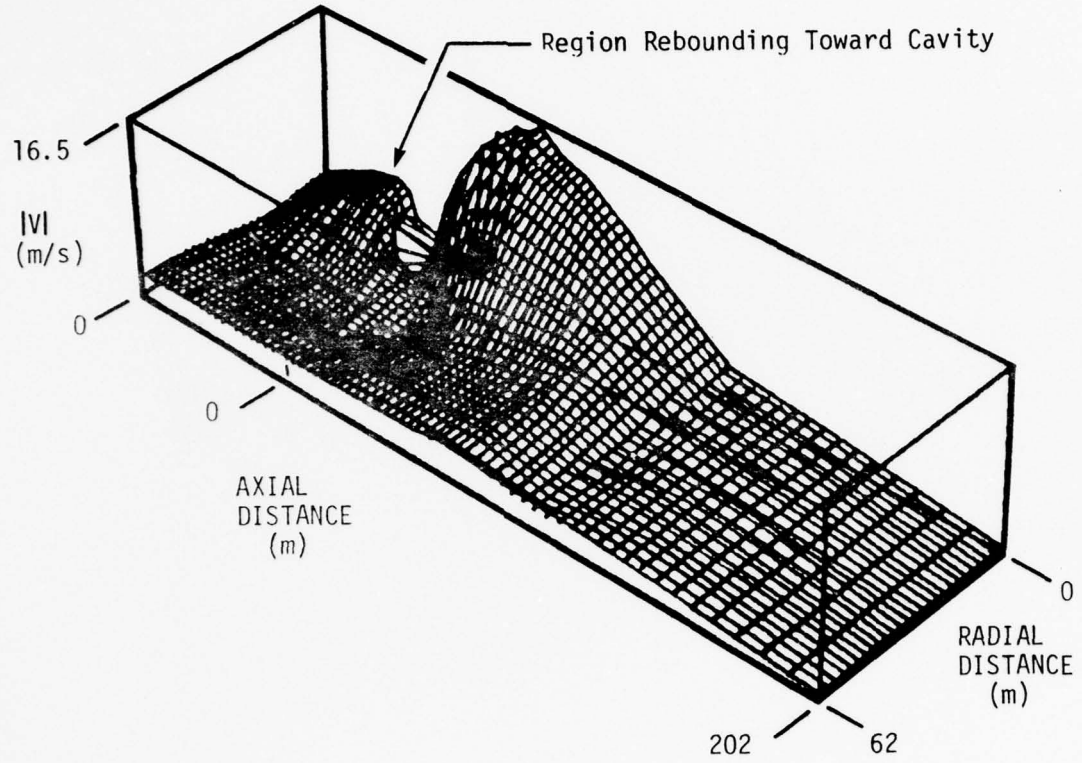

Figure 43. Isometric speed plot at 100 ms for conoidal chimney problem. Material below cavity is rebounding, while chimney material continues to move outward.

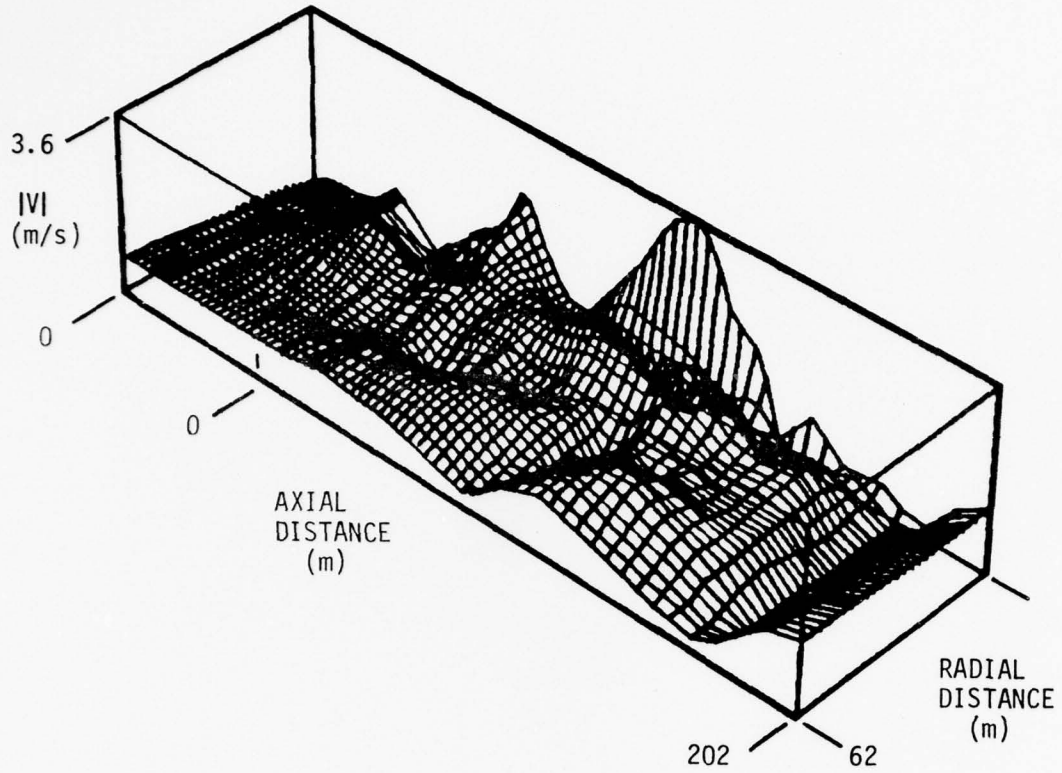

Figure 44. Isometric speed plot at 200 ms for conoidal chimney problem. Several regions of rebounding material exist.

on axis. Some elements of chimney material are already moving back towards the cavity in the conoidal chimney case at this time. This effect was also noted for the cylindrical chimney.

By 250 ms, the magnitude of the peak velocities is almost exactly an order of magnitude lower for the conoidal chimney; however, this velocity is in a direction back towards the cavity. The peak velocities from the cylindrical case were still moving outward at about 20 meters per second over a substantial length of the chimney with only a small region at about 2 meters per second moving back towards the cavity. For the conoidal chimney case, these low velocities continue to rattle around, but are no longer playing a role in establishing the residual stress field which is discussed below.

The most striking difference between the two chimney computations is that for the conoidal chimney, the residual stress fields which were established at 250 ms are not significantly different from what one would expect for a computation without a special chimney region. The residual hoop stress is shown at a time of 250 ms in Figure 45 for the conoidal chimney case. Note the near-symmetric magnitude of the hoop stress peaks around the cavity. It is seen that the hoop stress in the chimney region above the cavity is greater than that in surroundings and that the gradient moving away from the detonation point is somewhat lower than the region beneath the cavity. At 250 ms for the cylindrical chimney case, the residual stresses in the direction above the cavity were essentially completely eroded contrary to what is seen here for the conoidal case. This is what made the tensile "valley" in the cylindrical case appear to be ominous. Although such a valley also exists for the conoidal case, the fact that the residual stresses around the cavity are so high casts the evaluation of the low stress region in a substantially different light.

A more quantitative illustration of the hoop stress in different regions at 250 ms for the conoidal problem is shown in the contour plot of Figure 46. Notice the particular asymmetry of the region bounded by the 40 MPa contour. This region, which is of finite extent beneath the cavity, tapers away to a cusp before reaching the axis of symmetry above the cavity. Another asymmetry is that of the 10 MPa

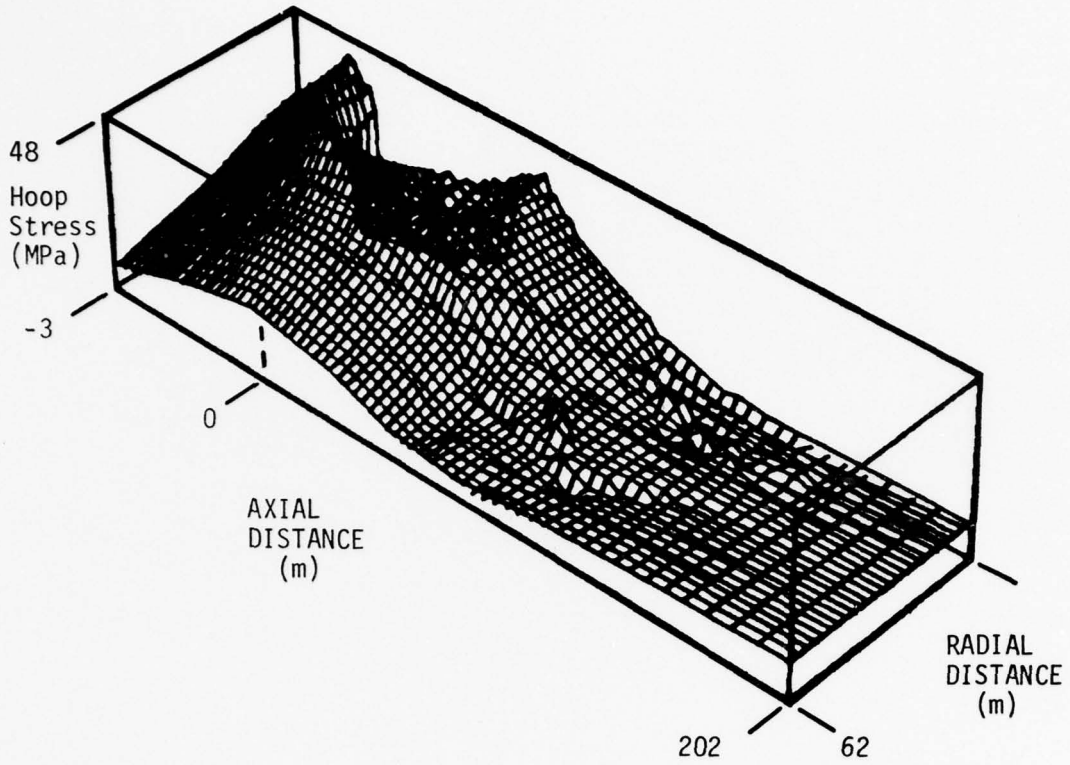

Figure 45. Isometric plot of residual hoop stress (at 250 ms) for conoidal chimney problem.

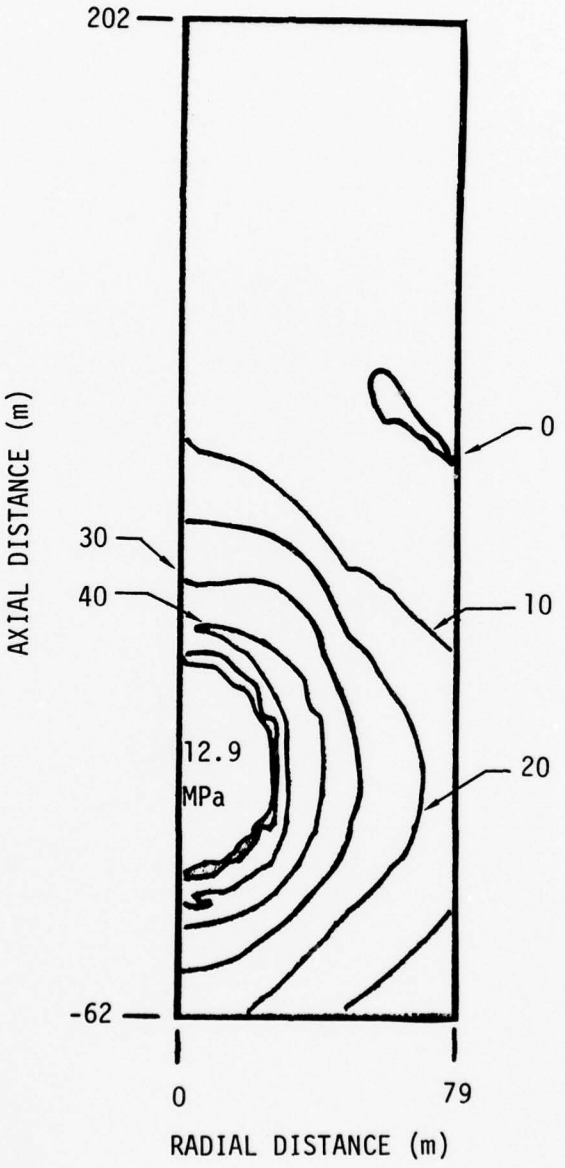

Figure 46. Contour plot of residual hoop stress at 250 ms for conoidal chimney problem. Contour interval 15 10 MPa.

contour which shows a kink at the chimney boundary. This is the same type of effect which was seen on the cylindrical chimney problem, but is of significantly less importance here. The small tensile region adjacent to the chimney also appears more clearly in the contour plot. In the cylindrical calculation this region was the beginning of the low stress valley to which reference was made. In the conoidal case, the cavity is clearly isolated from the tensile region by the development of the residual stress field which has formed.

4.3.3 Conclusions

The outstanding conclusion from the in-chimney study is that the properties of the material which fill the chimney region are of paramount importance regarding the formation of a competent residual stress field. The materials chosen here in one sense represent two bounds of what is likely to exist in an actual chimney. The distribution of cavity volume throughout the chimney in the cylindrical case provides an upper bound on what the air void content of the recompacted material at a chimney bottom is likely to be. While this may underestimate the amount of void in the upper levels of the chimney, it clearly overestimates the amount of void in the lower levels. The use of properties from overlying strata is probably reasonable in the cavity region, but underestimates the air voids in the rubble at higher levels of the chimney.

Because of the clear dependence of the residual stress field on the material properties for in-chimney configurations, one would have to carefully document the chimney properties during the exploratory phase of site selection. Extensive work to document these properties would have to be conducted on a case by case basis in order to qualify any particular site. Before the actual exploration, it would be prudent to perform computations which included the effects of layered media both in the chimney and the surrounding tuff.

5. REFERENCES

1. Letter by Col. Neuer, Defense Nuclear Agency, establishing guidelines for siting criteria for HLOS tests in Area 12 at NTS, 10 July 1969.

2. D. F. Patch, "Preliminary Results from Numerical Studies of Groundshock Interaction with a Nearby Chimney", Pacifica Technology, PT-U76-0081, 1976.

3. D. F. Patch and R. T. Allen, "Additional Studies of Groundshock Interaction with a Nearby Chimney", Pacifica Technology, PT-U78-0180, 1978.

4. M. L. Wilkens, "Calculation of Elastic-Plastic Flow", in Alder, B., Fernback, S. and Rotenberg, M., editors, Methods in Computational Physics, Academic Press, 1964.

5. R. L. Bjork and M. L. Gittings, "Wave Generation by Shallow Underwater Explosions", Defense Nuclear Agency, DNA 2949Z, December 1972.

6. D. F. Patch and J. E. Welch, "Phase II Ground Motion Calculations in Support of the Boeing Structures Experiment in Diablo Hawk", Pacifica Technology, PT-U78-0166, 26 January 1978.

7. N. Rimer and M. Friedman, "Residual Stress and Coupling from Nuclear Shots in a Cavity", Systems, Science and Software, SSS-R-78-3596, April 1978.

8. W. Herrmann, "Constitutive Equation for the Dynamic Compaction of Ductile Porous Materials", J. Appl. Phys., Vol. 40, No. 6, pp. 2490-2499, 1969.

9. L. Whitman and J. P. Wright, "Tensile Behavior of Geological Material in Ground Shock Calculations", Defense Nuclear Agency, DNA 3769T, June 1975.

10. Material response model developed by D. F. Patch and R. T. Allen, Pacifica Technology, for ground motion calculations of the Mighty Epic test site response, December 1975.

11. M. J. Cunningham, United States Geological Survey, private communication with G. I. Kent, 10 October 1975.

12. S. W. Butters, R. K. Dropek and A. H. Jones, "Material Properties of Nevada Test Site Tuff and Grout - With Emphasis on the Mighty Epic Event", Defense Nuclear Agency, DNA 4235F, November 1976.

13. S. W. Butter, Terra Tek, private communication of uniaxial response crush curves for tests summarized in Reference 12 above, October 1975.

14. S. W. Butters and D. S. Gardiner, "Physical and Mechanical Properties of Reconstituted Tuff", Terra Tek, TR77-94, October 1977.

15. M. Scott, Ken O'Brian Associates, private communication.

16. J. LaComb, Defense Nuclear Agency, Field Command, Test Directorate, Nevada Branch, 1977.

17. S. W. Butters, Terra Tek, personal communication of data contained in Terra Tek Report, TR 75-9, "Field, Laboratory and Modeling Studies on Mount Helen Welded Tuff for Earth Penetrator Test Evaluation", by S. W. Butters, et al., January 1975.

18. S. W. Butters, R. K. Dropek, S. J. Green and A. H. Jones, "Material Properties in Support of the Nevada Test Site Nuclear Test Program", Terra Tek, TR 75-27, October 1975.

19. D. S. Gardiner, Terra Tek, personal communication to J. W. LaComb, Defense Nuclear Agency, 14 September 1977.

20. E. Peterson, P. Lagus and K. Lie, "Summary of the Mighty Epic Tracer-Gas Chimney Pressurization Studies", Systems, Science and Software, SSS-R-78-3542, 9 January 1978.

DISTRIBUTION LIST

DEPARTMENT OF DEFENSE

Assistant to the Secretary of Defense
Atomic Energy
ATTN: Executive Assistant

Defense Documentation Center
12 cy ATTN: DD

Defense Nuclear Agency
ATTN: DDST
ATTN: SPTD, W. Summa
4 cy ATTN: TITL

Field Command
Defense Nuclear Agency
ATTN: FCPR
ATTN: FCTMC, C. Keller

Livermore Div., Field Command, DNA
Lawrence Livermore Laboratory
ATTN: FCPRL

Test Construction Div.
Field Command Test Directorate
Defense Nuclear Agency
ATTN: J. LaComb

Under Secretary of Defense for Rsch. & Engrg.
ATTN: Strategic & Space Systems (OS)

DEPARTMENT OF THE ARMY

Harry Diamond Laboratories
ATTN: DELHD-N-NP

DEPARTMENT OF THE NAVY

White Oak Laboratory
Naval Surface Weapons Center
ATTN: F31

DEPARTMENT OF THE AIR FORCE

Air Force Weapons Laboratory
ATTN: SUL

DEPARTMENT OF ENERGY

Nevada Operations Office
ATTN: R. Newman

OTHER GOVERNMENT AGENCY

Department of Commerce
US Geological Survey
Special Projects Branch
ATTN: R. Carroll

DEPARTMENT OF DEFENSE CONTRACTORS

General Electric Company—TEMPO
Center for Advanced Studies
ATTN: DASIAC

Lawrence Livermore Laboratory
University of California
ATTN: D. Oakley
ATTN: B. Hudson
ATTN: B. Terhune
ATTN: J. Shearer

Los Alamos Scientific Laboratory
ATTN: R. Brownlee
ATTN: F. App/E. Jones
ATTN: A. Davis
ATTN: L. Germain

Pacifica Technology
ATTN: G. Kent
ATTN: D. Patch
ATTN: J. Welch

Physics International Company
ATTN: E. Moore

Sandia Laboratories
ATTN: C. Mehl/C. Smith

SRI International
ATTN: A. Florence

Systems, Science & Software, Inc.
ATTN: R. Duff

Terra Tek, Inc.
ATTN: S. Green

END